ESL-TR-88-22

# HEAVY GAS DISPERSION TEST SUMMARY REPORT

D.L. ERMAK, R. CHAPMAN, H.C. GOLDWIRE,
F.J. GOUVEIA, H.C. RODEAN

LAWRENCE LIVERMORE
NATIONAL LABORATORY
LAWRENCE LIVERMORE NATIONAL LABORATORY
P.O. BOX 808
LIVERMORE CA 94550

JUNE 1989

FINAL REPORT

NOVEMBER 1985 — OCTOBER 1988





AIR FORCE ENGINEERING & SERVICES CENTER
ENGINEERING & SERVICES LABORATORY
TYNDALL AIR FORCE BASE, FLORIDA 32403

# NOTICE

PLEASE DO NOT REQUEST COPIES OF THIS REPORT FROM HQ AFESC/RD (ENGINEERING AND SERVICES LABORATORY). ADDITIONAL COPIES MAY BE PURCHASED FROM:

NATIONAL TECHNICAL INFORMATION SERVICE
5285 PORT ROYAL ROAD
SPRINGFIELD, VIRGINIA 22161

FEDERAL GOVERNMENT AGENCIES AND THEIR CONTRACTORS REGISTERED WITH DEFENSE TECHNICAL INFORMATION CENTER SHOULD DIRECT REQUESTS FOR COPIES OF THIS REPORT TO:

DEFENSE TECHNICAL INFORMATION CENTER
CAMERON STATION
ALEXANDRIA, VIRGINIA 22314

UNCLASSIFIED

SECURITY CLASSIFICATION OF THIS PAGE

# REPORT DOCUMENTATION PAGE

Form Approved OMB No. 0704-0188

| | |
|---|---|
| 1a. REPORT SECURITY CLASSIFICATION<br>Unclassified | 1b. RESTRICTIVE MARKINGS |
| 2a. SECURITY CLASSIFICATION AUTHORITY | 3. DISTRIBUTION/AVAILABILITY OF REPORT<br>Approved for Public Release<br>Distribution Unlimited |
| 2b. DECLASSIFICATION/DOWNGRADING SCHEDULE | |
| 4. PERFORMING ORGANIZATION REPORT NUMBER(S) | 5. MONITORING ORGANIZATION REPORT NUMBER(S)<br>ESL-TR-88-22 |
| 6a. NAME OF PERFORMING ORGANIZATION<br>Lawrence Livermore National Laboratory<br>6b. OFFICE SYMBOL (If applicable) | 7a. NAME OF MONITORING ORGANIZATION<br>Air Force Engineering and Services Center |
| 6c. ADDRESS (City, State, and ZIP Code)<br>Lawrence Livermore National Laboratory<br>P.O. Box 808<br>Livermore, CA 94550 | 7b. ADDRESS (City, State, and ZIP Code)<br>AFESC/RDVS<br>Tyndall AFB FL 32403-6001 |
| 8a. NAME OF FUNDING/SPONSORING ORGANIZATION Air Force Engineering and Services Center<br>8b. OFFICE SYMBOL (If applicable) RDVS | 9. PROCUREMENT INSTRUMENT IDENTIFICATION NUMBER<br>Contract #W-7405-ENG-48 |
| 8c. ADDRESS (City, State, and ZIP Code)<br>AFESC/RDVS<br>Tyndall AFB FL 72403-6001 | 10. SOURCE OF FUNDING NUMBERS<br>PROGRAM ELEMENT NO. 63723F; PROJECT NO. 2103; TASK NO. 50; WORK UNIT ACCESSION NO. 05 |

11. TITLE (Include Security Classification)

Heavy Gas Dispersion Test Summary Report

12. PERSONAL AUTHOR(S)

Ermak, Donald L; Chapman, Renee; Goldwire, Henry C., Jr.; Gouveia, Frank J.; Rodean, Howard C

| 13a. TYPE OF REPORT | 13b. TIME COVERED | 14. DATE OF REPORT (Year, Month, Day) | 15. PAGE COUNT |
|---|---|---|---|
| Final | FROM Nov. '85 TO Oct. '88 | June 1989 | 176 |

16. SUPPLEMENTARY NOTATION

Availability of this report is specified on reverse of front cover.

| 17. COSATI CODES | | | 18. SUBJECT TERMS (Continue on reverse if necessary and identify by block number) |
|---|---|---|---|
| FIELD | GROUP | SUB-GROUP | |
| 04 | 02 | | Model validation, model evaluation, diffusion model, hazard response model, AIR POLLUTION, Heavy gases, |
| 12 | 01 | | |

19. ABSTRACT (Continue on reverse if necessary and identify by block number)

This report summarizes the results from selected field-scale, heavy gas dispersion tests, which can be used to validate atmospheric dispersion models. A total of 26 benchmark tests were chosen from the Lawrence Livermore National Laboratory Burro (LNG), Coyote (LNG), Desert Tortoise (ammonia), and Eagle (nitrogen tetroxide) tests; the Shell Research Ltd. Maplin Sands tests (LNG and LPG); and the British Health and Safety Executive Thorney Island tests (freon-air mixtures). Only continuous finite duration releases were selected for the test summaries as they were considered to better represent typical accidental releases from a storage vessel or transportation vehicle. The test summaries describe the manner of release, the ambient meteorological conditions, and the resulting vapor cloud characteristics including peak concentration, average centerline concentration, and average height and width of the cloud, all as functions of downwind distance.

| 20. DISTRIBUTION/AVAILABILITY OF ABSTRACT | 21. ABSTRACT SECURITY CLASSIFICATION | |
|---|---|---|
| ☐ UNCLASSIFIED/UNLIMITED ☐ SAME AS RPT. ☐ DTIC USERS | Unclassified | |
| 22a. NAME OF RESPONSIBLE INDIVIDUAL<br>Capt. Michael T. Moss | 22b. TELEPHONE (Include Area Code)<br>(904) 283-4234 | 22c. OFFICE SYMBOL<br>AFESC/RDVS |

DD Form 1473, JUN 86 *Previous editions are obsolete.* SECURITY CLASSIFICATION OF THIS PAGE



UNCLASSIFIED

(The reverse of this page is blank.)

TABLE OF CONTENTS


| Section | Title | Page |
|---|---|---|
| I | INTRODUCTION | 1 |
| | A. OBJECTIVE | 1 |
| | B. BACKGROUND | 1 |
| | C. SCOPE | 4 |
| II | METHODS FOR DESCRIBING THE AMBIENT METEOROLOGICAL CONDITIONS | 5 |
| | A. ATMOSPHERIC STABILITY | 6 |
| | 1. Stability Classification Schemes | 6 |
| | 2. Surface Layer Similarity Theory | 11 |
| | 3. A Unifying Approach | 16 |
| | B. COMPUTATION OF METEOROLOGICAL PARAMETERS | 17 |
| | 1. Review of Methods | 18 |
| | 2. Proposed Approach | 23 |
| | 3. Application to LLNL, Shell, and HSE Tests | 27 |
| | C. UNCERTAINTY | 30 |
| | 1. Variation in Stability Category Classification Methods | 32 |
| | 2. Surface-Layer Theory | 39 |
| | 3. Variation in Friction Velocity | 46 |
| III | PARAMETERS USED TO DESCRIBE A DISPERSING DENSE-GAS CLOUD | 49 |
| | A. HEAVY GAS DISPERSION AND MODEL VALIDATION | 49 |
| | B. CHOICE OF CLOUD PARAMETERS | 52 |
| | C. CONCENTRATION AVERAGING TIME | 53 |
| | D. SELECTED MEASURES OF PLUME DISPERSION | 54 |
| IV | SUMMARY | 56 |
| | REFERENCES | 58 |
| APPENDIX | | |
| A | LLNL BURRO AND COYOTE TESTS (LNG) | 65 |
| B | LLNL Desert Tortoise Tests ($NH_3$) | 95 |
| C | LLNL Eagle Tests | 105 |
| D | Shell Continuous Release Tests (LNG and LPG) | 117 |
| E | HSE Continuous Release Tests (Freon) | 153 |




The reverse of this page is blank.

## PREFACE

This report was prepared by Lawrence Livermore National Laboratory (LLNL), P. O. Box 808, Livermore, California 94550, under contract W-7405-ENG-48, for the Air Force Engineering and Services Center, Engineering and Services Laboratory (AFESC/RDVS), Tyndall Air Force Base, Florida 32403-6001.

This report summarizes work done between November 1985 and February 1988. The principal investigator at LLNL was Donald L. Ermak. Captains Lawrence E. Key and Michael T. Moss were the AFESC/RDVS Project Officers.

This report has been reviewed by the Public Affairs Office (PA) and is releasable to the National Technical Information Service (NTIS). At NTIS, it will be available to the general public, including foreign nationals.

This technical report has been reviewed and is approved for publication.

MICHAEL T. MOSS, Captain, USAF
Project Officer

NILS AKERLIND, JR., Major, USAF
Chief, Environics Division

KENNETH T. DENBLEYKER, Major, USAF
Chief, Environmental Sciences Branch

LAWRENCE D. HOKANSON, Colonel, USAF
Director, Engineering and Services Laboratory

| Accession For | |
|---|---|
| NTIS GRA&I | ☒ |
| DTIC TAB | ☐ |
| Unannounced | ☐ |
| Justification | |
| By | |
| Distribution/ | |
| Availability Codes | |
| Dist | Avail and/or Special |
| A-1 | |



(The reverse of this page is blank.)

## LIST OF FIGURES


| Figure | Title | Page |
|---|---|---|
| 1 | Curves of $\sigma_y$ and $\sigma_z$ for Pasquill's Turbulence Types (Reference 17) | 8 |
| 2 | Curves by Golder (Reference 40) Showing Pasquill's Stability Classes as a Function of the Monin-Obukhov Length and the Surface Roughness Length | 18 |
| 3 | Stability as a Function of Heat Flux and Windspeed as Given by Pasquill (Reference 54) | 35 |
| A-1 | Sensor Array for the Burro Series Experiments | 68 |
| A-2 | Sensor Array for the Coyote Series Experiments. "Old" Locations Refer to Those that were the Same as in the Burro Series | 69 |
| B-1 | Sensor Array for the Desert Tortoise Series Experiments | 98 |
| C-1 | Sensor Array for the Eagle Series Experiments | 108 |
| D-1 | Sensor Array for the Shell Tests at Maplin Sands | 119 |
| E-1 | Sensor Array for the Continuous HSE Tests at Thorney Island: (a) Far-Field Layout; (b) Near-Field Layout | 156 |




The reverse of this page is blank.

LIST OF TABLES


| Table | Title | Page |
|---|---|---|
| 1 | Meteorological Conditions Defining Pasquill Turbulence Types | 8 |
| 2 | Pasquill Stability Categories $\sigma_\theta$ | 9 |
| 3 | Power-Law Approximations $\sigma_z = ax^s$ in F.B. Smith's (Reference 29) Revision of Pasquill's (Reference 17) Values (Surface Release) $\sigma$ and x in km | 10 |
| 4 | Brigg's $\sigma_y(x)$ and $\sigma_z(x)$ Formulae for Elevated Small Releases, $0.1 \leq x \leq 10$ km | 10 |
| 5 | Typical Values of Surface Roughness | 20 |
| 6 | Average Ratio of Velocity and Potential Temperature Terms | 26 |
| 7 | Summary of Datafit Results | 28 |
| 8 | Modified Pasquill Stability Categories | 34 |
| 9 | Stability Class: Average Value and Standard Deviation | 38 |
| 10 | Distribution of Chosen Stability Values | 38 |
| 11 | Estimated Error | 41 |
| 12 | Friction Velocity ($U_*$ m/s) | 43 |
| 13 | Scaling Potential Temperature ($\theta_*$ °K) | 44 |
| 14 | Nine-Minute Average of $[-\langle U' \cdot W' \rangle]^{1/2}$ for Burro 7, 8, and 9 | 47 |
| 15 | Comparison of Friction Velocity Values ($U_*$) | 47 |
| 16 | Description of Dense-Gas Cloud Parameters | 51 |
| D-1 | Radial Locations of Useful Gas Concentration Data | 148 |




(The reverse of this page is blank.)

# SECTION I

# INTRODUCTION

## A. OBJECTIVE

The U.S. Air Force (USAF) is updating its atmospheric dispersion modeling capability. Several models are being considered as possible replacements for the operational dispersion model being used to predict toxic corridors resulting from an accidental spill or release of toxic gases. Of particular interest is the dispersion of heavier-than-air gases because several gases of concern to the USAF take on heavier-than-air characteristics when released to the atmosphere (nitrogen tetroxide, for example). This report summarizes the results from selected field-scale, heavy gas dispersion tests, which can be used to validate atmospheric dispersion models.

## B. BACKGROUND

The USAF focus on the dispersion of heavier-than-air gases reflects the state of the art in atmospheric dispersion modeling. Results of trace gas dispersion experiments have been analyzed extensively to characterize atmospheric dispersion quantitatively under various conditions. One such study, by the Air Resources Atmospheric Turbulence and Diffusion Laboratory, resulted in the well-known Briggs Gaussian plume parameters for the dispersion of a trace pollutant over open country. The amount of experimentation and analysis for heavy gas releases is considerably less than for trace gas releases. However, several well-instrumented, heavy-gas dispersion tests have been conducted over the past ten years. The major test series were those performed by Lawrence Livermore National Laboratory (LLNL), Shell Research Ltd., and the British Health and Safety Executive (HSE).

LLNL has conducted field-scale tests of dense-gas dispersion under a variety of sponsors. We performed liquefied natural gas (LNG) tests for the U.S. Department of Energy in 1978 (the Avocet series) and 1980 (the Burro series), and again in 1981 (the Coyote series) with additional sponsorship by the Gas Research Institute. Altogether, 22 LNG field-scale spill tests were performed in the three test series. The Avocet series was performed mainly for instrumentation evaluation; the Burro series (References 1-3) investigated heavy-gas dispersion; and the Coyote series (References 3, 4) studied rapid-phase change and combustion phenomena as well as heavy-gas dispersion. In 1983, LLNL performed four ammonia dispersion tests (References 5, 6) for the U.S. Coast Guard and the Fertilizer Institute and performed six nitrogen tetroxide spill experiments (References 6-8) for the USAF. Six hydrogen fluoride dispersion and mitigation tests were performed in 1986; however, the results from these tests are not available as yet. All of the LLNL tests involved continuous, finite duration releases, some as a relatively quiescent evaporating pool formed from a liquid release onto the ground or a small water pond and some as a high-speed horizontal momentum jet formed from a pressurized pipe release. In 1980, Shell Research performed 34 spill tests (References 9-12) using LNG and refrigerated liquid propane (LPG) to study the dispersion and combustion of releases of dense flammable gases. Both continuous, finite duration releases and instantaneous liquid releases were performed onto the sea with the subsequent dispersion also occurring over the sea. The HSE field tests (References 13-16), performed in 1982 and 1983, were designed to study the dispersion of instantaneous, fixed volume releases of heavy gas (freon-air mixtures), but were extended to include three tests on steady, continuous releases.

Of these tests, 26 were chosen as benchmark tests, and their results are summarized in Appendices A-E. By mutual agreement with the sponsor, only the continuous, finite duration releases and the momentum jet releases were considered for the test summaries because they better represent typical accidental releases from a storage vessel or a transportation vehicle. The test summaries describe the manner of release, the ambient meteorological

conditions, and the resulting vapor cloud characteristics, including peak concentration, average centerline concentration, and average height and width of the cloud, all as functions of downwind distance.

This choice of cloud characteristics was based primarily on perceived USAF needs and capabilities for model validation and on the nature of heavier-than-air dispersion in the atmosphere. Atmosphere dispersion models for use by the USAF must run on minicomputers in times of a few minutes. This generally restricts the numerical complexity of the models to ones that require numerical integration in only one dimension, usually downwind distance or time. Consequently, these models use similarity profiles to describe the concentration distribution (and other properties) in the crosswind plane. Since crosswind profiles are readily changed, they did not appear to be as important in testing the model as the variation in centerline characteristics with downwind distance. However, heavy gases tend to change the shape of dispersing vapor clouds, making them lower and wider than equivalent trace gas vapor clouds. Consequently, a measure of cloud height and width was considered to be important in attempting to evaluate the performance of denser-than-air dispersion models.

The ability of a model to simulate the dispersion of a particular release is strongly dependent upon the degree to which the meteorological conditions are known. Several methods that are commonly used to characterize the ambient meteorological conditions are described in this report. These methods fall into two main categories: stability classification schemes and atmospheric surface-layer theory. Both use varying amounts of ambient wind velocity data, temperature data, and other measurements. The approach proposed in this report is based on surface-layer theory; it requires mean wind velocity and temperature gradient information, and includes a method for converting to and from the stability classification approach.

## C. SCOPE

In this report, we describe the methods used to characterize the ambient meteorological conditions and the uncertainty associated with such parameters. We also discuss the various methods used to describe a dense-gas cloud as it disperses in the atmosphere, the reasons for using a variety of cloud parameters (in addition to cloud concentration) when dense-gas dispersion phenomena are occurring, and the parameters we selected to describe the characteristics of the cloud resulting from a continuous denser-than-air vapor release. Finally, we present the test summaries, including a brief description of the series from which the selected tests were chosen and extensive notes on how the cloud characteristics were obtained.

## SECTION II

## METHODS FOR DESCRIBING THE AMBIENT METEOROLOGICAL CONDITIONS

In atmospheric dispersion models, numerous input parameters are used to describe the ambient meteorological conditions and simulate cloud dispersion. The most common meteorological data are windspeed and air temperature, often given at several heights. Additional data and inferred quantities include surface roughness, friction velocity, Richardson number, vertical flux of sensible heat, Monin-Obukhov length scale, height of the mixing layer, Deardorff convective velocity, and variances of the wind velocity components. These quantities are used to describe the two main transport properties in the atmosphere: wind convection and turbulent mixing. Wind convection is generally defined by either a constant windspeed or windspeed as a function of height; some complex dispersion models use a temporal and spatially varying wind field. Turbulent mixing of the vapor release with the ambient atmosphere is generally characterized by either an atmospheric stability classification, such as the method proposed by Pasquill, or by an atmospheric stability parameter, such as the Monin-Obukhov length.

Several classification methods have been proposed to determine the level of atmospheric stability based on common meteorological measurements. In each method, the stability is classified into one of six or seven levels. In simpler models, the dispersion coefficients $\sigma_y$ and $\sigma_z$ are determined empirically and used to estimate the rate of dispersion of the mixing cloud as it is transported downwind. More complex models characterize atmospheric dispersion by either a diffusion coefficient or an entrainment rate that is based on theoretical considerations such as surface-layer theory for the atmosphere. For these models, the turbulence parameter is a function of several meteorological parameters such as friction velocity, surface roughness, and Monin-Obukhov length, which are in turn determined from basic meteorological measurements.

In this section, we describe the two main approaches for describing atmospheric stability as well as a method for unifying the two approaches. Then we present several methods for computing the meteorological parameters required for our models. We also discuss the uncertainty that can be expected when classifing atmospheric stability in this manner.

## A. ATMOSPHERIC STABILITY

### 1. Stability Classification Schemes

Probably the most widely used classification scheme is based on the methods proposed by Pasquill (17). Pasquill presented information on the lateral spreading, $\theta$, and vertical spreading, h, of diffusing plumes as functions of six atmospheric stability classes, designated A to F. Class A corresponds to extremely unstable conditions and Class F to stable conditions. The quantities $\theta$ and h are the 10% points of the plume concentration distributions relative to its mean centerline value. The applicable stability category relates these quantities to observed windspeed, cloud cover, and insolation conditions, as shown in Table 1.

Gifford (Reference 18) converted Pasquill's plume spreading data into curves of the standard deviations, $\sigma_y$ and $\sigma_z$, for the plume concentration distributions (Figure 1). Gifford chose the standard deviation because it is a commonly used statistic and it emphasizes that the method could be readily used with a Gaussian plume formula. Pasquill's scheme is usually used in the form of these or similar graphs of $\sigma_y$ and $\sigma_z$, frequently called the Pasquill-Gifford curves.

Other stability classification schemes have been introduced. For example, Turner (References 19, 20, 21) published a version in which the incoming solar radiation is classified in terms of elevation angle and cloud amount and height. His expressions for $\sigma_y$ and $\sigma_z$ are functions of travel time, and he includes seven stability curves that are labeled from 1 (for extreme instability) to 7 (for extreme stability). Other schemes include

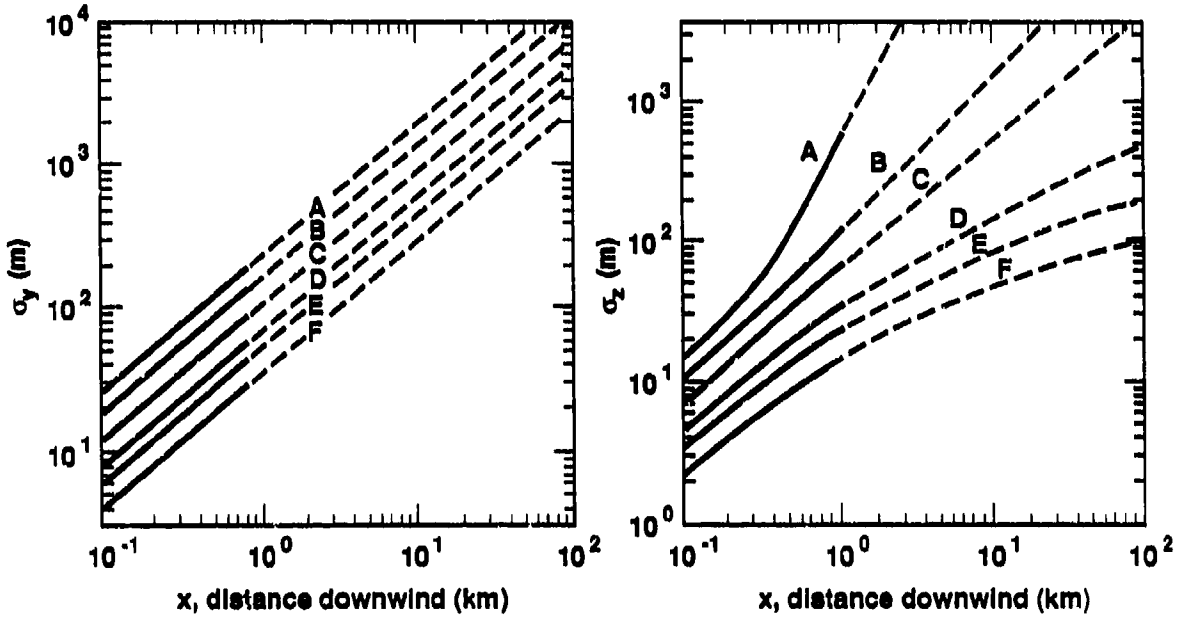


Figure 1. Curves of $\sigma_y$ and $\sigma_z$ for Pasquill's Turbulence Types (Reference 17).

MB-002-U-0692-001

TABLE 1. METEOROLOGICAL CONDITIONS DEFINING PASQUILL TURBULENCE TYPES.

| | |
|---|---|
| A: Extremely unstable conditions | D: Neutral conditions[a] |
| B: Moderately unstable conditions | E: Slightly stable conditions |
| C: Slightly unstable conditions | F: Moderately stable conditions |

| Surface wind-speed (m/s) | Daytime insolation | | | Nighttime conditions | |
|---|---|---|---|---|---|
| | Strong | Moderate | Slight | Thin overcast or ≥4/8 cloudiness[b] | ≤3/8 cloudiness |
| <2 | A | A-B | B | | |
| 2 | A-B | B | C | E | F |
| 4 | B | B-C | C | D | E |
| 6 | C | C-D | D | D | D |
| >6 | C | D | D | D | D |

[a]Applicable to heavy overcast day or night.
[b]The degree of cloudiness is defined as that fraction of the sky above the local apparent horizon that is covered by clouds.

those by Klug (Reference 22), Cramer (References 23, 24), and Carpenter (Reference 25). For a more complete review, see Gifford (Reference 26), and Pasquill and Smith (Reference 27).

Pasquill's concept of characterizing the stability of the ambient atmosphere by six or seven stability classes has been widely accepted. In addition to his original scheme for determining the stability class (Table 1), a number of other methods have been proposed. One common approach presented (Reference 28) is to classify stability class by relating it to measured values of the standard deviation of the horizontal wind direction $\sigma_\theta$ (Table 2). Other schemes for determining the stability class are given later in this report in a study of the uncertainty in stability category as determined by these various methods.

Other studies have tried to improve the $\sigma_y$ and $\sigma_z$ curves that correspond to each stability class. For example, Smith (Reference 29) provided estimates based on several numerical solutions of the two-dimensional

TABLE 2. STABILITY CATEGORIES AS A FUNCTION OF $\sigma_\theta$

| Stability Category | $\sigma_\theta$ |
|---|---|
| A, extremely unstable | 25.0° |
| B, moderately unstable | 20.0° |
| C, slightly unstable | 15.0° |
| D, neutral | 10.0° |
| E, slightly stable | 5.0° |
| F, moderately stable | 2.5° |

Source: Slade (Reference 28)

diffusion equation using empirically derived values for the vertical profile of the diffusivity. Smith's revision includes surface roughness $Z_0$ and thermal stratification. Table 3 gives a simple approximation to Smith's $\sigma_z(x)$ for $0.1 \leq x \leq 10.0$ km.

Briggs (Reference 30) revised the Pasquill-Gifford $\sigma_y$ and $\sigma_z$ estimates specifically for elevated releases. The Briggs formulae are presented in terms of algebraic equations as a function of stability category and downwind distance (Table 4). Briggs used two sets of curves: one for open country and one for urban areas. The open country values apply to a surface roughness of approximately 10 cm.

These systems predict the ambient conditions in two steps. First, they classify the ambient meteorological conditions into one of six or seven stability categories using routine measurements such as cloud cover, standard deviation in horizontal wind direction, average wind velocity, and temperature gradient. Second, they estimate dispersion parameters $\sigma_y$ and $\sigma_z$, which are functions of the downwind distance and correspond to the respective stability categories. These dispersion curves can then be used in Gaussian plume or similar models to predict concentration as a function of downwind distance from the source.

TABLE 3. SMITH'S POWER-LAW APPROXIMATIONS $\sigma_z = ax^s$.[a]

| Stability category ↓ | $z_0$ → | Coefficient a | | | Index s | | |
|---|---|---|---|---|---|---|---|
| | | 1 cm | 10 cm | 1 m | 1 cm | 10 cm | 1 m |
| A | 0.102 | 0.140 | 0.190 | 0.94 | 0.90 | 0.83 | |
| B | 0.062 | 0.080 | 0.110 | 0.89 | 0.85 | 0.77 | |
| C | 0.043 | 0.056 | 0.077 | 0.85 | 0.80 | 0.72 | |
| D | 0.029 | 0.038 | 0,050 | 0.81 | 0.76 | 0.68 | |
| E | 0.017 | 0.023 | 0.031 | 0.78 | 0.73 | p.65 | |
| F | 0.009 | 0.012 | 0.017 | 0.72 | 0.67 | 0.58 | |

Source: Smith (Reference 29).

[a]The form $\sigma_z = ax^s$ was fitted at $x = 0.3$ and 3 to estimates from nomograms. These estimates lie on log-log plots that are concave to the log x axis; with respect to these curves, the power-law fittings generally underestimate $\sigma_z$ at $x = 1$ km by about 5 % and overestimate $\sigma_z$ at $x = 0.1$ or 10 km by about 10 %. The error in this representation of the nomogram increases rapidly beyond $x = 10$ km.

TABLE 4. BRIGG'S $\sigma_y(x)$ AND $\sigma_z(x)$ FORMULAE FOR ELEVATED SMALL RELEASES, $0.1 \leq x \leq 10$ KM.

| | Stability category | $\sigma_y$ | $\sigma_z$ |
|---|---|---|---|
| Open country | A | $0.22x(1 + 0.1x)^{-1/2}$ | $0.20x$ |
| | B | $0.16x(1 + 0.1x)^{-1/2}$ | $0.12x$ |
| | C | $0.11x(1 + 0.1x)^{-1/2}$ | $0.08x(1 + 0.2x)^{-1/2}$ |
| | D | $0.08x(1 + 0.1x)^{-1/2}$ | $0.06x(1 + 1.5x)^{-1/2}$ |
| | E | $0.06x(1 + 0.1x)^{-1/2}$ | $0.03x(1 + 0.3x)^{-1}$ |
| | F | $0.04x(1 + 0.1x)^{-1/2}$ | $0.016x(1 + 0.3x)^{-1}$ |
| Urban areas | A-B | $0.32x(1 + 0.4x)^{-1/2}$ | $0.24x(1 + 0.1x)^{-1/2}$ |
| | C | $0.22x(1 + 0.4x)^{-1/2}$ | $0.20x$ |
| | D | $0.16x(1 + 0.4x)^{-1/2}$ | $0.14x(1 + 0.3x)^{-1/2}$ |
| | E-F | $0.11x(1 + 0.4x)^{-1/2}$ | $0.08x(1 + 0.15x)^{-1/2}$ |

## 2. Surface-Layer Similarity Theory

The surface layer is usually defined as the lowest 10-20 m of the atmosphere boundary layer where the fluxes of momentum and heat may be considered to be constant. This layer has two important sources of turbulent energy. The first source arises from the instability of the windspeed gradients, which are caused by the mechanical drag of the underlying surface. The second source (or sink) is generated by buoyancy forces arising mainly from the input (or withdrawal) of sensible heat into the air at the ground. More detailed discussions of the theoretical treatment of the surface layer are given in Pasquill and Smith (Reference 27), Businger (Reference 31), Priestly (Reference 32), Lumley and Panofsky (Reference 33), and Monin and Yaglom (Reference 34). This theory, which combines theoretical considerations and empirical findings, is based on the widely accepted similarity arguments of Monin and Obukhov.

The basic identify in this approach is obtained by assuming that the vertical turbulence flux, taken to be constant, is proportional to the product of an eddy diffusion coefficient K and the vertical gradient of the transported property S. (Here S is either the horizontal mean velocity U or the sensible heat $\rho c_p \theta$, where $\theta$ is the potential temperature.) Thus,

$$\frac{\text{Flux of } S}{\rho} = -\overline{S' \cdot W'} = K \cdot (\partial S / \partial Z) = \text{constant} \quad , \tag{1}$$

where $\rho$ is the atmospheric density; S' is the random part of the property $S = \overline{S} + S'$; W' is the random part of the vertical velocity $W = \overline{W} + W'$; and Z is height. Introducing the friction velocity $U_*$ and the scaling potential temperature $\theta_*$, both assumed to be constant within the surface layer, the corresponding relations for the vertical fluxes of momentum and heat are

$$K_m \cdot (\partial U / \partial Z) = U_*^2 \quad ; \tag{2a}$$

$$K_h \cdot (\partial\theta/\partial Z) = \theta_* U_* \quad . \tag{2b}$$

To determine the diffusivities and the velocity and potential temperature profiles, additional assumptions must be made. A fundamental assumption is that each quantity can be determined by the parameters $Z$, $\rho$, $g/\theta_o$, $U_*$, and $\theta_*$, where $g$ is the acceleration of gravity, $\theta_o$ is the potential temperature at the height $Z_o$, and $Z_o$, called the surface roughness, is the height where the horizontal velocity is zero. Using the mixing length model of Prandtl (Reference 35) or simply by dimensional analysis, the eddy diffusion coefficients are assumed to have the form:

$$K_m = k \cdot U_* \cdot Z / \phi_m(Z/L) \quad , \tag{3a}$$

$$K_h = k \cdot U_* \cdot Z / \phi_h(Z/L) \quad , \tag{3b}$$

where $k = 0.41$ is the von Karman constant; $\phi$ is a Monin-Obukhov similarity profile function used to describe the atmospheric stability and is equal to 1 under neutral conditions ($\theta_* = 0$); and $L$ is the Monin-Obukhov length, which is a measure of atmospheric stability.

With this definition of the eddy diffusivities and the constant flux relationship, the velocity and heat gradients become

$$\frac{\partial U}{\partial Z} = \frac{U_* \cdot \phi_m(Z/L)}{k \cdot Z} \quad , \tag{4a}$$

$$\frac{\partial \theta}{\partial Z} = \frac{\theta_* \cdot \phi_h(Z/L)}{k \cdot Z} \quad . \tag{4b}$$

Integrating these equations yields the following mean horizontal velocity and potential temperature:

$$U(Z) = (U_*/k) \cdot [\ln(Z/Z_o) - \psi_m(Z/L)] \quad , \tag{5a}$$

$$\theta(Z) = \theta_o + (\theta_*/k)\cdot[\ln(Z/Z_o) - \psi_h(Z/L)] \quad , \tag{5b}$$

$$\partial\psi/\partial Z = [1 - \phi(Z/L)]/Z \quad . \tag{5c}$$

Under neutral conditions, $\psi = 0$ and the well-known logarithmic profiles are obtained.

In the absence of a theoretical derivation, the forms of the Monin-Obukhov similarity functions $\phi(Z/L)$, and consequently $\psi(Z/L)$, must be specified empirically. The vertical fluxes of heat and momentum have been measured in several field studies aimed at more firmly establishing the behavior of the Monin-Obukhov functions. These studies showed discrepancies that remain unresolved; possible sources of the discrepancies include experimental error, nonconformity to ideal fetch and exposure, and inadequacy of sampling duration.

In a review of these studies, Yaglom (Reference 36) provided a comprehensive table and graphical summary of the various analytic forms of $\phi(Z/L)$ proposed to represent the average trend indicated by particular sets of data. According to this review, if we assume $k = 0.4$, then $\phi_m(o)$ ranges from 0.93 to 1.14. Therefore, k can range from 0.43 to 0.35 if $\phi_m(o) = 1.00$. Correspondingly, $\phi_h(o)$ can range from 0.84 to 0.98. Pasquill and Smith (Reference 27) noted that for many purposes these uncertainties may be unimportant; unfortunately, in nonneutral conditions they become considerably wider, for example, reaching a factor of 1.5 for $\phi_h$ in unstable conditions and a factor of about 3 for $\phi_m$ in stable conditions. Consequently, there are corresponding uncertainties in the eddy diffusion coefficients defined in Equations (3a) and (3b).

In our study, we used the similarity functions presented by Dyer (Reference 37). For the stable region where $L \geq 0$, these functions are

$$\varphi_m(Z/L) = \phi_h(Z/L) = 1 + 5 \cdot Z/L \quad ,$$

$$\psi_m(Z/L) = \psi_h(Z/L) = -5 \cdot Z/L \quad . \tag{6a}$$

For the unstable region where $L < 0$, they are

$$\phi_m(Z/L) = 1/x \quad ,$$

$$\psi_m(Z/L) = 2 \cdot \ln[(1 + x)/2] + \ln[(1 + x^2)/2] - 2 \cdot \tan^{-1}(x) + \pi/2 \quad ,$$

$$\phi_h(Z/L) = 1/x^2 \quad , \tag{6b}$$

$$\psi_h(Z/L) = 2 \cdot \ln[(1 + x^2)/2] \quad ,$$

where $x = (1 - 16 \cdot Z/L)^{1/4}$ .

The parameters $U_*$, $\theta_*$, $\theta_o$, and L are all related by the definition of the Monin-Obukhov length given by:

$$L = U_*^2 \cdot \theta_o / g \cdot k \cdot \theta_* \quad , \tag{7}$$

where K, the von Karman constant 0.41, and g, the acceleration of gravity = 9.81 $m/s^2$. When considering stability, we often use the inverse Monin-Obukhov length $L^{-1}$ rather than L because $L^{-1}$ is proportional to $\theta_*$. Under neutral conditions ($\theta_* = 0$), $L^{-1} = 0$; under stable conditions; $L^{-1} > 0$; and under unstable conditions $L^{-1} < 0$.

The potential temperature and the actual temperatures are related by the definition:

$$\theta = T \cdot (P_o/P)^{\kappa} \quad , \tag{8a}$$

where $T$ = ambient temperature (K)
$P$ = ambient pressure
$P_0$ = standard pressure = 1000 mb
$\kappa = R/C_p = 0.285$
$R$ = gas constant for air = 287 J/kg-K
$C_p$ = specific heat of air = 1006 J/kg-K .

If we differentiate Equation (8a) and use the hydrostatic approximation, $\partial P = -g \cdot \rho \cdot \partial Z$, and the ideal gas law, $P = \rho \cdot R \cdot T$, we obtain:

$$\partial\theta = (\theta/T) \cdot (\partial T + \gamma \cdot \partial Z) \quad , \tag{8b}$$

where $\gamma = g/C_p = 0.00975$ K/m.

If $\theta/T$ is essentially constant for the height range of interest, we can integrate Equation (8b) with respect to height to obtain the potential temperature as a function of temperature and height:

$$\theta = (P_0/P_r)^{\kappa} \cdot [T + \gamma \cdot (Z - Z_r)] \quad . \tag{8c}$$

Here, subscript $r$ denotes reference value. Equation (8c) was used in this study to calculate the potential temperature from the temperature data.

Another measure that is often used to characterize stability within the surface layer is the Richardson number, which is defined and calculated from the Monin-Obukhov similarity functions as follows:

$$Ri(Z/L) = (g/\theta_0) \cdot (\partial\theta/\partial Z)/(\partial U/\partial Z)^2 = (Z/L) \cdot \phi_h(Z/L)/\phi_m^2(Z/L) \quad . \tag{9a}$$

If Equation (8b) is substituted into Equation (9a) and we assume that $\theta/T$ is essentially constant for the height range of interest, then the Richardson number can be expressed in terms of the temperature and temperature gradient. This manner of expressing the Richardson number, namely

$$Ri(Z/L) = (g/T_o)\cdot(\partial T/\partial Z + \gamma)/(\partial U/\partial Z)^2 \quad , \qquad (9b)$$

is used widely in the published literature.

3. A Unifying Approach

Gifford (Reference 26) reviewed several attempts to relate empirical stability categories (such as those by Pasquill) to boundary-layer turbulence criteria. The various turbulence criteria that have been considered include turbulence intensity, lapse rate, Richardson number, and Monin-Obukhov length. In addition, such properties as surface roughness, which varies from site to site, have been considered, although they are not specifically allowed for in simple stability classification schemes. These approaches have met with varying degrees of success and acceptance, and a summary of Gifford's work is presented here.

Studies by Luna and Church (References 38, 39), Goldner (Reference 40), and others show that qualitative stability categories correspond generally to direct measurements of boundary-layer turbulence intensity but that scatter is considerable. The correspondence with lapse rate (for example, see Carpenter, Reference 25) has been attempted; however, it has also proven to be an uncertain discriminator, partly because lapse rate varies with height. Material dispersing from surface sources experiences a much wider range of lapse rate conditions compared to those experienced by elevated emissions.

Using the Richardson number as defined previously, Islitzer (Reference 41) gave Richardson numbers for the Pasquill types ranging from -0.26 for type A to 0.046 for type F. The values were calculated from micrometeorological profile data measured on a 45-meter mast at the Idaho National Engineering Laboratory. The Richardson number contains the required information, but it varies with height in the steady-state boundary layer--although not as rapidly as lapse rate near the ground surface.

A more useful index of the state of the boundary-layer turbulence is the Monin-Obukhov length, also defined previously. Generally, the Monin-Obukhov length and the parameters used to define it can be assumed to be constant or to vary only slowly in a steady-state boundary layer. Gifford (Reference 42) estimated order-of-magnitude relations between stability class and Monin-Obukhov length ranging from $\pm 10^3$ m for near-neutral conditions to +10 m for very stable and -10 m for very unstable conditions. These values were chosen arbitrarily, based on qualitative indications provided by studies of boundary-layer wind profiles in conditions of varying stability. Pasquill and Smith (Reference 43), guided by detailed atmospheric diffusion experiments with accompanying micrometeorological profile data, provided more refined estimates, specifically tailored to the Pasquill stability categories, for flow over a fairly smooth surface (short grass, $Z_0$ = 1 cm).

A more general approach, and the one used in this study to relate Pasquill stability class to the turbulence parameters of the surface layer, is that proposed by Golder (Reference 40). Using five detailed micrometeorological data sets, Golder calculated Monin-Obukhov lengths and Pasquill stability classes, and derived a relationship between these two and the surface roughness (Figure 2). Gifford noted that in principle, this method should provide stability class estimates exhibiting less scatter than the lapse-rate method because it accounts for variations in thermal and mechanical turbulence parameters from site to site.

## B. COMPUTATION OF METEOROLOGICAL PARAMETERS

### 1. Review of Methods

The mean horizontal velocity and potential temperature as previously derived are given by:

$$U(Z) = (U_*/k)\cdot[\ln(Z/Z_0) - \psi_m(Z/L)] \quad ,$$

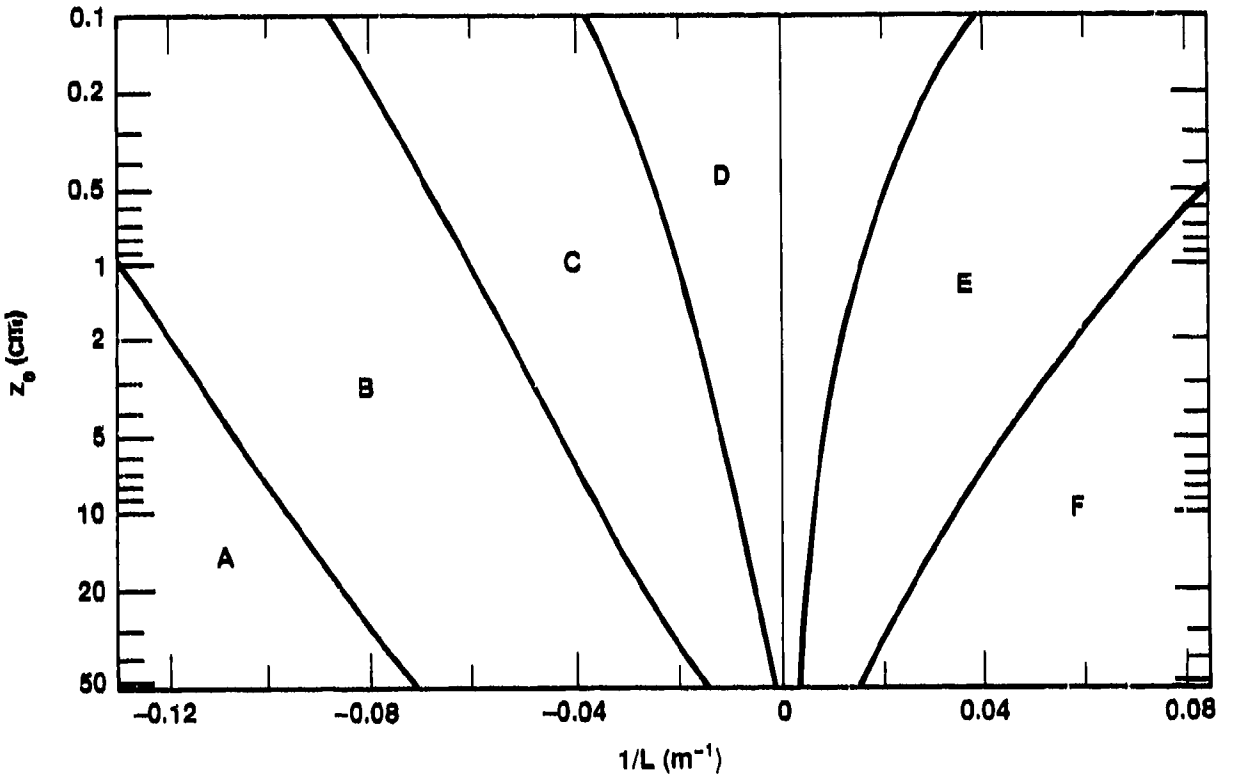


Figure 2. Curves by Golder (Reference 40) Showing Pasquill's Stability Classes as a Function of the Monin-Obukhov Length and the Surface Roughness Length

$$\theta(Z) = \theta_o + (\theta_*/k)\cdot[\ln(Z/Z_o) - \psi_h(Z/L)] \quad ,$$

where $L^{-1} = g\cdot k\cdot\theta_*/\theta_o\cdot U_*^2$, and $\psi_m(Z/L)$ and $\psi_h(Z/L)$ are defined in Equation (6b)--although only their dependence on the Monin-Obukhov length L is important here and not the specific form of the equations. Thus, five meteorological paramenters are of interest in defining these profiles: $Z_o$, $U_*$, $\theta_*$, $\theta_o$, and L. Since L is defined in terms of the other parameters, we have only four independent parameters. While the choice of the four independent parameters is arbitrary, it is usually dictated by the available meteorological data and the method chosen for fitting the profiles to the data. Here, we choose $Z_o$, $U_*$, $\theta_*$, and $\theta_o$ as the four independent meteorological parameters. Consequently, both U(Z) and $\theta$(Z) are functions of all four independent variables; that is

$$U(Z) = U(Z, Z_o, U_*, \theta_*, \theta_o) \quad ,$$

$$\theta(Z) = \theta(Z, Z_o, U_*, \theta_*, \theta_o) \quad .$$

Surface roughness $Z_o$ is generally estimated in one of two ways. The first method, and usually the more reliable, is to extrapolate measured velocity profile data (i.e., $U(Z_{i_1})$, $i_1 = 1,N$) under neutral stability conditions back to where U(Z) = 0. This can be done by either a least-squares fit to determine $U_*$ and $Z_o$ or by plotting the data on a semilog plot and linearly extrapolating until U(Z) = 0. Similarly, measured values of $U_*$ and U(Z) under neutral conditions can be used to estimate $Z_o$ if they are available. The second method uses values of $Z_o$ that have been empirically determined for various ground surface conditions, such as those listed in Table 5. From Meteorology and Atomic Energy, 1968 (Reference 44), with either method, the value of $Z_o$ that is obtained is assumed to be a function of the location and therefore is taken to be constant despite variations in the other meteorological parameters. However, these estimates of $Z_o$ are not very accurate because of the logarithmic dependence of the wind profile on $Z_o$. In

addition, $Z_0$ depends on the value chosen for the von Karman constant k. Although a value of k = 0.4 is commonly used, values suggested in the literature range from 0.35 to 0.43. Here, we use k = 0.41.

TABLE 5. TYPICAL VALUES OF SURFACE ROUGHNESS

| Type of surface | Surface roughness, $Z_0$ (cm) |
|---|---|
| Smooth mud flats; ice | 0.001 |
| Smooth snow | 0.005 |
| Smooth sea | 0.02 |
| Level desert | 0.03 |
| Snow surface; lawn to 1 cm high | 0.1 |
| Lawn, grass to 5 cm | 1-2 |
| Lawn, grass to 60 cm | 4-9 |
| Fully grown root crops | 14 |

In practice, the value of $\theta$, expressed in absolute degrees (i.e., K), does not vary much from the value of $\theta_0$. Consequently, a reasonable estimate of $\theta_0$ can be made from the average potential temperature data (i.e., $\theta_0 \approx \bar{\theta}$) and used to define the Monin-Obukhov length L. If the potential temperature is expressed as a difference

$$d(Z) = \theta(Z) - \theta(Z_1) \quad ,$$

where $Z_1$ is a reference height, then the zero level potential temperature $\theta_0$ is eliminated from the equations for U(Z) and d(Z). Thus, only two independent variables, $U_*$ and $\theta_*$ must be determined. (If the value for the potential temperature $\theta$ is desired, a more accurate value of $\theta_0$ can be calculated by a fit to the potential temperature data once $U_*$ and $\theta_*$ have been determined from the velocity $U_1$ and the potential temperature difference $d_1$ data.)

Several methods have been proposed for determining $U_*$ and $\theta_*$ (often expressed as $T_*$), most involving some type of least-squares fit. Krüermeyer (Reference 45) fit the measured profiles to a specified function of height. Then he found the surface-layer parameters by comparing the differential of this function with the empirical relation for the gradients. The disadvantage to this approach is that the approximation of the profile gradients is relatively inaccurate. Klug (Reference 46) used a method by which the surface-layer parameters are found from a least-squares fit of only the wind profile data to a wind profile relation. Consequently, temperature information is neglected. Paulson (Reference 47) used both the wind and temperature profiles to estimate the surface-layer parameters. In this method, the estimate of $U_*$ is primarily derived from the wind profile and the estimate of $T_*$ ($\theta_*$) from the temperature data.

A general least-squares approach, proposed by Nieuwstadt (Reference 48), uses the velocity and temperature data simultaneously to estimate $U_*$ and $\theta_*$. This method starts by defining two square difference functions:

$$E_1 = \sum_{i=1}^{N_1} [U_i - U(Z_i)]^2 \quad ;$$

$$E_2 = \sum_{i=2}^{N_2} [d_i - d(Z_i)]^2 \quad ;$$

where

$U_i$ = the measured velocity at height $Z_i$,

$d_i$ = $\theta_i - \theta_1$ = the difference between the measured potential temperature at heights $Z_i$ and $Z_1$,

$U(Z_i)$ = the value of the velocity profile function at height $Z_i$,

$d(Z_i)$ = the potential temperature difference function at height $Z_i$,

$N_1$ = the number of velocity measurement heights,

$N_2$ = the number of potential temperature measurement heights.

Therefore, both $E_1$ and $E_2$ are functions of the meteorological parameters $U_*$ and $\theta_*$. (In keeping with our previous arguments, we assumed that $Z_o$ and $\theta_o$ have been determined for the purpose of evaluating L.) The two functions are then combined in a weighted average as follows:

$$E(U_*, \theta_*) = E_1/\Delta U^2 + E^2/'\theta^2 \quad ,$$

where $\Delta U$ and $\Delta\theta$ are the measuring errors, respectively, in $U_i$ and $\theta_i$.

The parameters $U_*$ and $\theta_*$ are then found by minimizing $E(U_*, \theta_*)$. This is done by setting the derivative of E with respect to $U_*$ and $\theta_*$ equal to zero. Thus, $\partial E/\partial U_* = 0$, and $\partial E/\partial\theta_* = 0$. This produces two coupled nonlinear equations, which can be solved using iterative methods to determine $U_*$ and $\theta_*$.

The weighting factors used to define $E(U_*, \theta_*)$ are based on the assumption that the difference between the measurements and the profile functions is caused only by random measurement errors. Furthermore, these errors are assumed to be independent of the measurement height and the errors in the velocity and temperature measurements are uncorrelated. In practice, other errors can be significant and are often difficult to estimate. For example, the measured average quantity may not be a good estimate of the average steady-state condition because the averaging time is too short. Also, this theory (profile functions) does not an exactly represent reality--the "true" average velocity and temperature.

Such nonmeasurement errors limit the use of the approach as given above. Namely, all nonrandom measurement errors must be insignificant compared to the random measurement errors. Since nonmeasurement errors, as well as measurement errors for the field experiments of concern, may be difficult to estimate accurately, we recommend an alternative least-squares fit approach that does not depend on estimates of the errors between the measurements and the profile functions.

## 2. Proposed Approach

In the method presented here, the value of the surface roughness $Z_o$ is obtained by one of the methods given previously and is taken to be constant for any given series of field tests. The remaining three meteorological parameters, $U_*$, $\theta_*$, and $\theta_o$, are simultaneously determined by a least-squares fit using both the velocity and the temperature data.

For the remainder of this section, the following notation will be used to describe the data:

$$U_i = \text{measured velocity at height } Z_i \ (i = 1, N_1) \ ,$$
$$T_i = \text{measured temperature at height } Z_i \ (i = 1, N_2) \ ,$$
$$\theta_i = (P_o/P_r)^{\kappa} \cdot [T_i + \gamma(Z_i - Z_r)] = \text{potential temperature} \ ,$$

where $P_r$ = pressure at height $Z_r$ ,
$P_o$ = standard pressure = 1000 mb ,
$\kappa = R/C_p = 0.285$ ,
$\gamma = g/C_p = 0.00975$ ,

and $d_i = \theta_i - \theta_1$ = potential temperature difference (sub 1 → $Z_1$).

The velocity and potential temperature profiles are expressed here in a slightly different form so that the identities $U(Z_o) = 0$ and $\theta(Z_o) = \theta_o$ rigorously hold at $Z = Z_o$. With this slight modification:

$$U(Z_i) = (U_*/k) \cdot [\ln(Z_i/Z_o) - \psi_m(Z_i/L) + \psi_m(Z_o/L)] \ ,$$

$$\theta(Z_i) = \theta_o + (\theta_*/k) \cdot [\ln(Z_i/Z_o) - \psi_h(Z_i/L) + \psi_h(Z_o/L)] \ , \qquad (10)$$

$$d(Z_i) = \theta(Z_i) - \theta(Z_1) = (\theta_*/k) \cdot [\ln(Z_i/Z_1) - \psi_h(Z_i/L) + \psi_h(Z_1/L)] \ .$$

where $\psi_m$ and $\psi_h$ are as given in Equations (6a) and (6b).

With this notation for the data and these definitions of the profile functions, three square difference functions can be defined:

$$E_1(U_*, \theta_*, \theta_o) = \sum_{i=1}^{N_1} [U_i - U(Z_i)]^2 \quad ,$$

$$E_2(U_*, \theta_*, \theta_o) = \sum_{i=2}^{N_2} [d_i - d(Z_i)]^2 \quad , \tag{11}$$

$$E_3(U_*, \theta_*, \theta_o) = \sum_{i=1}^{N_2} [\theta_i - \theta(Z_i)]^2 \quad .$$

These functions are minimized by simultaneously minimizing $E_1$ with respect to $U_*$, $E_2$ with respect to $\theta_*$, and $E_3$ with respect to $\theta_o$. This is done by taking the appropriate derivatives and setting them equal to zero as follows:

$$\frac{\partial E_1}{\partial U_*} = 0; \quad \frac{\partial E_2}{\partial \theta_*} = 0; \quad \frac{\partial E_3}{\partial \theta_o} = 0 \quad . \tag{12}$$

With some mathematical manipulation, these equations can be rearranged to yield equations for $U_*$, $\theta_*$, and $\theta_o$, respectively. With the definition for $L^{-1}$, they are

$$U_* = k \cdot \left[ \sum_{i=1}^{N_1} U_i \cdot F_2(Z_i, L) \right] \Big/ \left[ \sum_{i=1}^{N_1} F_1(Z_i, L) \cdot F_2(Z_i, L) \right] ,$$

$$\theta_* = k \cdot \left[ \sum_{i=2}^{N_2} d_i \cdot G_2(Z_i, L) \right] \Big/ \left[ \sum_{i=2}^{N_2} G_1(Z_i, L) \cdot G_2(Z_i, L) \right] , \qquad (13)$$

$$\theta_o = \left\{ \sum_{i=1}^{N_2} H_2(Z_i, L) \cdot \left[ \theta_i - (\theta_*/k) \cdot H_1(Z_i, L) \right] \right\} \Big/ \sum_{i=1}^{N_2} H_2(Z_i, L) ,$$

$$L^{-1} = g \cdot k \cdot \theta_* / U_*^2 \cdot \theta_o ,$$

where the functions F, G, and H are

$$F_1(Z_i, L) = \ln(Z_i/Z_o) - \psi_m(Z_i/L) + \psi_m(Z_o/L) ,$$

$$F_2(Z_i, L) = F_1(Z_i, L) + \phi_m(Z_i/L) - \phi_m(Z_o/L) ,$$

$$G_1(Z_i, L) = \ln(Z_i/Z_1) - \psi_h(Z_i/L) + \psi_h(Z_1/L) ,$$

$$G_2(Z_i, L) = G_1(Z_i, L) + \phi_h(Z_i, L) - \phi_h(Z_1/L) ,$$

$$H_1(Z_i, L) = \ln(Z_i/Z_o) - \psi_h(Z_i/L) + \psi_h(Z_o/L) ,$$

$$H_2(Z_i, L) = 1 - (\theta_*/k \cdot \theta_o) \cdot [\phi_h(Z_i/L) - \phi_h(Z_o/L)] .$$

The equations for $U_*$, $\theta_*$, $\theta_o$, and $L^{-1}$ given in Equation (13) are coupled, nonlinear equations. Consequently, they were solved iteratively following the sequence shown. We began the iteration by assuming that $L^{-1} = 0$. In subsequent iterations, the sign of $L^{-1}$ (or equivalently $\theta_*$) determined which set of functions (stable or unstable) we used for the $\psi$ and $\phi$ functions [see Equations (6a) and (6b)].

Some assumptions with regard to Equations (11) and (12) are implicit. Namely, these equations suggest that $E_1$ is primarily a function of $U_*$, $E_2$ is primarily a function of $\theta_*$, and $E_3$ is primarily a function of $\theta_o$. If we express the velocity and potential temperature profiles, respectively, as

$$U = U_B + U_C \quad ,$$
$$\theta = \theta_A + \theta_B + \theta_C \quad , \tag{14}$$

where $\theta_A = \theta_o$, $U_B$ and $\theta_B$ are the logarithmic terms, and $U_C$ and $\theta_C$ are the Monin-Obukhov stability profile terms, then our approach suggests that in general

$$U_B >> U_C \quad ,$$
$$\theta_A >> \theta_B >> \theta_C \quad . \tag{15}$$

To test this assumption, the ratios $U_C/U_B$, $\theta_B/\theta_A$, and $\theta_C/\theta_B$ were calculated at three heights (1, 3, 10 m) for each test considered in the LLNL and Shell series. Then the ratios were averaged over the number of tests (Table 6). In general, the conditions of Equation (15) are well met for this set of tests. The maximum value of $U_C/U_B$ was 0.31, and the maximum value of $\theta_C/\theta_B$ was 0.31, which agrees with Equation (15).

TABLE 6. AVERAGE RATIO OF VELOCITY AND POTENTIAL TEMPERATURE TERMS.

| Z (m) | $\langle U_C/U_B \rangle$ | $\langle \theta_B/\theta_A \rangle$ | $\langle \theta_C/\theta_B \rangle$ |
|---|---|---|---|
| 1 | 0.013 | 0.010 | 0.021 |
| 3 | 0.027 | 0.011 | 0.041 |
| 10 | 0.059 | 0.012 | 0.082 |

## 3. Application to LLNL, Shell, and HSE Tests

This method was used to estimate the meteorological parameters of the ambient surface-layer in the LLNL, Shell, and HSE field experiments. Table 7 lists the resulting values of $U_*$, $\theta_*$, $\theta_o$, and $L^{-1}$, as well as the root mean square difference in the velocity profile fit $E_u$ and the temperature profile fit $E_T$. These functions express the accuracy with which the respective profiles fit the data. The root mean square difference of X is defined as:

$$E = \frac{1}{N-N_c} \cdot \sum_{i=1}^{N} [X_i - X(Z_i)]^2 \; ^{1/2} \qquad (16)$$

where N = number of data points,
$N_c$ = number of determined coefficients, 1 for the velocity profile and 2 for the temperature profile.

Most data sets had 3 data points for the velocity profile fit and for the temperature fit. The two exceptions were Desert Tortoise, which had only 2 velocity data points per test, and Eagle which had only 3 temperature points per test. In calculating $E_T$, the potential temperature profile function $\theta(Z_i)$ was converted to temperature $T(Z_i)$ using Equation (8c) and was compared with the measured temperature $T_i$ in the root mean square function $E_T$.

For the Shell tests, the surface roughness length $z_o$ was obtained from the logarithmic velocity profile:

$$U = (U_*/k) \cdot \ln(Z/Z_o)$$

for neutral stability conditions, where the ratio of the friction velocity $U_*$ to the velocity at 10 m $U_{10}$ is

$$U_*/U_{10} = 0.034 \quad .$$

TABLE 7. RESULTS OF DATA FIT.

| Test | $u_*$(m/s) | $\theta_*$(K) | $\theta_o$(K) | $L^{-1}$($m^{-1}$) | $E_u$ | $E_T$ |
|---|---|---|---|---|---|---|
| B1 | 0.2058 | -0.5982 | 319.00 | -0.1779 | 0.0139 | 0.3620 |
| B2 | 0.2555 | -0.6144 | 328.74 | -0.1150 | 0.0489 | 0.3248 |
| B3 | 0.2597 | -0.9870 | 331.10 | -0.1775 | 0.0592 | 0.1385 |
| B4 | 0.4099 | -0.3836 | 321.86 | -0.0285 | 0.0469 | 0.3133 |
| B5 | 0.3442 | -0.3835 | 327.49 | -0.0397 | 0.0397 | 0.2996 |
| B6 | 0.4087 | -0.3223 | 325.30 | -0.0238 | 0.0407 | 0.2300 |
| B7 | 0.3772 | -0.0981 | 314.45 | -0.0088 | 0.0106 | 0.0952 |
| B8 | 0.0747 | 0.0287 | 310.76 | 0.0665 | 0.0170 | 0.0218 |
| B9 | 0.2535 | -0.0092 | 314.21 | -0.0018 | 0.0287 | 0.0449 |
| C3 | 0.3100 | -0.8656 | 334.43 | -0.1082 | 0.1024 | 0.2120 |
| C4A | 0.2359 | -0.3070 | 315.35 | -0.0703 | 1.409 | 0.1490 |
| C4B | 0.2739 | -0.1939 | 312.30 | -0.0332 | 0.2568 | 0.1421 |
| C4C | 0.3818 | -0.1271 | 309.31 | -0.0113 | 0.1196 | 0.1399 |
| C5 | 0.4796 | -0.5440 | 318.12 | -0.0299 | 0.4370 | 0.1341 |
| C6 | 0.2213 | 0.0448 | 301.52 | 0.0122 | 0.3116 | 0.0965 |
| C7 | 0.2864 | 0.0113 | 303.29 | 0.0018 | 0.0965 | 0.1005 |
| C8A | 0.3910 | -0.1365 | 304.04 | -0.0118 | 0.0299 | 0.1369 |
| C8B | 0.4622 | -0.0583 | 301.95 | -0.0036 | 0.1140 | 0.1129 |
| C8C | 0.4425 | -0.0079 | 300.14 | -0.0005 | 0.3706 | 0.0975 |
| C9A | 0.1262 | -0.1387 | 307.69 | -0.1138 | 0.4088 | 0.1415 |
| C9B | 0.2040 | -0.1429 | 308.30 | -0.0448 | 0.0497 | 0.1639 |
| C9C | 0.1893 | -0.0314 | 305.57 | -0.0115 | 0.1595 | 0.1367 |
| D1 | 0.4360 | 0.1602 | 308.14 | 0.0110 | 0.0866 | 0.0471 |
| D2 | 0.3124 | 0.0907 | 310.58 | 0.0120 | 0.0509 | 0.0273 |
| D3 | 0.4424 | 0.0032 | 315.60 | 0.0002 | 0.0307 | 0.1330 |
| D4 | 0.2499 | 0.1240 | 312.88 | 0.0255 | 0.1246 | 0.0478 |
| E1 | 0.3068 | -0.3743 | 323.34 | -0.0494 | 0.0950 | 0.0222 |
| E2 | 0.2837 | -0.0315 | 311.40 | -0.0050 | 0.1239 | 0.1546 |
| E3 | 0.1293 | 0.0749 | 301.93 | 0.0596 | 0.4378 | 0.0368 |
| E4 | 0.2453 | -0.1389 | 309.53 | -0.0300 | 0.0733 | 0.0501 |
| E5 | 0.1136 | 0.0082 | 303.99 | 0.0084 | 0.2163 | 0.0981 |
| E6 | 0.2328 | 0.1396 | 303.44 | 0.0034 | 0.0548 | 0.0112 |
| S9 | 0.3118 | -0.0990 | 292.34 | -0.0140 | 0.3286 | 0.0596 |
| S15 | 0.1280 | 0.0029 | 288.29 | 0.0025 | 0.1919 | 0.0379 |
| S27 | 0.2030 | -0.1339 | 291.32 | -0.0448 | 0.0929 | 0.0377 |
| S29 | 0.2630 | 0.0073 | 289.08 | 0.0015 | 0.3525 | 0.0140 |
| S34 | 0.3155 | -0.1009 | 290.89 | -0.0140 | 0.3667 | 0.0425 |
| S35 | 0.3526 | -0.1683 | 293.45 | -0.0185 | 0.1951 | 0.0314 |
| S37 | 0.1639 | 0.0098 | 289.02 | 0.0051 | 0.2267 | 0.0056 |
| S39 | 0.1263 | 0.0364 | 2880.92 | 0.0318 | 0.1118 | 0.0294 |
| S56 | 0.1721 | -0.0012 | 2830.80 | -0.0006 | 0.1858 | 0.0094 |

TABLE 7. RESULTS OF DATA FIT (CONCLUDED).

| Test | $U_*$(m/s) | $\theta_*$(K) | $\theta_0$(K) | $L^{-1}(m^{-1})$ | $E_U$ | $E_T$ |
|---|---|---|---|---|---|---|
| S42 | 0.1208 | 0.0129 | 2910.14 | 0.0122 | 0.0672 | 0.0121 |
| S43 | 0.1809 | 0.0001 | 2900.17 | 0.0001 | 0.3295 | 0.0097 |
| S45 | 0.0653 | -0.2321 | 2950.05 | -0.7410 | 0.2425 | 0.0367 |
| S46 | 0.2839 | 0.0090 | 2910.64 | 0.0015 | 0.3004 | 0.0043 |
| S47 | 0.1932 | 0.0150 | 2900.19 | 0.0055 | 0.1999 | 0.0198 |
| S49 | 0.2122 | 0.0580 | 2840.98 | 0.0182 | 0.5021 | 0.0557 |
| S50 | 0.2600 | 0.0347 | 2820.68 | 0.0073 | 0.1837 | 0.0258 |
| S51 | 0.2317 | -0.0304 | 2820.94 | -0.0080 | 0.2371 | 0.0276 |
| S52 | 0.2585 | 0.0340 | 2840.11 | 0.0072 | 0.3515 | 0.0433 |
| S54 | 0.1260 | 0.0195 | 2810.06 | 0.0176 | 0.2061 | 0.0058 |
| S55 | 0.1880 | 0.0254 | 2820.82 | 0.0102 | 0.3071 | 0.0175 |
| S22 | 0.1864 | -0.0244 | 2920.68 | -0.0096 | 0.2015 | 0.0087 |
| S23 | 0.2131 | 0.0105 | 2900.90 | 0.0032 | 0.2911 | 0.0170 |
| S63 | 0.1165 | -0.0088 | 2820.49 | -0.0093 | 0.5029 | 0.0175 |
| H45 | 0.083 | 0.037 | 2850.33 | 0.075 | --- | --- |
| H47 | 0.049 | 0.017 | 2870.03 | 0.100 | --- | --- |

This value was typical for neutral conditions (Colenbrander and Puttock, Reference 49). Therefore if k = 0.41, the surface roughness is

$$Z_o = 5.8 \times 10^{-5} \text{ m} \quad .$$

Note that the value of $Z_o$ depends on the value chosen for k, the von Karman constant. If k = 0.35, then $Z_o = 3.4 \times 10^{-4}$m.

In the HSE tests, the surface roughness length ranged from 1 to 25 mm (Reference 50). The logarithmic mean value of $Z_o$ = 5 mm = 0.005 meter was chosen for the surface roughness length in these calculations. The remaining input data from the HSE tests differed from that of the LLNL and Shell tests. Rather than the average velocity at three heights and the average temperature at four heights, the HSE tests used a single average velocity and a single temperature measurement plus the stability classification, A to F. Consequently, the procedure for calculating the meteorological parameters, $U_*$, $\theta_*$, $\theta_o$, and $L^{-1}$ was altered to be compatible with the input data.

For these tests, the inverse Monin-Obukhov length $L^{-1}$ was determined from the Golder curves using the surface roughness length $Z_o$ and the stability classification. The friction velocity was then determined using the single mean velocity U(Z) and the measurement height Z as well as $Z_o$, $L^{-1}$, and the velocity profile function. Thus, the friction velocity was given by:

$$U_* = k \cdot U(Z) / [\ln(Z/Z_o) - \psi_m(Z/L) + \psi_m(Z_o/L)] \quad .$$

After converting the mean temperature T(Z) to potential temperature $\theta(Z)$, we determined the ground level potential temperature $\theta_o$ in a similar manner, using $\theta(Z)$, $L^{-1}$, and $U_*$ in the potential temperature profile equation. Expressing the scaling potential temperature $\theta_*$ in terms of $U_*$, $L^{-1}$, and $\theta_o$, we obtained:

$$\theta_o = \theta(Z) / \{1 + (U_*/g \cdot k^2 \cdot L) \cdot [\ln(Z/Z_o - \psi_h(Z/L) + \psi_h(Z_o/L)]\} \quad .$$

Finally, the scaling potential temperature $\theta_*$ was determined from the definition of the Monin-Obukhov length L, expressed as follows:

$$\theta_* = (\theta_o \cdot U_*^2) / (g \cdot k \cdot L) \quad .$$

Since only one velocity and temperature measurement was available, the profiles fit the data exactly and an estimate of the error could not be made.

C. UNCERTAINTY

Several factors contribute to the uncertainty in the meteorological parameters that are assumed, according to surface layer theory, to describe a unique, steady-state condition in the atmosphere. For example:

- Measurement errors in the data are included in the calculation of the average velocity and temperature.

- The calculated mean velocity and temperature can be in error if the averaging time is inappropriate.
- The state of the atmosphere is complex because of turbulent processes. Consequently, it cannot be characterized by a limited number (typically less than 10) of temperature and wind velocity measurements. For a given set of measurements, a range in dispersive characteristics is observed. Thus, we have an ensemble average condition with a surrounding range of conditions, all of which might occur given the same meteorological parameters.
- Although the atmosphere is assumed to be in a steady state, this may not be true and conditions may be continually changing.
- Surface-layer theory and the set of Monin-Obukhov similarity parameters are a model for the atmosphere in the layer closest to the ground. There is some degree of difference between the model description and the actual mean quantities in the atmosphere even if steady-state conditions are met.

These factors add to the uncertainty in describing the particular state of the atmosphere. Of particular difficulty to quantify are the nonmeasurement errors and uncertainties. To obtain some quantitative measure of uncertainty, three analyses are presented.

The first analysis studies the variation in the predicted Pasquill-Gifford stability class when several methods are used. Since stability class defines the dispersion curves ($\sigma_y$, $\sigma_z$) in this approach to describing ambient conditions, the variation in stability class can be used directly to determine the variation in plume dispersion parameters ($\sigma_y$, $\sigma_z$) and the resulting variation in concentration as a function of downwind distance. The data used in this analysis were taken from 27 of the HSE tests.

The second analysis studies the importance of using both velocity and temperature gradient information. In the method proposed in this report, the

surface-layer parameters $U_*$, $\theta_*$, and $\theta_o$ are determined from a mix of temperature data and velocity data using a least-squares fit. Theoretically, these parameters can be determined from two or more mean velocity measurements at different heights and a single mean temperature measurement or from three or more mean temperature measurements all at different heights. Although many methods rely heavily on one type of data or the other, these two approaches represent extreme cases: one determines the mean temperature gradient ($\theta_*$) using only velocity information, and the other determines the mean velocity gradient ($U_*$) using only temperature data. Using the LLNL and Shell data, we compared these approaches with each other and with our approach, which uses all available velocity and temperature data. Our purpose is not to quantify the uncertainty in the meteorological parameters, but to demonstrate that both temperature and velocity data are needed to fit both profiles well.

In the third analysis, two different methods are used to calculate the friction velocity $U_*$. The first method, which is presented in this report, is based on surface-layer theory for the vertical profiles of the mean velocity and temperature. The second method uses the basic definition of the friction velocity [see Equation (10)]:.

$$U_*^2 = -\langle U' \cdot W' \rangle \quad ,$$

where U' and W' are the random components of the horizontal and vertical components of the wind velocity. The results from these two methods are then compared as a measure of the uncertainty in the predicted value of $U_*$. This comparison is applied to the LLNL Burro data for which the high-resolution windspeed data were available.

1. Variation in Stability Category Classification Methods

Seven methods were used to determine the atmospheric stability in the HSE Thorney Island tests of heavy gas dispersion. These methods are as follows (Reference 51):

a. Visual Observation. The amount of cloud cover or the judged level of incoming solar radiation and the value of the windspeed were recorded based on visual observation (see Table 8).

b. Temperature Difference. Temperature difference is one of two methods suggested by the U.S. Nuclear Regulatory Commission (NRC). This difference was calculated as:

$$\frac{DT}{DZ} = \frac{T_{30} - T_9}{21} \cdot 100.00 \quad .$$

The NRC tables, see e.g., Sedefian and Bennett (Reference 52) or McQuaid (Reference 53), were then consulted to determine the appropriate stability.

c. Solarimeter. Insolation measured by a solarimeter was used with the windspeed to determine the stability based on the information presented in Pasquill (Reference 54, Figure 6.13) and presented here as Figure 3.

d. Heat Flux. Heat flux (H) was calculated from the insolation (R) by the formula $H = 0.4(R - 10.0)$ based on the suggestion by Smith (Reference 55). Pasquill's Figure 6.13 (Reference 54) (our Figure 3) was then consulted to determine the stability. This method therefore agrees generally with the previous method.

e. Richardson Number. The Richardson number is calculated according to Sedefian and Bennett (Reference 52) as:

$$R_i = \frac{g(D\theta/DZ)}{T(DU/DZ)^2} \quad ,$$

where $\theta$ is the potential temperature and T is the actual temperature, in this case at 16 m above the ground. $D\theta/DZ$ was calculated as:

$$\frac{T_{30} - T_9}{21} + 0.00986 \quad ,$$

TABLE 8. MODIFIED PASQUILL STABILITY CATEGORIES.

| Wind-speed[a] | Daytime (excluding 1 hr after sunrise and 1 hr before sunset) | | | | Nighttime | | | |
|---|---|---|---|---|---|---|---|---|
| | Incoming solar radiation ($W\ m^{-2}$) | | | | Within 1 hr before or after sunset[b] | Cloud amount (oktas) | | |
| | Strong (>600) | Moderate (300-600) | Slight (<300) | Overcast | | 0-3 | 4-7 | 8 |
| <3 | A | A-B | B | C | D | F or G[c] | F | D |
| 4-5 | A-B | B | C | C | D | F | E | D |
| 6-9 | B | B-C | C | C | D | E | D | D |
| 10-12 | C | C-D | D | D | D | D | D | D |
| >12 | C | D | D | D | D | D | D | D |

From Meteorological Office

[a]1 kt = 0.52 m/s.

[b]Night was originally defined to include periods of 1 hr before sunset and after sunrise. These two hours are always categorized here as D.

[c]Pasquill said that in light winds on clear nights the vertical spread may be less than for category F but excluded such cases because the surface plume is unlikely to have any definable travel. However, they are important when considering pollution buildup so category G (nighttime, 0-1 okta of cloud, windspeed 0-1 kt) was added.

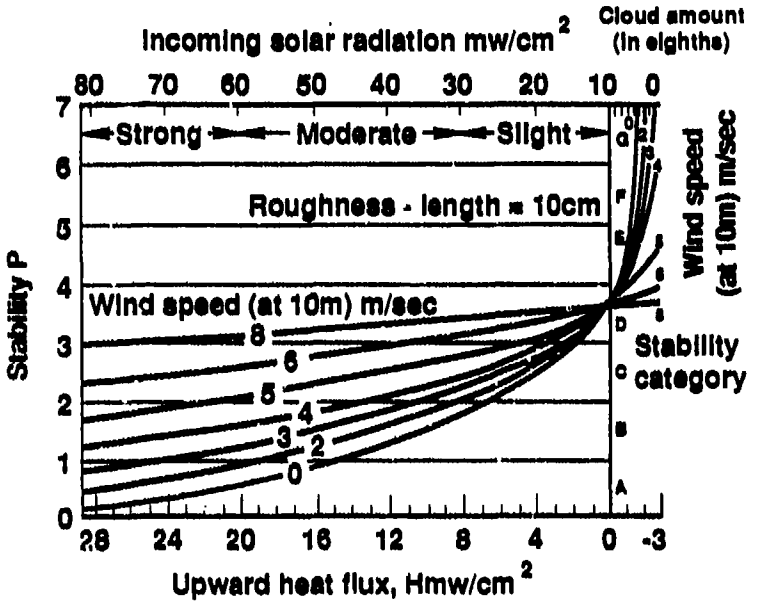


Figure 3. Stability as a Function of Heat Flux and Windspeed as Given by Pasquill (Reference 54).

and DU/DZ was calculated as:

$$\frac{U_{30} - U_{10}}{20} .$$

Sedefian and Bennett calculate the limits of the Richardson number for the various stability categories; however, the limits they presented were valid for measurements at heights whose geometric mean was 22 meters. Since the measurement stations were at 30, 9 and 16 meters, the limits were recalculated to correspond to a geometric mean height of 16 meters.

f. Bulk Richardson Number. The bulk Richardson number was also calculated according to Sedefian and Bennett (Reference 52) as:

$$R_{i\infty} = \frac{g(D\theta/DZ)\bar{Z}^2}{T\bar{U}^2} ,$$

where $\bar{Z}$ is the geometric mean height = $\sqrt{9 \times 30}$; T is the temperature at 16 meters above the ground; and $\bar{U}$ is the mean windspeed at 30 meters.

Again, the limits of $R_{i\infty}$ were recalculated to correspond to a geometric mean height of 16 meters.

g. Standard Deviation of Wind Heading. The standard deviation of wind heading was calculated from the Porton wind vane, which has a resolution bandwidth of 11°. The resulting accuracy is predicted to be about ±2°, assuming a Gaussian distribution of wind direction. These estimates were compared with the simple assumption that the standard deviation is approximately 1/6 (maximum-minimum angle). The NRC limits for $\sigma_\theta$ are then used to determine the appropriate stability category.

To compare the different methods, the stability classes A to F were given numerical values 1 to 6, respectively. When two classes were given, the numerical value halfway between the two was used (for example,

B/C → 2.5). Using this numerical approach, we calculated the average numerical stability class and the standard deviation about the average for each test. Then we averaged the standard deviation over 27 of the HSE tests, namely, tests 5-29 and 45-47. The results are presented in Table 9. The average standard deviation for these tests was 1.0, or one stability class.

If we assume that all seven methods for calculating stability class are equally reliable, then this analysis suggests that the uncertainty in identifying the stability class is plus or minus one class, where standard deviation has been used as the measure of uncertainty. In the HSE data summaries, a chosen stability class was also given. This class was apparently selected in some qualitative manner based on the seven quantitative approaches. In our study, the average difference and the root mean square difference between this chosen value and the average value of the seven methods were also calculated. The average difference for all 27 tests was -0.14 or essentially zero, suggesting no particular bias between the chosen class and the average class. The root mean square difference was 0.60 or about one-half class. Further interpretation of uncertainty is difficult since the "true" stability class for each test is unknown. However, a trained meteorologist who witnessed the experiment and reviewed all the data might be able to reduce the uncertainty (standard deviation) in stability class to about plus or minus one-half class.

Our analysis involved only 27 tests at one location. Furthermore, the distribution of stability class over the six possible classes was not uniform, as shown in Table 10. In about 50% of the tests, the stability class was neutral (D stability class) and in the remaining 50% it was distributed among Class B, C, E, and F.

TABLE 9. STABILITY CLASS: AVERAGE VALUE AND STANDARD DEVIATION.

| Test | Average value | Sigma[a] |
|---|---|---|
| 5 | 2.643 | 1.376 |
| 6 | 3.286 | 2.307 |
| 7 | 5.357 | 1.180 |
| 8 | 4.500 | 1.354 |
| 9 | 5.786 | 0.994 |
| 10 | 3.286 | 0.809 |
| 11 | 4.143 | 0.378 |
| 12 | 5.286 | 0.756 |
| 13 | 3.786 | 0.393 |
| 14 | 3.571 | 0.450 |
| 15 | 3.214 | 1.286 |
| 16 | 4.071 | 0.932 |
| 18 | 3.929 | 0.189 |
| 19 | 4.500 | 0.764 |
| 20 | 4.286 | 1.380 |
| 21 | 5.000 | 1.155 |
| 22 | 4.571 | 0.787 |
| 23 | 4.500 | 0.764 |
| 24 | 4.429 | 0.787 |
| 25 | 5.571 | 1.272 |
| 26 | 4.071 | 1.835 |
| 27 | 4.571 | 1.512 |
| 28 | 4.143 | 0.378 |
| 29 | 4.643 | 0.748 |
| 45 | 4.929 | 1.170 |
| 46 | 4.429 | 0.787 |
| 47 | 5.286 | 1.380 |

[a]Average sigma = 1.005.

TABLE 10. DISTRIBUTION OF CHOSEN STABILITY VALUES.

| Class | Number[a] | Percentage |
|---|---|---|
| A | 0 | 0 |
| B | 2 | 7.4 |
| C | 2.5 | 9.3 |
| D | 13.5 | 50.0 |
| E | 5.5 | 20.4 |
| F | 3.5 | 13.0 |

[a]For this particular table, when two values were listed, a weighting of 0.5 was given to each class. For example, when B/C was listed as the chosen class, 0.5 was added to the number in each of the B and C classes.

## 2. Surface-Layer Theory

As previously stated, a severe test of the accuracy of the mean temperature and velocity data and of the applicability of surface-layer theory is to predict the scaling potential temperature $\theta_*$ without temperature gradient information or to predict the friction velocity $U_*$ without velocity information. To do this, two least-squares fit codes were developed. The first, called VELFIT, uses the velocity equation:

$$U(Z) = (U_*/k)[\ln(Z/Z_o) - \psi_m(Z/L) + \psi_m(Z_o/L)] \quad ,$$

and the velocity data to determine $U_*$ and L. Then the potential temperature equation:

$$\theta(Z) = \theta_o\{1 + (U_*^2/g \cdot k^2 \cdot L) \cdot [\ln(Z/Z_o) - \psi_h(Z/L) + \psi_h(Z_o/L)]\} \quad ,$$

and the potential temperature data are used to determine $\theta_o$. Finally, the scaling potential temperature $\theta_*$ is determined from the Monin-Obukhov length equation expressed as:

$$\theta_* = (U_*^2 \cdot \theta_o)/(g \cdot k \cdot L) \quad .$$

The second code, called TMPFIT, is similar, only it uses no velocity data since $U_o$ is defined as zero. The three meteorological parameters $\theta_*$, $\theta_o$, and L are determined from the potential temperature equation:

$$\theta = \theta_o + (\theta_*/k) \cdot [\ln(Z/Z_o) - \psi_h(Z/L) + \psi_h(Z_o/L)] \quad ,$$

and the potential temperature data. The friction velocity $U_*$ is then given by:

$$U_* = (g \cdot k \cdot L \cdot \theta_*/\theta_o)^{1/2} \quad .$$

The general error formula that is used to evaluate the fit between the profile functions and the data is

$$E_x = \{(N - N_c)^{-1} \cdot \sum_{i=1}^{N} [X_i - X(Z_i)]^2\}^{1/2} \quad ,$$

where $N$ = number of data points,
$N_c$ = number of determined coefficients,
$X_i$ = mean temperature or velocity,
$X(Z_i)$ = temperature or velocity profile value.

The tests in this study generally use three velocity data points and four temperature data points. The Desert Tortoise tests used only two velocity data points per test. Consequently, in VELFIT there are no degrees of freedom in the velocity fit ($N = 2$ and $N_c = 2$) so the error is indeterminant. The Eagle tests had only three temperature data points per test. Consequently, in TMPFIT there are no degrees of freedom in the temperature fit ($N = 3$ and $N_c = 3$) so again the error is indeterminant.

The analysis was applied to the LLNL (References 56-59) data (B - Burro, C - Coyote, D - Desert Tortoise, E - Eagle) and the Shell (Reference 60) data (S - Shell). The results of the analysis for the DATAFIT method as well as the VELFIT and TMPFIT approaches are given in Table 11. In general, the DATAFIT code presented the best overall fit, as expected since it used all the data to determine $U_*$ and $\theta_*$. For example, in the Burro tests, $E_U$ = 0.034 m/s and $E_T$ = 0.20K. The velocity fit was exceptionally good for the Burro tests, and both the velocity and temperature fits were quite good for the Desert Tortoise tests. The temperature fit was good in the Shell tests; however, most of these tests were conducted under near-neutral conditions where $\theta_*$ and $L^{-1} \sim 0$, and $\theta \sim \theta_o$. In general, VELFIT did a much better job of fitting the temperature data than TMPFIT did in fitting the velocity data. For example, in the Burro tests, the estimated VELFIT temperature error $E_T$ was

TABLE 11. ESTIMATED ERROR.

| | Velocity data ($E_u$) | | | Temperature data ($E_T$) | | |
|---|---|---|---|---|---|---|
| Test | DATAFIT | VELFIT | TMPFIT | DATAFIT | VELFIT | TMPFIT |
| B1 | 0.0139 | 0.0191 | 1.510 | 0.3620 | 0.2981 | 0.0576 |
| 2 | 0.0489 | 0.0017 | 1.609 | 0.3248 | 0.3788 | 0.1933 |
| 3 | 0.0592 | 0.0098 | 7.038 | 0.1385 | 0.4356 | 0.1875 |
| 4 | 0.0469 | 0.0043 | 7.117 | 0.3133 | 0.3386 | 0.0791 |
| 5 | 0.0397 | 0.0070 | 5.254 | 0.2996 | 0.2963 | 0.1991 |
| 6 | 0.0407 | 0.0107 | 5.463 | 0.2300 | 0.2736 | 0.1914 |
| 7 | 0.0106 | 0.0082 | 7.170 | 0.0952 | 0.0805 | 0.0192 |
| 8 | 0.0170 | 0.0025 | 0.6836 | 0.0218 | 0.0294 | 0.0268 |
| 9 | 0.0287 | 0.0028 | 5.923 | 0.0449 | 0.0648 | 0.0348 |
| C3 | 0.1024 | 0.0278 | 5731.0 | 0.2120 | 0.6288 | 0.4348 |
| 4A | 1.409 | 0.2355 | 15.01 | 0.1490 | 2.578 | 0.2213 |
| 4B | 0.2568 | 0.1464 | 5.297 | 0.1421 | 0.4238 | 0.1917 |
| 4C | 0.1196 | 0.1243 | 1.453 | 0.1399 | 0.3856 | 0.1759 |
| 5 | 0.4370 | 0.5946 | 8.234 | 0.1341 | 1.483 | 0.1734 |
| 6 | 0.3116 | 0.3933 | 5.337 | 0.0965 | 0.2659 | 0.2440 |
| 7 | 0.0965 | 0.0599 | 6.745 | 0.1005 | 0.1923 | 0.1522 |
| 8A | 0.0299 | 0.0235 | 0.4303 | 0.1369 | 0.1150 | 0.1868 |
| 8B | 0.1140 | 0.1311 | 6.438 | 0.1129 | 0.2916 | 0.1431 |
| 8C | 0.3706 | 0.2992 | 9.542 | 0.0975 | 2.258 | 0.1216 |
| 9A | 0.4088 | 0.0330 | 5.318 | 0.1415 | 0.3663 | 0.1992 |
| 9B | 0.0497 | 0.0499 | 7.006 | 0.1639 | 0.2300 | 0.2384 |
| 9C | 0.1595 | 0.1507 | 4.372 | 0.1367 | 0.1346 | 0.1887 |
| D1 | 0.0866 | I | 2.148 | 0.0471 | 0.6136 | 0.0574 |
| 2 | 0.0509 | I | 0.8091 | 0.0273 | 0.2816 | 0.0365 |
| 3 | 0.0307 | I | 7.885 | 0.1330 | 0.2965 | 0.1958 |
| 4 | 0.1246 | I | 1.607 | 0.0478 | 0.6485 | 0.0406 |
| E1 | 0.0950 | 0.0290 | 0.7398 | 0.0222 | 0.4350 | I |
| 2 | 0.1239 | 0.0001 | 6.795 | 0.1546 | 0.1631 | I |
| 3 | 0.4378 | 0.0910 | 4.490 | 0.0368 | 0.3603 | I |
| 4 | 0.0733 | 0.0846 | 5.666 | 0.0501 | 0.1315 | I |
| 5 | 0.2163 | 0.0690 | 2.849 | 0.0981 | 2.692 | I |
| 6 | 0.0548 | 0.0334 | 5.096 | 0.0112 | 0.0492 | I |
| S9 | 0.3286 | 0.4429 | 6.372 | 0.0596 | 0.0923 | 0.0929 |
| 15 | 0.1919 | 0.0591 | 3.436 | 0.0379 | 0.2027 | 0.0567 |
| 27 | 0.0929 | 0.0899 | 34.89 | 0.0377 | 0.1332 | 0.0680 |
| 29 | 0.3525 | 0.1509 | 7.040 | 0.0140 | 0.6366 | 0.0288 |
| 34 | 0.3667 | 0.1781 | 3.729 | 0.0425 | 2.318 | 0.0653 |
| 35 | 0.1951 | 0.0006 | 13.82 | 0.0314 | 0.5807 | 0.0636 |
| 37 | 0.2267 | 0.0191 | 4.424 | 0.0056 | 0.2419 | 0.0321 |

TABLE 11. ESTIMATED ERROR (CONCLUDED).

| | Velocity data ($E_U$) | | | Temperature data ($E_T$) | | |
|---|---|---|---|---|---|---|
| Test | DATAFIT | VELFIT | TMPFIT | DATAFIT | VELFIT | TMPFIT |
| S39 | 0.1118 | 0.0921 | 3.619 | 0.0294 | 0.0528 | 0.1783 |
| 56 | 0.1858 | 0.2357 | 3.998 | 0.0094 | 0.0433 | 0.0111 |
| 42 | 0.0672 | 0.0917 | 3.311 | 0.0121 | 0.0110 | 0.0486 |
| 43 | 0.3295 | 0.3466 | 4.831 | 0.0097 | 0.1431 | 0.0138 |
| 45 | 0.2425 | 0.0467 | 1836. | 0.0367 | 0.1151 | 0.0452 |
| 46 | 0.3004 | 0.0005 | 6.973 | 0.0043 | 0.5239 | 0.0036 |
| 47 | 0.1999 | 0.0501 | 5.219 | 0.0198 | 0.1509 | 0.0501 |
| 49 | 0.5021 | 0.1018 | 5.918 | 0.0557 | 0.7350 | 0.2280 |
| 50 | 0.1837 | 0.2461 | 7.048 | 0.0258 | 0.0626 | 0.1133 |
| 51 | 0.2371 | 0.1110 | 2.056 | 0.0276 | 0.1671 | 0.0149 |
| 52 | 0.3515 | 0.4567 | 7.008 | 0.0433 | 0.1502 | 0.1091 |
| 54 | 0.2061 | 0.2182 | 3.500 | 0.0058 | 0.0524 | 0.0801 |
| 55 | 0.3071 | 0.3379 | 5.136 | 0.0175 | 0.0990 | 0.0916 |
| 22 | 0.2015 | 0.1713 | 0.9876 | 0.0087 | 0.0948 | 0.0028 |
| 23 | 0.2911 | 0.1750 | 5.726 | 0.0170 | 0.2299 | 0.0350 |
| 63 | 0.5029 | 0.6772 | 827.5 | 0.0175 | 0.0569 | 0.0252 |

about 0.25K, while the estimated TMPFIT velocity error $E_U$ was about 4.6 m/s. For the same data, the estimated VELFIT velocity error was $E_U$ = 0.007 m/s (essentially a perfect fit) and the estimated TMPFIT temperature error was $E_T$ = 0.110 K. Thus, TMPFIT provides the best temperature fit but the poorest velocity fit. Combining the errors $E_U$ and $E_T$ and assuming equal accuracy in the velocity and temperature data, we obtain to a relative error of 1.0, 1.2, and 22.0 for DATAFIT, VELFIT, and TMPFIT, respectively.

The friction velocity results from all three fitting codes are given in Table 12, and, the scaling potential temperature results are given in Table 13. The DATAFIT and VELFIT values for the friction velocity $U_*$ are generally in good agreement. The agreement between the DATAFIT results and the TMPFIT and VELFIT results for scaling potential temperature $\theta_*$ are nearly equal. In the Shell series, many of the tests were conducted in near-neutral conditions where the value of $\theta_*$ is essentially zero. Under neutral conditions, where $\theta_* = L^{-1} = 0$, TMPFIT cannot predict the value of $U_*$ because the ratio $\theta_*/L^{-1}$ is indeterminant. Consequently, as conditions approach

TABLE 12. FRICTION VELOCITY, $U_*$ (m/s).

| Test | DATAFIT | VELFIT | TMPFIT |
|---|---|---|---|
| B1 | 0.2058 | 0.2051 | 0.1373 |
| 2 | 0.2555 | 0.2488 | 0.1841 |
| 3 | 0.2597 | 0.2503 | 0.5473 |
| 4 | 0.4099 | 0.4058 | 0.1119 |
| 5 | 0.3442 | 0.3403 | 0.1234 |
| 6 | 0.4087 | 0.4053 | 0.1805 |
| 7 | 0.3772 | 0.3765 | 0.0771 |
| 8 | 0.0747 | 0.0757 | 0.1050 |
| 9 | 0.2535 | 0.2554 | 0.0007 |
| C3 | 0.3100 | 0.2976 | 244.7 |
| 4A | 0.2359 | 0.1535 | 0.8679 |
| 4B | 0.2739 | 0.2588 | 0.4970 |
| 4C | 0.3818 | 0.3884 | 0.3222 |
| 5 | 0.4796 | 0.4958 | 0.8169 |
| 6 | 0.2213 | 0.2327 | I |
| 7 | 0.2864 | 0.2922 | I |
| 8A | 0.3910 | 0.3892 | 0.4100 |
| 8B | 0.4622 | 0.4671 | 0.1928 |
| 8C | 0.4425 | 0.4742 | 0.0411 |
| 9A | 0.1262 | 0.0997 | 0.3485 |
| 9B | 0.2040 | 0.2084 | 0.4986 |
| 9C | 0.1893 | 0.1824 | I |
| D1 | 0.4360 | 0.4510 | 0.5591 |
| 2 | 0.3124 | 0.3213 | 0.3589 |
| 3 | 0.4424 | 0.4484 | I |
| 4 | 0.2499 | 0.2718 | 0.3434 |
| E1 | 0.3068 | 0.2923 | 0.2766 |
| 2 | 0.2837 | 0.2740 | 0.0010 |
| 3 | 0.1293 | 0.1636 | 0.3278 |
| 4 | 0.2453 | 0.2392 | 0.0018 |
| 5 | 0.1136 | 0.3214 | I |
| 6 | 0.2328 | 0.2365 | 0.0130 |
| S9 | 0.3118 | 0.3073 | 0.5483 |
| 15 | 0.1280 | 0.1452 | I |
| 27 | 0.2030 | 0.2101 | 1.505 |
| 29 | 0.2630 | 0.2904 | I |
| 34 | 0.3155 | 0.3599 | 0.4531 |
| 35 | 0.3526 | 0.3709 | 0.8665 |
| 37 | 0.1639 | 0.1821 | I |

TABLE 12. FRICTION VELOCITY, $U_*$ (m/s) (CONCLUDED).

| Test | DATAFIT | VELFIT | TMPFIT |
|---|---|---|---|
| S39 | 0.1263 | 0.1305 | I |
| 56 | 0.1721 | 0.1684 | 0.0236 |
| 42 | 0.1208 | 0.1216 | I |
| 43 | 0.1809 | 0.1712 | I |
| 45 | 0.0653 | 0.0489 | 68.95 |
| 46 | 0.2839 | 0.3066 | 0.0191 |
| 47 | 0.1932 | 0.2045 | I |
| 49 | 0.2122 | 0.2500 | I |
| 50 | 0.2600 | 0.2574 | I |
| 51 | 0.2317 | 0.2217 | 0.1565 |
| 52 | 0.2585 | 0.2523 | I |
| 54 | 0.1260 | 0.1319 | I |
| 55 | 0.1880 | 0.1961 | I |
| 22 | 0.1864 | 0.1792 | 0.2226 |
| 23 | 0.2131 | 0.2015 | I |
| 63 | 0.1165 | 0.1099 | 31.16 |

TABLE 13. SCALING POTENTIAL TEMPERATURE, $\Theta_*$ (K).

| Test | DATAFIT | VELFIT | TMPFIT |
|---|---|---|---|
| B1 | -0.5982 | -0.5528 | -0.3628 |
| 2 | -0.6144 | -0.2727 | -0.4291 |
| 3 | -0.9870 | -0.3630 | -0.3799 |
| 4 | -0.3836 | -0.2198 | -0.6997 |
| 5 | -0.3835 | -0.2291 | -0.5319 |
| 6 | -0.3223 | -0.1956 | -0.4415 |
| 7 | -0.0981 | -0.0827 | -0.2022 |
| 8 | 0.0287 | 0.0265 | 0.0364 |
| 9 | -0.0092 | -0.0355 | -0.0332 |
| C3 | -0.8656 | -0.2084 | -0.4888 |
| 4A | -0.3070 | 0.3683 | -0.2104 |
| 4B | -0.1939 | 0.0534 | -0.1775 |
| 4C | -0.1271 | -0.3550 | -0.1725 |
| 5 | -0.5440 | -1.898 | -0.5637 |
| 6 | 0.0448 | -0.0767 | 0. |
| 7 | 0.0113 | -0.0744 | 0. |
| 8A | -0.1365 | -0.0892 | -0.1611 |
| 8B | -0.0583 | -0.1973 | -0.1165 |
| 8C | -0.0079 | -1.886 | -0.0594 |
| 9A | -0.1387 | 0.0610 | -0.0859 |

TABLE 13. SCALING POTENTIAL TEMPERATURE, $\theta_*$ (K) (CONCLUDED).

| Test | DATAFIT | VELFIT | TMPFIT |
|---|---|---|---|
| C9B | -0.1429 | -0.2926 | -0.1136 |
| 9C | -0.0314 | 0.0253 | 0. |
| D1 | 0.1602 | 0.0021 | 0.1715 |
| 2 | 0.0907 | 0.0243 | 0.0947 |
| 3 | 0.0032 | -0.0890 | 0. |
| 4 | 0.1240 | -0.0130 | 0.1437 |
| E1 | -0.3743 | -0.0482 | -0.3669 |
| 2 | -0.0315 | 0.0356 | -0.0789 |
| 3 | 0.0749 | -0.0245 | 0.1107 |
| 4 | -0.1389 | -0.0465 | -0.2432 |
| 5 | 0.0082 | 77.99 | 0. |
| 6 | 0.1396 | -0.0049 | 0.0034 |
| S 9 | -0.0990 | -0.0137 | -0.0801 |
| 15 | 0.0029 | -0.5368 | 0. |
| 27 | -0.1339 | -0.4271 | -0.0686 |
| 29 | 0.0073 | -1.413 | 0. |
| 34 | -0.1009 | -8.962 | -0.0886 |
| 35 | -0.1683 | -1.357 | -0.1233 |
| 37 | 0.0098 | -0.4960 | 0. |
| 39 | 0.0364 | 0.0212 | 0. |
| 56 | -0.0012 | 0.0180 | -0.0043 |
| 42 | 0.0129 | 0.0100 | 0. |
| 43 | 0.0001 | 0.0525 | 0. |
| 45 | -0.2321 | 0.0107 | -0.0345 |
| 46 | 0.0090 | -0.9044 | 0.0028 |
| 47 | 0.0150 | -0.1532 | 0. |
| 49 | 0.0580 | -10.722 | 0. |
| 50 | 0.0347 | 0.0549 | 0. |
| 51 | -0.0304 | 0.0505 | -0.0417 |
| 52 | 0.0340 | 0.0807 | 0. |
| 54 | 0.0195 | -0.0040 | 0. |
| 55 | 0.0254 | -0.0391 | 0. |
| 22 | -0.0244 | 0.0275 | -0.0224 |
| 23 | 0.0105 | 0.0835 | 0. |
| 63 | -0.0088 | 0.0176 | -0.0068 |

neutral, TMPFIT becomes sensitive to $L^{-1}$ and the uncertainty in predicted $U_*$ becomes very large. This does not occur in VELFIT. In VELFIT, as conditions approach neutral and $L^{-1}$ approaches zero, $\theta_*$ linearly approaches zero and is therefore well defined.

3. Variation in Friction Velocity

As previously discussed, the friction velocity is defined by the flux relationship:

$$U_*^2 = -\langle U' \cdot W' \rangle \quad , \tag{17}$$

where U' and W' are the random parts of the horizontal and vertical components of the wind velocity. The average and random parts of each component are defined as follows:

$$U = \overline{U} + U' \quad ; \quad \langle U \rangle = \overline{U} \quad ; \quad \langle U' \rangle = 0 \quad ;$$
$$V = \overline{V} + V' \quad ; \quad \langle V \rangle = \overline{V} = \langle V' \rangle = 0 \quad ;$$
$$W = \overline{W} + W' \quad ; \quad \langle W \rangle = \overline{W} \quad ; \quad \langle W' \rangle = 0 \quad .$$

Consequently, if high time resolution data of the horizontal and vertical components of the wind velocity are available, the friction velocity $U_*$ can be calculated according to Equation (17).

Such data were available for the LLNL Burro Tests 7, 8, and 9 (Reference 61) and the results are summarized in Table 14. Three stations were available in Tests 7 and 9, and four stations were available in Test 8 Measurements were made at three heights: 1, 3, and 8 m, except for Station T4 where measurements were made at only the two lower heights. The average $U_*$ from all measurements, plus the standard deviation (sigma) and the ratio of sigma to the average $U_*$ are also listed in Table 14. The ratio of sigma to the average $U_*$ ranges from 10 to 20% for these tests. Table 14 also lists the average $U_*$ obtained from Station T1 the station from which the surface-layer prediction of $U_*$ was made using the mean velocity and temperature profiles.

Table 15 compares the friction velocity calculated from the surface-layer profile fit method with the value obtained from the mean flux method of Equation (17), first for the measurements only at Station T1 and then for all

TABLE 14. NINE-MINUTE AVERAGE OF $[-\langle U' \cdot W' \rangle]^{1/2}$ FOR BURRO TESTS 7, 8, AND 9.

| Station and elevation (m) | Burro 7 | Burro 8 | Burro 9 |
|---|---|---|---|
| T1Z1 | 0.4093 | 0.0782 | 0.2483 |
| Z3 | 0.5069 | 0.0941 | 0.2776 |
| Z8 | 0.4440 | 0.0824 | 0.2613 |
| Average T1 | 0.4534 | 0.0849 | 0.2624 |
| T2Z1 | 0.3858 | 0.0754 | 0.2683 |
| Z3 | 0.4262 | 0.0726 | 0.3371 |
| Z8 | 0.4152 | 0.1197 | 0.4288 |
| T3Z1 | -- | 0.1174 | -- |
| Z3 | -- | 0.1023 | -- |
| Z8 | -- | 0.1119 | -- |
| T4Z1 | 0.5148 | 0.0909 | 0.3575 |
| Z3 | 0.4678 | 0.0836 | 0.2796 |
| Average $U_*$ | 0.4463 | 0.0935 | 0.3073 |
| Sigma | 0.0431 | 0.0162 | 0.0581 |
| Sigma/average $U_*$ | 0.0966 | 0.1737 | 0.1890 |

TABLE 15. COMPARISON OF FRICTION VELOCITY VALUES ($U_*$).

| | | Burro 7 | Burro 8 | Burro 9 |
|---|---|---|---|---|
| I. | Surface-layer theory Station T1 | 0.377 | 0.075 | 0.254 |
| II. | Equation 17 Average of Station T1 | 0.453 | 0.085 | 0.262 |
| III. | Equation 17 Average of all stations | 0.446 | 0.094 | 0.307 |
| IV. | $[(I - III)^2/(I \cdot III)]^{1/2}$ | 0.17 | 0.23 | 0.19 |

available stations. As expected, the comparisons with the measurements at Station T1 were as good as or better than those using all stations. The difference between the two methods for calculating $U_*$ is about 20 percent, and in all three cases, the mean flux method gave the higher value.

The amount of data used in this analysis was limited. Consequently, an estimate of the general uncertainty in the calculation of friction velocity is risky. The variation of $U_*$ using the mean flux method at various field locations ranged from 10 to 20 percent, and the variation between the mean profile fit method and the mean flux method was typically 20 percent. Thus, from these limited comparisons, an uncertainty of about 20 percent can be expected in the estimate of the friction velocity $U_*$.

## SECTION III

## PARAMETERS USED TO DESCRIBE A DISPERSING DENSE-GAS CLOUD

### A. HEAVY GAS DISPERSION AND MODEL VALIDATION

Modeling the atmospheric dispersion of heavy gases requires a somewhat different approach from the one used for the dispersion of trace gases. In a trace gas release, the quantity of material released to the atmosphere is too small to affect the atmospheric flow into which it is mixing. Consequently, trace gas dispersion is controlled solely by the advective and diffusive properties of the ambient atmosphere. However, a dense gas release behaves more like an independent, continuous cloud whose physical properties (density, temperature, turbulence level) differ significantly from those of the ambient atmosphere. Furthermore, the dispersion of a heavy gas cloud is controlled as much, if not more, by these in-cloud properties as by the conditions existing in the ambient atmosphere.

Basically, three major effects are observed in the dispersion of dense gas clouds that are not observed in the dispersion of trace emissions. First, turbulent mixing within the vapor cloud is reduced because of stable stratification of the dense layer. Second, gravity spreading and self-induced vortices occur because of density gradients in the horizontal direction. These two effects produce a lower and significantly wider cloud than is observed when a trace or neutral density gas is released. Third, cloud lingering occurs when the dense gas cloud travels downwind at a slower rate than the ambient windspeed because of reduced mixing between the dense gas layer and the ambient atmosphere.

These effects are most pronounced when the ambient windspeed is low and the atmospheric conditions are stable. As the cloud mixes with the surrounding ambient atmosphere, the cloud becomes more dilute, the in-cloud

properties approach ambient levels, and the above-mentioned effects begin to play a less significant role. Eventually, after a considerable amount of dilution, the originally heavy gas cloud begins to disperse in a manner similar to a trace gas cloud, where dispersion is primarily controlled by the ambient windspeed and atmospheric stability.

To determine whether a model accurately predicts these effects, we can compare the predictions against the results of field-scale dispersion experiments. The varied interests of model developers, users, and evaluators has led to the use of numerous cloud parameters in comparing model predictions with observation. For example, a model developer interested in evaluating the gravity spread aspects of a model might use the location of the leading edge of the cloud or the cloud width as measures for comparison. In a hazard assessment, one might be interested in the average concentration above some specified lower limit and the area exposed to these levels of concentration. Some more common parameters include height and width of the cloud, velocity of the leading edge, maximum extent of the lower flammability limit (LFL) in combustible gas releases, and horizontal extent of the visible cloud, as well as average and peak concentration. Various cloud parameters used in model validation studies are given in Table 16 (from Reference 62).

The number of cloud parameters creates some confusion regarding the best way to compare model predictions with observation; in addition, another element that is often overlooked not only adds confusion but can render the comparison meaningless. This element is the definition of the particular cloud parameter and the essential requirement that a single definition of the parameter be used for all models and field data. Thus, if average concentration is used in a comparison, the duration of the averaging time must be the same for all data and it must be equal to that assumed in the models. Similarly, when cloud parameters such as height, width, and location of the leading edge are used, they must be defined uniformly for both the model predictions and the experimental observation. The limitations of data collection and the specific requirements of certain models will, at times, require some compromise; however, this must be noted and done judiciously.

TABLE 16. DESCRIPTION OF DENSE-GAS CLOUD PARAMETERS.

| | |
|---|---|
| $R(t)$, $R(x)$ | Radius as a function of time and downwind distance, respectively. Some models use crosswind width and downwind length. |
| $h(t)$, $h(x)$ | Height as a function of time and downwind distance, respectively. |
| $x_{CEN}(t)$ | Location of cloud center as a function of time. |
| $x_{LE}(t)$ | Location of cloud leading edge as a function of time. |
| $x_{TE}(t)$ | Location of cloud trailing edge as a function of time. |
| $x_{MAX}(t)$ | Location of the maximum concentration as a function of time. |
| $\bar{C}(t)$, $\bar{C}(x)$ | Bulk concentration as a function of time and downwind distance, respectively |
| $C(L,t)$ | Concentration at location L and at time t. |
| $C_{MAX}(t)$, $C_{MAX}(x)$ | Peak concentration as a function of time and downwind distance, respectively. |
| $x_{LFL}$, $x_{1/2\text{-}LFL}$ | Maximum downwind extent of the LFL and 1/2-LFL concentration, respectively. |
| Concentration contours[a,b] | Horizontal and vertical contours at specified levels. |
| UFL/LFL contours | Contours of the upper and lower flammability levels. |

Source: Reference 62.

[a]Contours also have been obtained from the visible outline of LNG and LPG spills and compared with model predictions (Reference 9).

[b]Comparisons using horizontal contours could give cloud width and those using vertical contours could give cloud height as functions of time or downwind distance. However, they may not do so explicitly.

## B. CHOICE OF CLOUD PARAMETERS

The physical processes associated with the atmospheric dispersion of a dense gas release significantly modify the entire three-dimensional concentration distribution in time and space. This effect is most easily observed in the exaggerated width and reduced height of a dispersing heavy gas cloud. Other phenomena include cloud bifurcation, where the cloud splits into two plumes with the cloud centerline becoming a relative minimum in concentration rather than a maximum, and cloud lingering, where the cloud travels downwind at a considerably slower rate than the ambient windspeed. Both effects have been observed under low windspeed, stable atmospheric conditions.

Because these dense gas phenomena interact in a complex manner, we can obtain good agreement between prediction and observation of one cloud parameter which can be more fortuitous than a measure of the model's validity. A model may appear to be quite accurate when actually one error is canceling another. For example, a model might predict the downwind centerline concentration quite well for a specific set of conditions while greatly underestimating the cloud width and overestimating the cloud height because gravity spread and turbulence damping are neglected. This result would undoubtedly be uncovered by expanding the meteorological conditions under which model-data comparisons are conducted. However, the deficiency in the model could be readily detected by a comparison based on cloud structure (such as a measure of cloud height and width) without obtaining more experimental data.

Consequently, heavy gas dispersion models can be best evaluated by using parameters associated with cloud structure as well as cloud concentration. Of particular concern in this study are models used to predict cloud dispersion from continuous sources where the major independent variable is the downwin direction. In this case, the simplest cloud parameters would be cloud width, height, and concentration (i.e., peak concentration, average concentration,

centerline concentration, etc.) all as a function of downwind distance. Using both cloud structure and concentration parameters to test dense gas dispersion models against field data obtained under various atmospheric and terrain conditions will result in greater confidence when applying the models beyond the range of observation.

## C. CONCENTRATION AVERAGING TIME

In general, the concentration measured in an atmospheric dispersion experiment is always an average concentration where the average is over some period of time ($\tau$). This averaging time $\tau$ is the instrument averaging or response time plus the time used to process the data to make the averaging time the same for all instruments. In denser-than-air dispersion, experiments, $\tau$ is generally short, typically between 1 and 10 seconds. These tests are designed to study the hydrodynamics of dense gas flow and/or the flammability limits resulting from the dispersion of combustible gases, both of which depend on the "instantaneous" concentration rather than a long-duration average concentration.

The experiments of interest in this study are assumed to approximate the ideal plume experiment, where the direction of the plume is constant and the cloud has reached a steady state for a significant part of the experiment. As discussed, the measured concentration at time t, designated as $C(t;\tau)$, is actually a short-duration average concentration. For the remainder of this report, the term "concentration" refers to the sequence of short-duration average concentration measurements $C(t;\tau)$ from the beginning to the end of the experiment. The term "average concentration," designated as $\bar{C}(\tau)$, refers to the average of these measurements taken over the steady-state period. Since variation in plume direction is assumed to be negligible, the average concentration $\bar{C}(\tau)$ approaches a well-defined and constant limiting value as the steady-state period T becomes sufficiently large.

## D. SELECTED MEASURES OF PLUME DISPERSION

The measures of plume dispersion used in this report are maximum concentration $C^m$, average concentration $\bar{C}$, average cloud half-width W, and average cloud height H. These characteristics are considered to be functions of downwind distance from the source. These characteristics were chosen because of the type of experiments from which the data are obtained---namely, steady-state experiments where the direction of the plume is assumed to be well-defined and steady. Consequently, the plume centerline is also well-defined.

The four plume characteristics are more fully described as follows:

$C^m_{(x)}$ = the maximum measured plume concentration $C(t;\tau)$ as a function of downwind distance x from the source. The maximum is chosen from all instrument locations at a given downwind distance from the source irrespective of the vertical and horizontal displacement from the plume centerline.

$\bar{C}(x)$ = the ground level, plume centerline average concentration $\bar{C}(\tau)$, or the ground level, lobe centerline average concentration if the plume is bifurcated as a function of downwind distance x from the source. The average is taken for the entire steady-state period. Clearly, some interpolation is generally needed since the data are measured at points that may not coincide with the plume centerline.

W(x) = the plume half-width, defined by $\bar{C}(x,W,0) = 0.1\ \bar{C}(x)$, where $\bar{C}(x)$ is the average ground level, centerline concentration as defined above. Thus, W is equal to the distance between the plume centerline and the point where the average concentration drops to 1/10 the centerline value.

H(x) = the plume height, defined by $\bar{C}(x,0,H) = 0.1\ \bar{C}(x)$, where $\bar{C}(x)$ is the average ground level, centerline concentration as defined above. Thus, H is equal to the distance between the plume centerline and the point where the average concentration drops to 1/10 the centerline value.

The maximum concentration was chosen as a plume characteristic because it is relevant to safety analysis. Furthermore, it is obtained directly from the data, often without further manipulation. The average centerline concentration was chosen as a plume descripter because it can be directly compared to model predictions. The centerline value as a function of downwind distance was chosen so that high concentrations would correspond to values obtained from the near-field region, and low concentrations would correspond to values obtained in the far field. Thus, we avoid the difficulties involved with treating low concentration levels at the edge of the plume.

Plume width and height were included to assess the effects of gravity flow on the height and width of the cloud as well as the effects of cloud dilution due to mixing with the surrounding atmosphere. The particular definition of height and width was not considered to be important. The particular choice was made because it is easier to implement this definition with the experimental data (since it is based directly on the average concentration) than it is other measures such as the root mean square.

These plume characteristics allow for considerable relaxation of time and space correlation between the observed and the predicted values. Since the comparisons are between steady-state values, time is essentially irrelevant. Correlation in space has been significantly relaxed since all parameters are functions of only downwind distance. Thus, correlation in the crosswind plane is totally neglected while correlation in the downwind distance is fully retained. The four measures of plume dispersion with their implied levels of relaxation in time and space correlation are believed to provide a description of the dispersing plume that is commensurate with the level of models that are of interest to the USAF.

# SECTION IV

## SUMMARY

A total of 26 tests were selected for this study. As mentioned, only continuous, finite duration releases from a direct vapor source, an evaporating pool, or a momentum jet were considered for the test summaries because they best represent typical accidental releases from a storage vessel or a transportation vehicle. Other criteria were qualitative in nature and fell into two dichotomous groups.

Our first goal was to have each test be a benchmark with a complete, high-quality set of ambient meteorological and gas cloud concentration data. To achieve this goal, we selected tests with the following characteristics:

- Most of the meteorological and gas sensing instruments were calibrated properly and functioned well during the test.
- Data acquisition and data storage systems operated properly througout the test.
- Wind direction remained nearly constant, and the dense gas plume centerline was well within the array of sensors throughout the test.
- Windspeed and atmospheric stability were nearly constant.

These characteristics reduced the number of acceptable tests for inclusion in the summaries.

Our second goal was to develop a broad data base of tests involving releases of various denser-than-air gases where dispersion occurred under a wide range of meteorological conditions. Therefore, we selected tests that:

- Involved releases of various denser-than-air gases.
- Were conducted under stable, neutral, and unstable atmospheric conditions as well as under low, medium, and high windspeeds.

To approach this goal we, at times, needed to reduce the criteria on data quality and completeness.

Summaries of the selected field experiments are presented in the appendices that correspond to the various test series conducted by LLNL, Shell, and the HSE. Each appendix includes a description of the test series, test summary notes that are specific to each series, and the selected test summaries. The test summaries are divided into five parts. Parts 1 and 2 provide a quantitative and narrative description of the test and the manner of release. Parts 3 and 4 quantitatively describe the ambient meteorolgical conditions and the vapor cloud characteristics. Part 5 lists specific comments regarding the test and the summarized data.

## REFERENCES


1. Koopman, R.P., et al., Burro Series Data Report, LLNL/NWC 1980 LNG Spill Tests, UCID-19075, Lawrence Livermore National Laboratory, Livermore, California, December 1982.

2. Koopman, R.P., et al., "Analysis of Burro Series 40-m³ LNG Spill Experiments," J. of Hazard. Mater., vol. 6, pp. 43-83, 1982.

3. Morgan, D.L., Jr., et al., Phenomenology and Modeling of Liquefied Natural Gas Vapor Dispersion, UCRL-53581, Lawrence Livermore National Laboratory, Livermore, California, April 1984.

4. Goldwire, H.C., Jr., et al., Coyote Series Data Report, LLNL/NWC 1981 LNG Spill Tests: Dispersion, Vapor Burn, and Rapid-Phase-Transition, UCID-19953, Lawrence Livermore National Laboratory, Livermore, California, October 1983.

5. Goldwire, H.C., Jr., et al., Desert Tortoise Series Data Report, 1983 Pressurized Ammonia Spills, UCID-20562, Lawrence Livermore National Laboratory, Livermore, California, December 1985.

6. Koopman, R.P., et al., "Results of Recent Large-Scale $NH_3$ and $N_2O_4$ Dispersion Experiments," in Heavy Gas and Risk Assessment--III (S. Hartwig, Ed.), D. Reidel Publ. Co., Boston, Massachusetts, 1984.

7. McRae, T.G., et al., Eagle Series Data Report: 1983 Nitrogen Tetroxide Spills, UCID-20063-Rev. 1, Lawrence Livermore National Laboratory, Livermore, California, March 1987.

8. McRae, T.G., Analysis and Model/Data Comparisons of Large-Scale Releases of Nitrogen Tetroxide, UCID-20388, Lawrence Livermore National Laboratory, Livermore, California, March 1985.

9. Puttock, J.S., Colenbrander, G.W., and Blackmore, D.R. "Maplin Sands Experiments 1980: Dispersion Results from Continuous Releases of Refrigerated Liquid Propane and LNG," in Air Pollution Modeling and Its Application III (C. DeWispelaere, Ed.), Plenum Press, New York, 1983.

10. Colenbrander, G.W., and Puttock, J.S., "Maplin Sands Experiments 1980: Interpretation and Modeling of Liquefied Gas Spills on Sea," in Atmospheric Dispersion of Heavy Gases and Small Particles (G. Ooms and H. Tennekes, Eds., Springer-Verlag, New York, 1984.

11. Puttock, J.S., Colenbrander, G.W., and Blackmore, D.R., "Maplin Sands Experiments 1980: Dispersion Results from Continuous Releases of Refrigerated Liquid Propane," in Heavy Gas and Risk Assessment--II S. Hartwig, Ed.), D. Reidel Publ. Co., Boston, Massachusetts, 1983.

12. Colenbrander, G.W., Evans, A., and Puttock, J.S. Spill Tests of LNG and Refrigerated Liquid Propane on the Sea, Maplin Sands, 1980: Dispersion Data Digests, Thornton Research Centre, Shell Research Limited, UK., 1984.

13. Health and Safety Executive, Heavy Gas Dispersion Trials Thorney Island 1982-3: Data for Trials, Research and Laboratory Services Division, Red Hill, Sheffield, UK, 1984.

14. McQuaid, J. (Ed.), "Heavy Gas Dispersion Trials at Thorney Island," special issue of J. of Hazard. Materials, vol. 11, 1987.

15. McQuaid, J. (Ed.), "Heavy Gas Dispersion Trials at Thorney Island-2," Special Issue of J. of Hazard. Materials, vol. 16, 1987.

16. McQuaid, J., and Roebuck, B., Large-Scale Field Trials on Dense Vapour Dispersion, Health and Safety Executive, Safety Engineering Laboratory, Sheffield, UK, 1987.

17. Pasquill, F., "The Estimation of the Dispersion of Windborne Material," Meteorol. Mag., vol. 90, pp. 33-49, 1961.

18. Gifford, F.A., Jr., "Use of Routine Meteorological Observations for Estimating Atmospheric Dispersion," Nucl. Safety, vol. 2, no. 4, pp. 47-57, 1961.

19. Turner, D.B., "Relationships Between 24-Hour Mean Air Quality Measurements and Meteorological Factors in Nashville, Tennessee," J. Air Pollut. Control Ass., pp. 483-489, 1961.

20. Turner, D.B., "A Diffusion Model for an Urban Area," J. Appl. Meteorol., vol. 3, no. 1, pp. 83-91, 1964.

21. Turner, D.B., "Workbook of Atmospheric Dispersion Estimates," U.S. Public Health Service, Publication 999-AP-26, Robert A. Taft Sanitary Engineering Center, Cincinnati, Ohio, 1967.

22. Klug, W., "Ein Verfabren zur Bestimmung der Ausbreitungsbedingungen aus synoptischen Beobachtungen" (in German), Staub, vol. 29, no. 4, pp. 143-147 (1969).

23. Cramer, H.E., "A Practical Method for Estimating the Dispersal of Atmospheric Contaminants," in Proceedings of the First National Conference on Applied Meteorology, Section C, pp. 33-55, American Meteorological Society, Hartford, Connecticut, 1957.

24. Cramer, H.E., "Engineering Estimates of Atmospheric Dispersion Capacity," presented at the annual meeting of the American Industrial Hygiene Association, Chicago, Illinois, April 30, 1959.

25. Carpenter, S.B., et al., "Principal Plume Dispersion Models: TVA Power Plants," J. Air Pollut. Control Ass., vol. 21, pp. 491-495, 1971.

26. Gifford, F.A., "Turbulent Diffusion-Typing Schemes: A Review," Nuclear Safety, vol. 17, no. 1, 1976.

27. Pasquill, F., and Smith, F.B., Atmospheric Diffusion, 3rd Ed., John Wiley and Sons, New York, 1983.

28. Meteorology and Atomic Energy--1968, D.H. Slade (Ed.), USAEC Report TID-24190, Environmental Science Services Administration, 1968.

29. Smith, F.B., "A Scheme for Estimating the Vertical Dispersion of a Plume from a Source near Ground Level," in Proceedings of the Third Meeting of the Expert Panel on Air Pollution Modeling, NATO-CCHS Report 14, North Atlantic Treaty Organization, Brussels, 1972.

30. Briggs, G.A., "Diffusion Estimation for Small Emissions," in Environmental Research Laboratories, Air Resources Atmosphere Turbulence and Diffusion Laboratory 1973 Annual Report, USAEC Report ATDL-106, National Oceanic and Atmospheric Administration, 1974.

31. Businger, J.A., "Turbulent Transfer in the Atmospheric Surface Layer," in Workshop on Micrometeorology, (D.A. Haugen, Ed.), American Meteorology Society, Boston, Massachusetts, 1972.

32. Priestly, C.H.B., Turbulent Transfer in the Lower Atmosphere, University of Chicago Press, 1959.

33. Lumley, J.L., and Panofsky, H.A., The Structure of Atmospheric Turbulence, John Wiley and Sons, New York, 1964.

34. Monin, A.S., and Yaglom, A.M., "Statistical Hydromechanics," in The Mechanics of Turbulence, Part 1, Trans-Joint Publication Research Service, Washington, 1965, JPRS, vol. 37, p. 763, 1966.

35. Prandtl, L., "Meteorologische Anwenderngen der Stromungslehre," Phys. Atmos., vol. 19, pp. 188-202, 1932.

36. Yaglom, A.M., Comments on wind and temperature flux-profile relationships, Boundary-Layer Meteorology, vol. 11, pp. 89-102, 1977.

37. Dyer, A.J., A review of flux-profile relationships, Boundary-Layer Meteorology, vol. 7, pp. 363-372, 1974.

38. Luna, R.E., and Church, H.W., "A Comparison of Turbulence Intensity and Stability Ratio Measurements to Pasquill Turbulence Types," in Conference on Air Pollution Meteorology, American Meteorological Society, April 5-9, 1971, Raleigh, North Carolina, available from the American Meteorological Society, Boston, Massachusetts; also, USAEC Report SC-DC-70-5443, Sandia National Laboratories, Livermore, California, 1970.

39. Luna, R.E. and Church, H.W., "A Comparison of Turbulence Intensity and Stability Ratio Measurements to Pasquill Stability Classes," J. Appl. Meteorol., vol. 11, no. 4, pp. 663-669, 1972.

40. Golder, D., "Relations among Stability Parameters in the Surface Layer," Boundary-Layer Meteor., vol. 3, pp. 47-58, 1972.

41. Islitzer, N.F., "Program Review and Summary of Recent Accomplishments at NRTS" in Conference on AEC Meteorological Activities, May 19-22, 1964, USAEC Report BNL-914, pp. 57-64, Brookhaven National Laboratory, Upton, New York, 1965.

42. Gifford, F., "Diffusion in the Diabatic Surface Layer," J. Geophys. Res., vol. 67, no. 8, pp. 3207-3212, 1962.

43. Pasquill, F., and Smith, F.B., "The Physical and Meteorological Basis for the Estimation of the Dispersion of Windborne Material," in Proceedings of the Second International Clean Air Congress, Washington, D.C., 1970, (H.M. Englund and W.T. Beery, Eds.), pp. 1067-1072, Academic Press, Inc., New York, 1971

44. Slade, D.H. (Ed.), Meteorology and Atomic Energy (1968), U.S. Atomic Energy Commission, Office of Information Services.

45. Krugermeyer, L., "Vertikale Transporte von Impuls, Sensibler und Latenter Warme aus Profilmessunger uber dem Tropischen Atlantik Wahrend APEX," Berichte des Inst. fur Radiometeorologie und Maritime Meteorologie, Hamburg, 1975.

46. Klug, W., "Determination of Turbulent Fluxes of Heat and Momentum from the Wind Profile," Quart. J. Roy. Meteor. Soc., vol. 93, pp. 101-104, 1967.

47. Paulsen, C.A., "The Mathematical Representation of Wind Speed and Temperature Profiles in the Unstable Atmospheric Surface Layer," J. Appl. Meteorol., vol 9, pp. 857-861, 1970.

48. Nieuwstadt, F, "The Computation of the Friction Velocity $U_*$ and the Temperature Scale $T_*$ from Temperature and Wind Velocity Profiles by Least Square Methods," Boundary-Layer Meteorol., vol. 14, pp. 235-246, 1978.

49. Colenbrander, G.W., and Puttock, J.S., "Maplin Sands Experiments 1980: Interpretation and Modelling of Liquefied Gas Spills onto the Sea," I.U.T.A.M. Symposium on Atmospheric Dispersion of Heavy Gases and Small Particles, Delft, 1983.

50. Davies, M.E., and Singh, S., "Thorney Island: Its Geography and Meteorology," J. Hazard Mater., vol. 11, pp. 91-124, 1985.

51. Health and Safety Executive, Heavy Gas Dispersion Trials Thorney Island 1982-3: Data for Trials, Research and Laboratory Services Division, Red Hill, Sheffield, 1984.

52. Sedefian, L., and Bennett, E., "A Comparison of Turbulence Classification Schemes," Atmospheric Environment, vol. 14, no. 7, pp. 741-750, 1980.

53. McQuaid, J., "Climatological Records from the Thorney Island Mast," Commercial in Confidence HGDT Report 1981/6, 1981.

54. Pasquill, F., Atmospheric Diffusion, 2nd Ed., Ellis Horwood Ltd., Chichester, 1974.

55. Smith, F.B., "The Relation between Pasquill Stability P and Kazanski-Monin Stability (Neutral and Unstable Conditions)," Atmospheric Environment, vol. 13, pp. 879-881, 1979.

56. Koopman, R.P., et al., Burro Series Data Report, LLNL/NWC 1980 LNG Spill Tests, UCID-19075, Lawrence Livermore National Laboratory, Livermore, California, December 1982.

57. Goldwire, H.C., Jr., et al., Coyote Series Data Report, LLNL/NWC 1981 LNG Spill Test: Dispersion, Vapor Burn, and Rapid-Phase Transition, UCID-19953, Lawrence Livermore National Laboratory, Livermore, California, October 1983.

58. Goldwire, H.C., Jr., et al., Desert Tortoise Series Data Report, 1983 Pressurized Ammonia Spills, UCID-20552, Lawrence Livermore National Laboratory, Livermore, California, December 1985.

59. McRae, T.G., et al., Eagle Series Data Report: 1983 Nitrogen Tetroxide Spills, UCID-20063-Rev. 1, Lawrence Livermore National Laboratory, Livermore, California, March 1987.

60. Colenbrander, G.W., Evans, A.E. and Puttock, J.S., Spill Tests of LNG and Refrigerated Liquid Propane on the Sea, Maplin Sands, 1980: Dispersion Data Digests, Thornton Research Centre, Shell Research Limited, UK, 1984.

61. Rodean, H.C., and Cederwall, R.T., Analysis of Turbulent Wind-Velocity and Gas-Concentration Fluctuations During the Burro Series 40-$m^3$ LNG Spill Experiments, UCRL-53353, Lawrence Livermore National Laboratory, Livermore, California, 1982.

62. Mercer, A., Methods of Validating Models of Dense Gas Dispersion: A Review, Health and Safety Executive, Research and Laboratory Services Division, Safety Engineering Laboratory, Sheffield, 1986.



The reverse of this page is blank.

# APPENDIX A

# LLNL BURRO AND COYOTE TESTS (LNG)

## A. DESCRIPTION OF TEST SERIES

### 1. History of the Burro and Coyote Series

Under the sponsorship of the U.S. Department of Energy and the Gas Research Institute, two series of field experiments with liquefied natural gas (LNG) were conducted jointly by Lawrence Livermore National Laboratory (LLNL) and the Naval Weapons Center (NWC) at the NWC facility in China Lake, California. The Burro series, conducted in 1980, was designed to determine the transport and dispersion of vapor from spills of LNG on water. The Coyote series, conducted in 1981, further investigated the phenomenology of rapid-phase-transition (RPT) explosions, which had been observed during two of the Burro experiments, as well as the characteristics of fires resulting from ignition of vapor clouds from LNG spills (Reference A-1).

### 2. Series Summary

Nine tests were completed between June 6 and September 17, 1980, during the Burro series. Burro 3, 7, 8, and 9 were nominally 40-$m^3$ spills with durations of 167, 174, 107, and 79 seconds, respectively (Reference A-2). The Coyote series consisted of ten experiments from September 3 to November 24, 1981. Spill volumes and durations were as follows: 14.6 $m^3$ and 65 seconds, 28.0 $m^3$ and 98 seconds, and 22.8 $m^3$ and 82 seconds for Coyote 3, 5, and 6, respectively (Reference A-3). Tests were initiated by spilling LNG onto the surface of a 1-m-deep pool of water. The LNG exited from a pipe 25 cm in diameter and about 1 meter above the surface of the pond, flowing straight down. A splash plate was installed below the spill pipe outlet at a shallow depth beneath the water surface to limit LNG penetration into the water. Consequently, after the LNG stream encountered the splash plate, it was directed radially outward along the surface of the water. The water basin was 58 m in diameter.

3. Terrain

Ground level immediately surrounding the water basin was about 1.5 meters above the water level. Downwind (northeast) of the spill pond, the terrain sloped upward, at about a 7° angle until it reached a height of 7 meters above the water level at a downwind distance of 80 meters, thereafter, it remained relatively flat. In this region, the terrain sloped slightly (less than 1°), rising to the left and dropping to the right. A gully just beyond the right side of the instrumentation array dropped to an elevation of 4 to 6 meters below the centerline of the array. The gully encompassed the southeast edge of the array at 140 meters downwind.

4. Instrumentation

A large array of instruments for sensing gas concentrations and measuring temperatures and windspeeds was deployed to measure the characteristics of both the dispersing LNG vapor cloud and the ambient atmosphere. The instrument array for the Burro series is shown on a map of the test area in Figure A-1, and the corresponding array for the Coyote series is shown in Figure A-2. The array centerline was oriented at 225° (from the southwest), which coincides with the prevailing southwesterly wind direction for the summer season. The acceptance angle for the array was about 50° (from 200° to 250°).

The array was made up of three groups of instruments: (1) cup-and-vane anemometers to map the wind field, (2) gas sensors at three heights to track the LNG vapor cloud, and (3) propeller bivane anemometers and fast gas sensors also at three heights to measure turbulence effects and to track the cloud. The first group consisted of 20 stations with a single anemometer mounted at an elevation of 2 meters. Five of these stations were deployed upwind on or near the array centerline to measure the direction and speed of the incoming wind. The remaining 15 stations were deployed fairly uniformly downwind of the spill point. There were 25 gas stations (24 in the Coyote

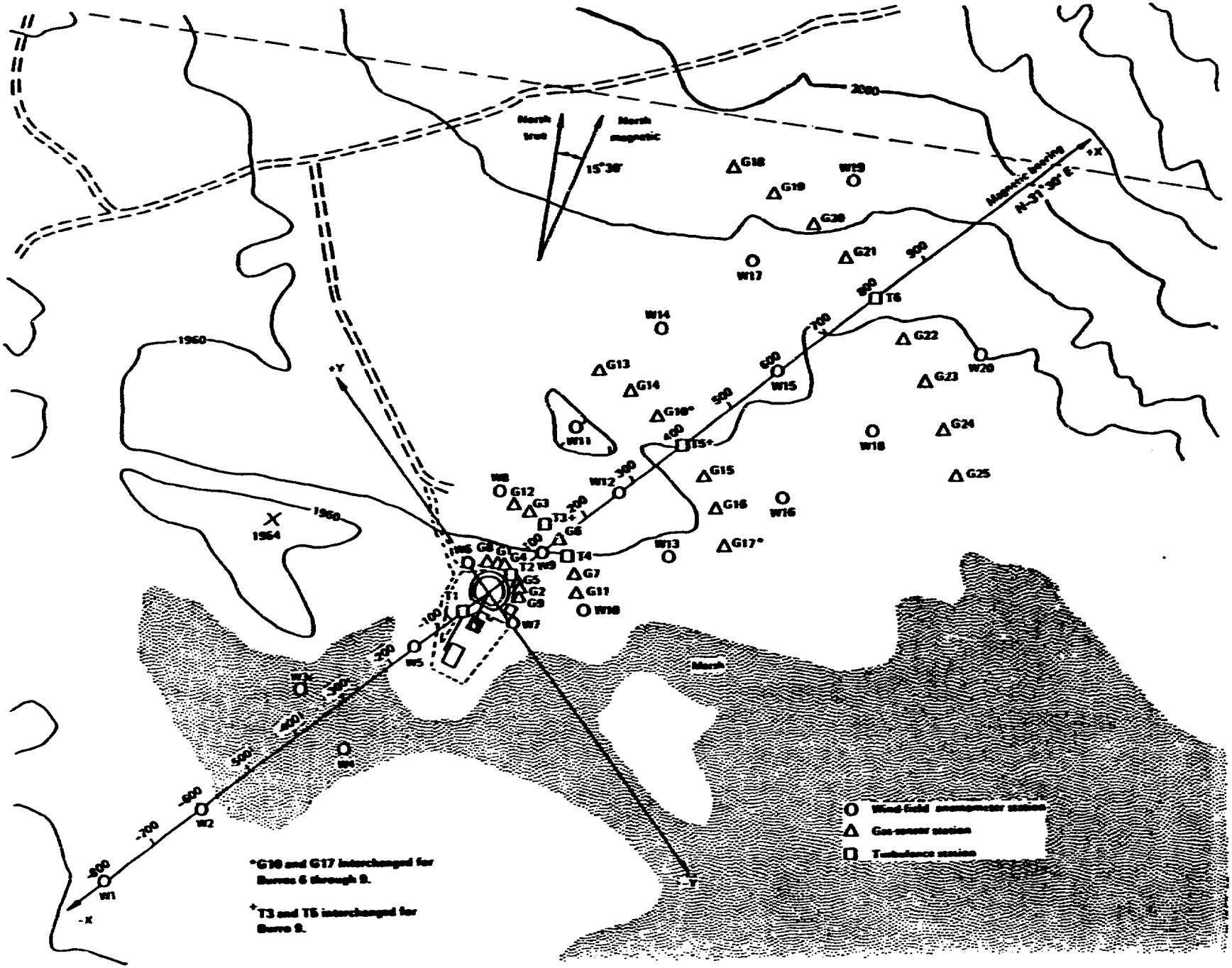


Figure A-1. Sensor Array for the Burro Series Experiments.

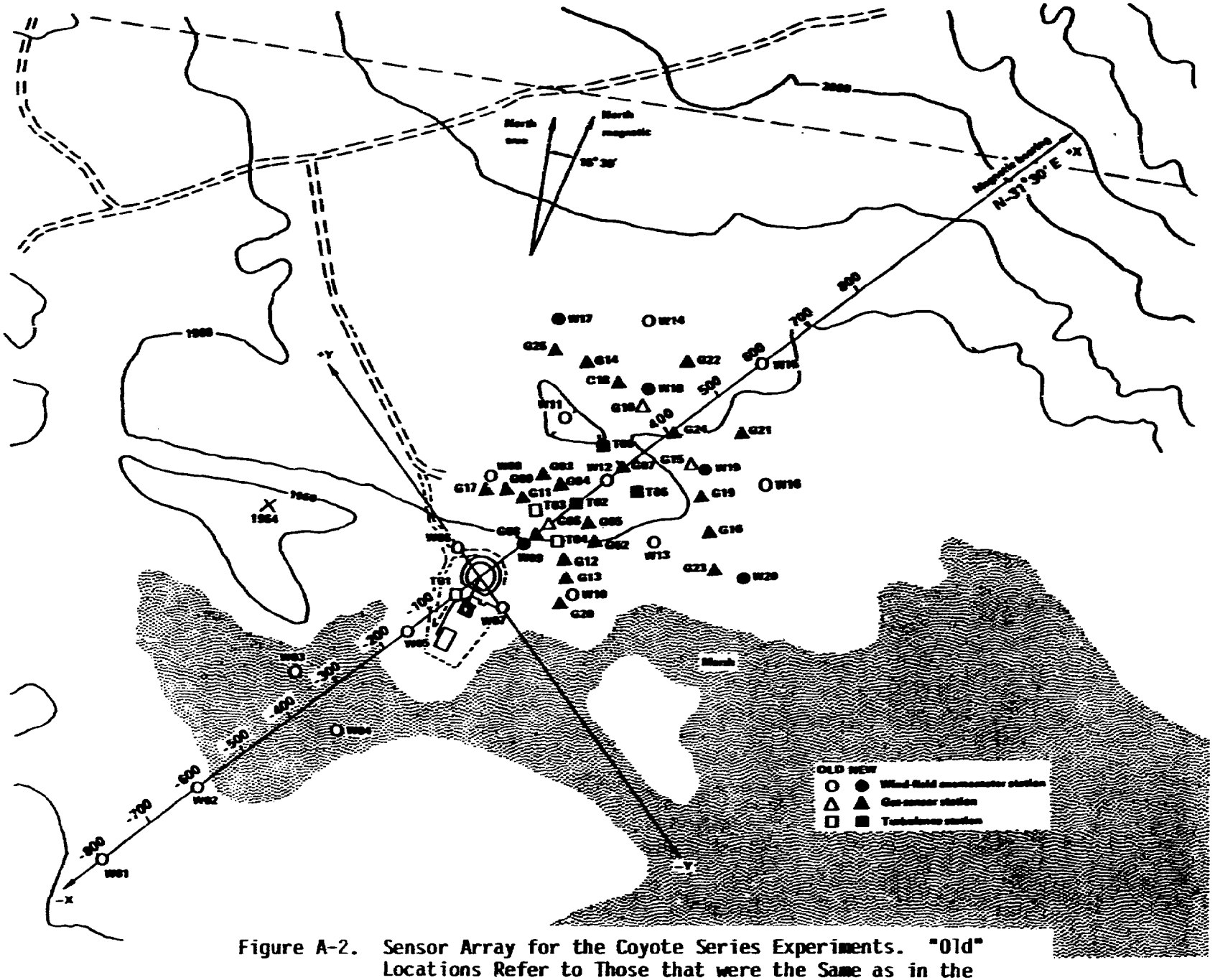


Figure A-2. Sensor Array for the Coyote Series Experiments. "Old" Locations Refer to Those that were the Same as in the Burro Series.

tests) and 5 turbulence stations arranged in arcs downwind from the spill point. In the Burro tests, the gas and turbulence stations were arranged in four arcs at 57, 140, 400, and 800 meters from the spill point. This array was rearranged in the Coyote series because of the special requirements of the vapor burn and RPT tests and because the Burro series demonstrated the desirability of concentrating the gas sensors in the zone from 100 to 500 meters downwind. In both test series, one turbulence station with no gas sensors was located just upwind of the spill basin.

Each turbulence station had three anemometers at heights of 1.36, 3, and 8 meters; three infrared (IR) gas sensors at 1, 3, and 8 meters; and thermocouples collocated with each gas sensor to provide temperature measurements of the gas cloud. The gas sensor stations were similar to these except they had no anemometers. Also, they took data at a slower rate than the turbulence stations (1 Hz as compared with 3.3 to 5 Hz), and they had some gas sensors other than the IR type. Seven gas stations had humidity and heat-flux sensors in addition to the gas and temperature sensors normally present.

5. Acquisition

All stations were battery powered and microprocessor controlled, with some onboard memory. They communicated with the data-recording trailer by radio telemetry, turning on instruments on command and sending back data when polled. Data were acquired at different rates from the various stations. The wind-field station data consisted of 10-s averages for speed, direction, and (new on the Coyote series) standard deviations of direction. Sensors on the gas stations were sampled at 1-second intervals, and those on the turbulence stations at 0.3- and 0.2-second intervals (Reference A-4).

B. Test Summaries

1. LLNL Burro 3

a. Test

| | |
|---|---|
| Name: | LLNL Burro 3 |
| Date: | July 2, 1980 |
| Material: | LNG (92.5% methane, 6.2% ethane, 1.3 propane) |
| Molecular Weight: | 0.016043 kg/mol (methane); 0.0307 kg/mol (ethane); 0.0411 kg/mol (propane) |
| Liquid Density: | 424.1 kg/m³ at -161.5°C (methane); 550 kg/m³ at -88.2°C (ethane); 580 kg/m³ at -42.1°C (propane) |
| Boiling Temperature: | 111.7 K (-161.5°C) (methane); 184.0 K (-88.2°C) (ethane); 231.1 K (-42.1°C) (propane) |
| Heat of Vaporization: | 8.18 kJ/mol at -161.5°C (methane); 15.02 kJ/mol at -88.2°C (ethane); 17.5 kJ/mol at -42.1°C (propane) |
| Heat Capacity (vapor): | 35.9 J/mol K (methane) |
| Release Mode: | Dispersion test. LNG was released through a 25-cm-diameter pipe, 1.5 m above the surface of the water basin. A splash plate was placed below the spill pipe outlet to limit LNG penetration into the water. The spill tank was pressurized with gaseous $N_2$. |

b. Source Data

| | |
|---|---|
| Spill Rate: | 88.4 kg/s |
| Spill Duration: | 166.8 s |
| Spill Mass: | 14752.6 kg |
| Spill Temperature: | 111.7 K (-161.5°C) |
| Source Description: | At approximately 150 s, the cloud bifurcated until 190 s. The bifurcation seems to be related to a local reduction in the windspeed near the spill pond. The cloud remained within the array except at the 57 m row, where it extended beyond both sides of the array during bifurcation. |

c. Atmospheric Conditions

| | | | |
|---|---|---|---|
| Avg. Windspeed: | 5.4 m/s at 2 m | $z_o$: | 0.0002 m |
| Sigma Windspeed: | 1.19 m/s | $U_*$: | 0.260 m/s |
| Sigma Wind Direction: | 13.3° | $\theta_*$: | -0.987 K |
| Avg. Temperature: | 306.95 K at 2 m | $\theta_o$: | 331.10 K |
| Barometric Pressure: | 948.0 mb | L: | -5.63 m |
| Relative Humidity: | 5.2% | Stability: | B |
| Cloud Cover: | -- | | |

d. Vapor Cloud Characteristics (Burro 3)

(1) Peak Concentration, $C_p$

| Downwind distance x (m) | Peak concentration, $C_p$ (vol%) | | |
|---|---|---|---|
| | 1 m | 3 m | 8 m |
| 57 | 28.3 | -- | -- |
| 140 | 9.0 | -- | -- |
| 400 | 0.8 | -- | 0.95 |
| 800 | 0.4 | 0.63 | -- |

(2) Average Cloud Characteristics

| Downwind distance, x (m) | Average Centerline concentration, C(x,0,0) (vol%) | Half-width, W (m) | Height, H (m) | Downwind flux ratio $Q_A/Q_s$ |
|---|---|---|---|---|
| 57 | 6.280 | 31.1 | 7.938 | 0.4680 |
| 140 | 6.248 | 70.4 | 7.621 | 0.9604 |
| 400 (N/A) | | | | |
| 800 (N/A) | | | | |

e. Comments

(1) Peak concentrations were measured at 1 m. Peak values at 3 m and 8 m are given when greater than 1 m peak values at 1 m.

(2) Widths at 57-m are time-averaged contour widths between 60 and 130 s.

(3) Heights at 57-m are 80-s averaged centerline heights for 5, 2, and 1% contours. A 3-point weighted least squares Gaussian fit of average centerline vertical values was used to get height parameters, C(x,0,0) and H.

(4) Heights of contours at 57-m were irregular so they were smoothed to get height parameters.

(5) Molecular weight of source gas was found by averaging the molecular weights of the components according to the composition.

(6) Heights at 140-m are 70-s averaged centerline heights for 5, 2, and 1%. A 3-point weighted least squares Gaussian fit of average centerline vertical values was used to get height parameters, C(x,0,0) and H.

The 100-s contour values were excluded because the crosswind centerline was slanted (1% and 2% peaks are about 60 m crosswind of 5% peak).

2. LLNL Burro 7

a. Test

| | |
|---|---|
| Name: | LLNL Burro 7 |
| Date: | August 27, 1980 |
| Material: | LNG (87% methane, 10.4% ethane, 2.6% propane) |
| Molecular Weight: | 0.016043 kg/mol (methane); 0.0307 kg/mol (ethane); 0.0411 kg/mol (propane) |
| Liquid Density: | 424.1 kg/m³ at -161.5°C (methane); 550 kg/m³ at -88.2°C (ethane); 580 kg/m³ at -42.1°C (propane) |
| Boiling Temperature: | 111.7 K (-161.5°C) (methane); 184.0 K (-88.2°C) (ethane); 231.1 K (-42.1°C) (propane) |
| Heat of Vaporization: | 8.18 kJ/mol at -161.5°C (methane); 15.02 kJ/mol at -88.2°C (ethane); 17.50 kJ/mol at -42.1°C (propane) |
| Heat Capacity (vapor): | 35.9 J/mol K (methane) |
| Release Mode: | Dispersion test. LNG was released through a 25-cm-diameter pipe, 1.5 m above the surface of the water basin. A splash plate was placed below the spill pipe outlet to limit LNG penetration into the water. The spill tank was pressurized with gaseous $N_2$. |

b. Source Data

| | |
|---|---|
| Spill Rate: | 99.9 kg/s |
| Spill Duration: | 174 s |
| Spill Mass: | 17385.1 kg |
| Spill Temperature | 111.7 K (-161.5°C) |
| Source Description: | The wind direction deviated 17° from the array centerline, causing the cloud to extend beyond the right side (northwest of the array during most of the test). The cloud bifurcated at 50 s and again at approximately 110 to 160 s. |

c. Atmospheric Conditions

| | | | |
|---|---|---|---|
| Avg. Windspeed: | 8.4 m/s at 2 m | $z_o$: | 0.0002 m |
| Sigma Windspeed: | 1.16 m/s | $U_*$: | 0.377 m/s |
| Sigma Wind Direction: | 5.21° | $\theta_*$: | -0.098 K |
| Avg. Temperature: | 306.85 K | $\theta_o$: | 314.45 K |
| Barometric Pressure: | 940.0 mb | L: | -113.5 m |
| Relative Humidity: | 71% | Stability: | D |
| Cloud Cover: | -- | | |

d. Vapor Cloud Characteristics (Burro 7)

(1) Peak Concentration, $C_p$

| Downwind distance, x (m) | Peak concentration, $C_p$ (vol%) | |
|---|---|---|
| | 1 m | 3 m |
| 57 | 17.5 | -- |
| 140 | 7.1 | 7.3 |
| 400 | 3.9 | -- |
| 800 | 0.55 | 0.79 |

(2) Average Cloud Characteristics

| Downwind distance, x (m) | Average Centerline concentration, C(x,0,0) (vol%) | Half-width, W (m) | Height, H (m) | Downwind flux ratio $Q_A/Q_s$ |
|---|---|---|---|---|
| 57 | 13.861 | 39.8 | 7.73 | 1.3041 |
| 140 | 5.739 | 39.5 | 7.772 | 0.7407 |
| 400 | 4.512 | 48.5 | 3.84 | 0.3396 |

e. Comments

(1) Peak concentrations were measured at 1 m. Peak values at 3 m are given when greater than peak values at 1 m.
(2) Widths at 57 m are time-averaged contour widths between 10 and 190 s excluding 50, 110, 140-160 values due to bifurcation.
(3) Heights at 57 m are 200-s average heights for 10, 5, 2, and 1% contours. A 4-point weighted least squares Gaussian fit of average centerline vertical values was used to get height parameters, C(x,0,0) and H.
(4) Average windspeed at tower T02 (57-m row) was used in place of the average ambient windspeed in $Q_A$ calculations.
(5) At 57 m, the centerline is near the edge of the grid, so contour height values may be good. However, width values are highly uncertain because a symmetric cloud shape about the array edge was assumed when the cloud may be asymmetric.
(6) Widths at 140 m are time-averaged contour widths between 140 and 160 s.
(7) Heights at 140 m are 30-s average heights for 5, 2, and 1% contours. A 3-point weighted least squares Gaussian fit of average centerline vertical values was used to get height parameters, C(x,0,0) and H (n = 1.852).
(8) Widths and heights at 400 m are from 180-s data only. A generalized exponential fit of centerline vertical values (1, 2, and 3.6%) was used to get height parameters, C(x,0,0) and H (n = 1.723).

3. LLNL Burro 8

a. Test

| | |
|---|---|
| Name: | LLNL Burro 8 |
| Date: | September 3, 1980 |
| Material: | LNG (87.4% methane; 10.3% ethane; 2.3% propane) |
| Molecular Weight: | 0.016043 kg/mol (methane); 0.0307 kg/mol (ethane); 0.0411 kg/mol (propane) |
| Liquid Density: | 424.1 kg/m³ at -161.5°C (methane); 550 kg/m³ at -88.2°C (ethane); 580 kg/m³ at 42.1°C (propane) |
| Boiling Temperature: | 111.7 K (-161.5°C) (methane); 184.0 K (-88.2°C) (ethane); 231.1 K (-42.1°C) (propane) |
| Heat of Vaporization: | 8.18 kJ/mol at -161.5°C (methane); 5.02 kJ/mol at -88.2°C (ethane); 17.50 kJ/mol at -42.1°C (propane) |
| Heat Capacity (vapor): | 35.9 J/mol K at 26.8°C |

Release Mode: Dispersion test. LNG was released through a 25-cm-diameter pipe, 1.5 m above the surface of the water basin. A splash plate was placed below the spill pipe outlet to limit LNG penetration into the water. The spill tank was pressurized with gaseous $N_2$.

b. Source Data

| | |
|---|---|
| Spill Rate: | 117 kg/s |
| Spill Duration: | 107 s |
| Spill Mass: | 12514 kg |
| Spill Temperature: | 111.7 K (-161.5°C) |

Source Description: The vapor cloud lingered over the source region for a considerable time after the spill was terminated. Photography showed that the cloud extended about 40 m upwind of the spill point as well as beyond both sides of the array. The cloud was bifurcated much of the time, probably due to the interaction between the lateral gravity flow and the longitudinal atmospheric flow. Both lobes appeared to be affected by the terrain.

c. Atmospheric Conditions

| | | | |
|---|---|---|---|
| Avg. Windspeed: | 1.8 m/s at 2 m | $z_o$: | 0.0002 m |
| Sigma Windspeed: | 0.27 m/s | $U_*$: | 0.075 m/s |
| Sigma Wind Direction: | 5.57° | $\theta_*$: | 0.029 K |
| Avg. Temperature: | 306.25 K at 2 m | $\theta_o$: | 310.76 K |
| Barometric Pressure: | 941.0 mb | L: | 15.1 m |
| Relative Humidity: | 4.6% | Stability: | E |
| Cloud Cover: | -- | | |

d. Vapor Cloud Characteristics (Burro 8)

(1) Peak Concentration, $C_p$

| Downwind distance, x (m) | Peak concentration, $C_p$ (vol%) | |
|---|---|---|
| | 1 m | 3 m |
| 57 | 56.0 | -- |
| 140 | 15.0 | 18.3 |
| 400 | 4.3 | 6.1 |
| 800 | 2.1 | -- |

(2) Average Cloud Characteristics

| Downwind distance, x (m) | | Average Centerline concentration, C(x,0,0) (vol%) | Half-width, W (m) | Height, H (m) | Downwind flux ratio $Q_A/Q_S$ |
|---|---|---|---|---|---|
| 57 | A | 24.098 | 34.1 | 5.093 | |
| | B | 27.248 | 30.8 | 4.286 | 0.2806 |
| 140 | A | 14.659 | 61.4 | 6.628 | |
| | B | 6.641 | 70.0 | 5.086 | 0.3436 |

e. Comments

(1) Peak concentrations were measured at 1 m. Peak values at 3 m are given when greater than peak values at 1 m.
(2) The plume bifurcated at 57 and 140 m and was lofted. Concentrations are less than 5% and 2% at 400 and 800 m, respectively, and are not analyzed for Section B.
(3) At 57 m, 20-s data between 40 and 200 s were treated separately in time and with respect to bifurcated plume. Contours were smoothed when irregular and assumed to be symmetric past grid boundaries. Fluxes from each portion of the plume were added at a given time and averaged. $Q_A/Q_S$ represents the average of the sum of the characteristics of the two lobes. Centerline concentration, half-width, and height are given for both lobes. Lobe A is on the left looking back toward the source; Lobe B is on the right.
(4) At 140 m, 20-s data between 80 and 280 s were treated similar to data at 57 m.
(5) Cloud speed at 1 m at 57 m was much less than the average ambient windspeed, $\bar{u}$ (1 m) = 0.8; $\bar{u}$ = 1.8 m/s. $Q_A$ calculation included 1-m cloud speed and not average ambient windspeed.
(6) Cloud speed at 1 m at 140 m varied for each lobe and was greater than average ambient windspeed. $Q_A$ calculation for each lobe included the 1-m windspeed for the lobe involved. T4 1-m windspeed was used for Lobe A; T3 1-m windspeed was used for Lobe B.

4. LLNL Burro 9

a. Test

| | |
|---|---|
| Name: | LLNL Burro 9 |
| Date: | September 17, 1980 |
| Material: | LNG (83.1% methane, 13.9% ethane, 3% propane) |
| Molecular Weight: | 0.016043 kg/mol (methane); 0.0307 kg/mol (ethane); 0.0411 kg/mol (propane) |
| Liquid Density: | 424.1 kg/m³ at -161.5°C (methane); 550 kg/m³ at -88.2°C (ethane); 580 kg/m³ at -42.1°C (propane) |
| Boiling Temperature: | 111.7 K (-161.5°C) (methane); 184.0 K (-88.2°C) (ethane); 231.1 K (-42.1°C) (propane) |
| Heat of Vaporization: | 8.18 kJ/mol at -161.5°C (methane); 15.02 kJ/mol at -88.2°C (ethane); 17.50 kJ/mol at -42.1°C (propane) |
| Heat Capacity (vapor): | 35.9 J/mol K |
| Release Mode: | Dispersion test. LNG was released through a 25-cm-diameter pipe, 1.5 m above the surface of the water basin. A splash plate was placed below the spill pipe outlet to limit the penetration of LNG into the water. The spill tank was pressurized with gaseous $N_2$. |

b. Source Data

| | |
|---|---|
| Spill Rate: | 136.7 kg/s |
| Spill Duration: | 79 s |
| Spill Mass: | 10799.9 kg |
| Spill Temperature: | 111.7 K (-161.5°C) |
| Source Description: | A series of RPT explosions occurred during this experiment. The large RPTs occurred at 21 and 35 s after the spill commenced releasing puffs of LNG vapor. |

c. Atmospheric Conditions

| | | | |
|---|---|---|---|
| Avg. Windspeed: | 5.7 m/s at 2 m | $z_o$: | 0.0002 m |
| Sigma Windspeed: | 0.74 m/s | $U_*$: | 0.254 m/s |
| Sigma Wind Direction: | 4.4° | $\theta_*$ | -0.009 K |
| Avg. Temperature: | 308.55 K at 2 m | $\theta_o$: | 314.21 K |
| Barometric Pressure: | 940.0 mb | L: | -544.5 m |
| Relative Humidity | 13.1% | Stability: | D |
| Cloud Cover: | 15% | | |

d. Vapor Cloud Characteristics (Burro 9)

(1) Peak Concentration, $C_p$

| Downwind distance, x (m) | Peak concentration, $C_p$ (vol%) | |
|---|---|---|
| | 1 m | 8 m |
| 57 | 10.0 | 11.75 |
| 140 | 10.6 | -- |
| 400 | 4.0 | 6.7 |
| 800 | 1.4 | 2.2 |

(2) Average Cloud Characteristics

| Downwind distance, x (m) | Average Centerline concentration, C(x,0,0) (vol%) | Half-width, W (m) | Height, H (m) | Downwind flux ratio $Q_A/Q_s$ |
|---|---|---|---|---|
| 57 | 5.530 | 30.1 | 11.3 | 0.3718 |
| 140 | 6.120 | 50.6 | 8.1 | 0.5225 |
| 400 | 4.105 | 85.0 | 13.9 | 1.9970 |

e. Comments

(1) Peak concentrations were measured at 1 m. Peak values are given at 8 m when greater than peak values at 1 m.
(2) At 57 m, the cloud became bifurcated between 30 and 40 s. Nonbifurcated cloud concentration contours were analyzed separately from bifurcated cloud concentration contours.
(3) Widths at 57 m are time-averaged contour widths between 30 and 80 s. Bifurcated plume widths were measured as though the cloud were a single plume.
(4) Heights at 57 m for the bifurcated stage are 30-s averaged centerline heights for 3, 2, and 1% contours for Lobe A and 5, 2, and 1% for Lobe B. Lobe A is on the left looking back toward source; Lobe B is on the right. Heights for the nonbifurcated stage are 50-s averaged centerline heights for 3, 2, and 1% contours. A 3-point weighted least squares Gaussian fit was used on each (Lobe A, Lobe B, nonbifurcated) to get height parameters and c(x,0,0).
(5) Average $Q_A$ was found by summing the $Q_A$ for each lobe and averaging the sum with nonbifurcated $Q_A$. The average C(x,0,0) is the average from each of the 3 fits. Average H was found by using the average of the highest $Z_e$ from Lobe A or B and the $Z_e$ from the nonbifurcated stage.
(6) Widths at 140 m are time-averaged contour widths between 30 and 110 s.
(7) Heights at 140 m are 90-s averaged centerline heights for 5, 2, and 1% contours. A 3-point weighted least squares Gaussian fit of average centerline vertical values were used to get height parameters, C(x,0,0) and H.
(8) Widths at 400 m are time-averaged contour widths between 110 and 150 s.
(9) Heights at 400 m are 60-s averaged centerline heights for 3.2 and 1% contours. A 3-point weighted least squares Gaussian fit of average centerline vertical values was used to get height parameters, C(x,0,0) and H.
(10) Errors in $Q_A$ calculation at 400 m can be attributed to low concentrations (hard measure) and a lofted plume. The peak concentration was assumed to be near the surface when in fact they were not.

5. LLNL Coyote 3

a. Test

| | |
|---|---|
| Name: | LLNL Coyote 3 |
| Date: | September 3, 1981 |
| Material: | LNG (79.4% methane, 16.4% ethane, 4.2% propane) |
| Molecular Weight: | 0.016043 kg/mol (methane); 0.0307 kg/mol (ethane); 0.0411 kg/mol (propane) |
| Liquid Density: | 424.1 kg/m³ at -161.5°C (methane) |
| Boiling Temperature: | 111.7 K (-161.5°C) (methane); 184.53 K (-88.63°C) (ethane); 231.09 K (-42.07°C) (propane) |
| Heat of Vaporization: | 8.18 kJ/mol at -161.5°C (methane) |
| Heat Capacity (vapor): | 35.9 J/mol K at 26.8°C (methane) |
| Release Mode: | Vapor burn test. LNG was released through a 25-m-diameter pipe, 1.5 m above the surface of the water basin. A splash plate was placed below the spill pipe outlet to limit LNG penetration into the water. The LNG was released at an average impact pressure of 6 psia with a maximum of 10 psia. The average exit temperature was -158°C. The spill tank was pressurized with gaseous $N_2$. |

b. Source Data

| | |
|---|---|
| Spill Rate: | 13.5 m³/min 95.42 kg/s |
| Spill Duration: | 65 s |
| Spill Mass: | 6202.4 kg (14.6 m³) |
| Spill Temperature: | 115 K (-158°C) |
| Source Description: | Data indicate turbulent cloud source. Visible cloud was about 2 m high with tufts to 6 or 7 m and extended 150 m downwind before disappearing. Leading edge of the cloud moved slower than the ambient windspeed from the source to 140 m. A cloud speed of about 3 m/s was assumed between the source and the igniter. The cloud was ignited 64.2 m downwind, 99.7 s after the valve opened. Flame or hot gas arrived 140 m downwind about 102 s after the spill began. The wind direction deviated 22° from the array centerline. |

c. Atmospheric Conditions

| | | | |
|---|---|---|---|
| Avg. Windspeed: | 6.0 m/s at 2 m | $z_0$: | 0.0002 m |
| Sigma Windspeed: | 0.9 m/s | $U_*$: | 0.310 m/s |
| Sigma Wind Direction: | 11° | $\theta_*$: | -0.866 K |
| Avg. Temperature: | 311.06 | $\theta_0$: | 334.43 K |
| Barometric Pressure: | 936. mb | L: | -9.24 m |
| Relative Humidity: | 11.3% | Stability: | B-C |
| Cloud Cover: | 15% | | |

d. Vapor Cloud Characteristics (Coyote 3)

(1) Peak Concentration, $C_p$

| Downwind distance x (m) | Peak concentration $C_p$ (vol%) |
|---|---|
| 110 | 7.3 |
| 140 | 8.4 |
| 200 | 4.5 |
| 300 | 2.0 at 3 m |
| 400 | 2.38 at 8 m |
| 500 | 0.76 at 3 m |

(2) Average Cloud Characteristics

| Downwind distance, x (m) | Average Centerline concentration, C(x,0,0) (vol%) | Half-width, W (m) | Height, H (m) | Downwind flux ratio $Q_A/Q_s$ |
|---|---|---|---|---|
| 140 | 6.28% | 56.9 | 8.66 | 0.9386 |
| 200 | 3.92 | 41.1 | 10.55 | 0.5864 |

e. Comments

(1) Peak concentrations were measured at 1 m except as noted.

(2) Widths at 140 m are time-averaged contour widths between 50 and 100 s. Widths at 200 m are time-averaged contour widths between 60 and 100 s.

(3) Heights at 140 m are 50-s average heights for 5, 2, and 1% contours. A generalized exponential fit of average centerline vertical values was used to get height parameters, C(x,0,0) and H (n = 1.419).

(4) Molecular weight of source gas was found by averaging components with respect to percentage of composition.

(5) Heights at 200 m row are 50-s average heights for 3, 2, and 1% contours. A 3-point weighted Gaussian fit of average centerline vertical values was used to get height parameters, C(x,0,0) and H.

6. LLNL Coyote 5

a. Test

| | |
|---|---|
| Name: | LLLNL Coyote 5 |
| Date: | October 7, 1981 |
| Material: | LNG (74.9% methane, 20.5% ethane, 4.6% propane) |
| Molecular Weight: | 0.016043 kg/mol (methane); 0.0307 kg/mol (ethane); 0.0411 kg/mol (propane) |
| Liquid Density: | 424.1 kg/m$^3$ at -161.5°C (methane) |
| Boiling Temperature: | 111.7 K (-161.5°C) (methane); 184.53 K (-88.63°C) (ethane); 231.09 K (-42.07°C) (propane) |
| Heat of Vaporization: | 8.18 kJ/mol at -161.5°C (methane) |
| Heat Capacity (vapor): | 35.9 J/mol K at 16.8°C (methane) |
| Release Mode: | Vapor burn test. LNG was released through a 25-cm-diameter pipe, 1.5 m above the surface of the water basin. A splash plate was placed below the spill pipe outlet to limit LNG penetration into the water. LNG was released at an average pressure of 8 psia with a maximum of 13 psia. The average exit temperature is unknown because the thermocouple was damaged. The spill tank was pressurized with gaseous $N_2$. |

b. Source Data

| | |
|---|---|
| Spill Rate: | 17.1 m$^3$/min 120.8 kg/s |
| Spill Duration: | 98 s |
| Spill Mass: | 11845.1 kg |
| Spill Temperature: | 112 K (-161°C) |
| Source Description: | The visible cloud was about 2 m high and extended 150 m downwind before disappearing. RPTs occurred between 101 and 105 s, sending large puffs of ethane-enriched gas into the cloud. The cloud was ignited at 79 m downwind, 132.7 s after the valve opened. Average flame or hot gas arrival at 140 m downwind was 138 s after the spill. Higher windspeeds during this test produced a narrower cloud than Coyote 3. Wind direction deviatied 2° from the array centerline. |

c. Atmospheric Conditions

| | | | |
|---|---|---|---|
| Avg. Windspeed: | 9.7 m/s at 2 m | $z_o$: | 0.0002 m |
| Sigma Windspeed: | 1.3 m/s | $U_*$: | 0.480 m/s |
| Sigma Wind Direction: | 7° | $\theta_*$: | -0.544 K |
| Avg. Temperature: | 301.05 K | $\theta_o$: | 318.12 K |
| Barometric Pressure: | 939 mb | L: | -33.5 m |
| Relative Humidity: | 22.1% | Stability: | C-D |
| Cloud Cover: | 44% | | |

d. Vapor Cloud Characteristics (Coyote 5)

(1) Peak Concentration, $C_p$

| Downwind distance x (m) | Peak concentration, $C_p$ (vol%) |
|---|---|
| 110 | 14.5 |
| 140 | 12.0 |
| 200 | 8.0 |
| 300 | 4.1 |
| 400 | 2.9 at 3 m |
| 500 | 1.93 at 3 m |

(2) Average Cloud Characteristics

| Downwind distance, x (m) | Average Centerline concentration, C(x,0,0) (vol%) | Half-width, W (m) | Height, H (m) | Downwind flux ratio $Q_A/Q_S$ |
|---|---|---|---|---|
| 140 | 6.285 | 43.5 | 9.47 | 1.231 |
| 200 | 7.955 | 53.0 | 9.24 | 1.881 |

e. Comments

(1) Peak concentrations were measured at 1 m except as noted.

(2) Widths at 140 m are time-averaged contour widths between 100 and 130 s. Widths at 200 m are time-averaged contour widths between 110 and 140 s.

(3) Heights at 140 and 200 m are 30-s average heights for 5, 2, and 1% contours. A 3-point weighted Gaussian fit of average centerline vertical values was used to get height parameters, C(x,0,0) and H.

(4) Molecular weight of source gas was found by averaging component molecular weight with respect to percentage of composition.

7. LLNL Coyote 6

a. Test

| | |
|---|---|
| Name: | LLNL Coyote 6 |
| Date: | October 27, 1981 |
| Material: | LNG (81.8% methane, 14.6% ethane, 3.6% propane) |
| Molecular Weight: | 0.016043 kg/mol (methane); 0.0307 kg/mol (ethane); 0.0411 kg/mol (propane) |
| Liquid Density: | 424.1 kg/m$^3$ at -161.5°C (methane) |
| Boiling Temperature: | 111.7 K (-161.5°C) (methane); 184.53 K (-88.63°C) (ethane); 231.09 K (-42.07°C) (propane) |
| Heat of Vaporization: | 8.18 kJ/mol at -161.5°C (methane) |
| Heat Capacity (vapor): | 35.9 J/mol K at 26.8°C (methane) |
| Release Mode: | Vapor burn test. LNG was released through a 25-cm-diameter pipe, 1.5 m above the surface of the water basin. A splash plate was placed below the spill pipe outlet to limit LNG penetration into the water. LNG was released at an average pressure of 8 psia with a maximum of 13 psia. The average exit temperature was -161°C. The spill tank was pressurized with gaseous $N_2$. |

b. Source Data

| | |
|---|---|
| Spill Rate: | 117.3 kg/s (16.6 m$^3$/min) |
| Spill Duration: | 82 s |
| Spill Mass: | 9621.4 kg |
| Spill Temperature: | 112 K (-161°C) |
| Source Description: | Data indicate a fairly constant, nonturbulent source. The visible cloud was slightly higher than 2 m and extended 160 m downwind before disappearing. The leading edge of the cloud moved approximately with the ambient windspeed. The cloud was ignited 79 m downwind, 108 s after the valve opened. Average flame or hot gas arrival at 140 m downwind was 112 s after the spill began. Slower windspeeds during this test produced a wider cloud than Coyote 3. Wind direction deviated 7° from the array centerline. |

c. Atmospheric Conditions

| | | | |
|---|---|---|---|
| Avg. Windspeed: | 4.6 m/s at 2 m | $z_o$: | 0.0002 m |
| Sigma Windspeed: | 0.6 m/s | $U_*$: | 0.221 m/s |
| Sigma Wind Direction: | 5° | $\theta_*$: | 0.045 K |
| Avg. Temperature: | 297.52 K | $\theta_o$: | 301.52 K |
| Barometric Pressure: | 942 mb | L: | 82.0 m |
| Relative Humidity: | 22.8% | Stability: | D |
| Cloud Cover: | 60% | | |

d. Vapor Cloud Characteristics (Coyote 6)

(1) Peak concentration, $C_p$

| Downwind distance, x (m) | Peak concentration, $C_p$ (vol%) |
|---|---|
| 110 | 6.8 |
| 140 | 11.5 |
| 200 | 9.0 |
| 300 | 3.43 at 3 m |
| 400 | 3.1 |
| 500 | 2.6 |

(2) Average Cloud Characteristics

| Downwind distance, x (m) | Average Centerline concentration, C(x,0,0) (vol%) | | Half-width, W (m) | Height, H (m) | Downwind flux ratio $Q_A/Q_S$ |
|---|---|---|---|---|---|
| 140 | 6.855 | 60.2 | 8.66 | 0.7887 | |
| 200 | 5.640 | 64.4 | 6.55 | 0.4593 | |

e. Comments

(1) Peak concentrations were measured at 1 m except as noted.

(2) Widths at 140 m are time-averaged contour widths between 50 and 110 s.

(3) Heights at 140 m are 70-s averaged heights for 5, 2, and 1% contours. A 3-point weighted least squares Gaussian fit of average centerline vertical values was used to get height parameters, C(x,0,0) and H.

(4) Molecular weight of source gas was found by averaging component molecular weight with respect to percentage of composition

(5) Widths at 200 m are time-averaged contour widths.

(6) Heights at 200 m are average heights for 5, 2, and 1% contours. A 2-point Gaussian fit of average centerline vertical values was used to get height parameters, C(x,0,0) and H.

C. TEST SUMMARY NOTES--Burro and Coyote Series

1. General

a. Liquid density of the LNG mixture, spill mass, and spill rate were found in the following manner, given spill volume and spill duration:

(1) Liquid density of the LNG mixture was found using a weighted average of the component densities. The weighting factors used were the percentage of each component in the mixture. For example, the Burro 3 LNG mixture consisted of 92.5 percent methane, 6.2 percent ethane, and 1.3 percent propane. Therefore, to determine the liquid density of this mixture we used 0.925, 0.062, and 0.013 as weighting factors. Then liquid density = 0.925 x 424.1 kg/m$^3$ + 0.062 x 550 kg/m$^3$ + 0.013 x 580 kg/m$^3$ = 433.9 kg/m$^3$.

(2) Spill mass (kg) was found by multiplying the spill volume (m$^3$) by the liquid density of LNG mixture (kg/m$^3$).

(3) The average spill rate (kg/s) was found by dividing the spill mass (kg) by the spill duration (s).

b. Peak concentrations at the downwind arrays were usually taken from the 1-meter concentration time series. Peaks at 3 meters and/or 8 meters were given when they were greater than the 1-meter values.

c. Steady-state periods were identified from concentration time series as periods where the concentration rose to near its peak value and remained nearly constant. The average height of the contours from the vertical cross sections during these periods were input to a FORTRAN program that fit the height and concentration data to four curves: a generalized exponential fit to the three lowest points; a Gaussian fit to the two lowest points; a least squares Gaussian fit to all points; and a weighted least squares Gaussian fit to all points.

Output consisted of predicted concentration at each given height using each fit. Predicted surface centerline concentration, effective cloud height, and the value for n in the exponential fit were also given.

The fit chosen was the one with the smallest residuals. When n is close to 2.0, the data nearly have a Gaussian distribution and Gaussian fits were considered. Gaussian fits were also considered when the surface centerline cone from the exponential fit was much greater than the measured average peak concentration or when the effective cloud height was considered too low even if n was not close to 2.0.

Although the exponential fits often returned small residuals (always 0 for the lowest 3 points), they do not estimate cloud parameters as accurately as the Gaussian fits. Exponential fits return larger values for surface centerline concentration and smaller values for effective cloud height than the Gaussian fits. Among the Gaussian fits, the weighted least squares fit usually returned the smallest residuals; therefore, it was commonly chosen except where noted.

d. Downwind flux ($Q_A$) was calculated assuming a cloud shape of the form:

$$C(x,y,z) = C_g(x) \cdot \exp(-y^2/y_e^2) \exp(-z^n/z_e^n) \quad , \tag{A-1}$$

where

C = volume concentration,

$C_g$ = centerline volume concentration.

Substituting into the flux formula:

$$Q_A = \int_{-\infty}^{\infty} \int_0^{\infty} \rho \cdot m \cdot u \; \partial z \; \partial y \quad , \tag{A-2}$$

we obtain

$$Q_A = \pi^{1/2} \cdot \rho_s \cdot (T_s/T_g) \cdot u \cdot C_g \cdot y_e \cdot z_e \cdot \Gamma(1 + 1/n) \quad , \tag{A-3}$$

where

$\rho_s$ = source gas density (kg/m$^3$);
$T_g$ = cloud temperature at the downwind distance;
$u$ = average ambient windspeed (m/s), unless otherwise noted;
$C_g$ = centerline concentration (vol) given by the chosen fit;
$y_e$ = effective cloud width (m);
$z_e$ = effective cloud height (m) given by the chosen fit.

The source gas density, $\rho_s$, was found by:

$$\rho_s = \frac{M_s \, P}{R \, T_x} \quad , \tag{A-4}$$

where

$M_s$ = molecular weight of the source gas,
$P$ = pressure (1 atm),
$R$ = gas constant (8.250575 x $10^{-5}$ J/K mol),
$T_s$ = source gas temperature (K).

In Equation (A-4), the molecular weight of the source gas, $M_s$, was found by averaging the molecular weights of the components of LNG with respect to its percentage of the total composition (kg/mol).

The cloud temperature at the downwind distance, $T_g$ in Equation (A-3), was found by assuming adiabatic mixing between the cloud and the ambient air:

$$T_g = \frac{C_{pa} \cdot T_a \cdot (1 - m_g) + C_{ps} \cdot T_s \cdot m_g}{C_{pa} \cdot (1 - m_g) + C_{ps} \cdot m_g} \quad , \tag{A-5}$$

where

$C_{pa}$ = specific heat for air (1005.9 J/kg K),
$T_a$ = average ambient temperature (K),
$m_g$ = mass concentration,
$C_{ps}$ = specific heat of the source gas.

In Equation (A-5), the mass concentration, $m_g$, was found by:

$$m_g = \frac{M_s \cdot C_g}{M_a + (M_s - M_a) \cdot C_g} \quad , \tag{A-6}$$

where $M_a$ is the molecular weight of air (0.02896 kg/mol).

Also, in Equation (A-5), the specific heat of the source gas, $C_{ps}$, was found by averaging the specific heats for each component of LNG with repect to its percentage of the total composition.

The effective cloud width, $y_e$ in Equation (A-3), was found by:

$$y_e = \frac{W}{2.3^{1/2}} \quad , \tag{A-7}$$

where W, the average half width, is taken to be one-half the width of the contour that is 10 percent of the peak concentration.

e. Cloud height was found using:

$$H = 2.3^{1/n} z_e \quad , \tag{A-8}$$

where n is given in the exponential fit output (n = 2 if Gaussian fit is chosen).

f. The downwind flux ratio is simply $Q_A/Q_S$, where $Q_s$ is the average spill rate.

2. Specific

Our analysis was completed as previously described. Exceptions and difficulties are discussed in the remainder of this appendix.

a. Burro 3

Contour heights and widths from 60 to 130 s were averaged at the 57-m row. Contours chosen were 15, 10, 5, 2, and 1 percent. Residuals for all fits were large and not smooth, so the 15 percent contour height was omitted and the program failed to converge on a solution. Removal of the 15 and 10-percent contour heights yielded the smallest errors in the 3-point weighted least squares Gaussian fit.

Contour heights and widths from 60 to 120 seconds were averaged at the 140-meter row. Contours chosen were 5, 2, and 1 percent A 3-point weighted least squares Gaussian fit was chosen, and the ratio of downwind flux to source flux was greater than 1. Height values at 100 seconds were higher than the other values because the centerline was slanted (with height). New averages were calculated neglecting the 100-second values, and $Q_A/Q_S$ was reduced slightly (1.08 → 1.02).

Concentrations at the 400- and 800-meter rows were too low to analyze. Peak values were less than 1 percent.

Irregular contours were smoothed to be more Gaussian in shape where necessary, which may alter centerline vertical values.

b. Burro 7

Contour heights and widths from 10 to 190 seconds were averaged at the 57-meter row; however, values at 50, 110, and 140-160 seconds were excluded because of bifurcation. Contours chosen were 15, 10, 5, 2, and 1 percent.

Residuals were somewhat larger using all 5 points. The 15 percent contour was eliminated and the residuals improved. A weighted least squares Gaussian fit was chosen yielding a $Q_A/Q_S$ of 1.991. For tower T02 (near centerline), the average windspeed at 57 meters was only 5.5 m/s and not the ambient average of 8.4 m/s. $Q_A/Q_S$ using 5.5 m/s was 1.30, which was much more acceptable. The ratio may be greater than 1 because the cloud was only half contained in the array. Errors arise in the assumption of symmetric Gaussian cloud shape and placement of the centerline at the edge of the array. Hence, the cloud may not be as wide as assumed.

Contour heights and widths from 180 seconds only were used at the 400-meter row because this was the only time for which the cloud was completely contained within the array. Contours chosen were 3.6, 2, 1.5, and 1 percent. A generalized exponential fit with n = 1.723 was chosen because residuals were zero and the centerline concentration and effective cloud height were about the same as for Gaussian fits. $Q_A/Q_S$ is small (0.33) due probably to the single point analysis.

Concentrations at the 800-meter row were too low to analyze. The peak value was less than 1 percent.

c. Burro 8

Because of plume bifurcation, each lobe of the plume at the 57- and 140-meter rows was analyzed separately. A $Q_A$ value was calculated for each 20-second period from 40 to 200 seconds at the 57-meter row. Fits were done using contours available for a given time. In general, a weighted least squares Gaussian fit was chosen. $Q_A$ for both lobes were added at a given time to find $Q_A/Q_S$ for that time. $Q_A$ was calculated three different ways: using (1) average ambient windspeed, (2) 3-meter windspeed, and (3) 1-meter windspeed. The 1- and 3-meter windspeeds were taken from time series data as the average for the 20-second time period involved. Although $Q_A/Q_S$ for 1-meter windspeed is lower than for the other two, it was chosen because the higher

concentrations were below 3 meters and would be advected with the lower windspeed. Average centerline concentration, half-width, and cloud height are given for Lobes A and B (Lobe A is on the left looking back toward the source). $Q_A/Q_S$ is the whole cloud average.

Total mass also was calculated to check this method. The total amount of LNG (12,514 kg) was taken as the average flux ($Q_A$) calculated with a particular windspeed multiplied by 180 seconds (the peak concentration of steady-state period). Percentage of total mass released was also found. Values for 1-meter windspeed $Q_A$ were lowest (39.2 percent); 3-meter windspeed $Q_A$ accounted for 88.3 percent; and average ambient windspeed $Q_A$ accounted for nearly all of the released mass (95.5 percent).

Data from 80 to 280 seconds at the 140-meter row were handled similarly to the 57-meter row data. Again, 1-meter windspeed $Q_A/Q_S$ was chosen since it is probably more representative of the advecting wind. Windspeeds for Lobe A were taken from tower T04 time series; T03 time series provided Lobe B windspeeds. Again, total mass was calculated. All values for each windspeed $Q_A$ were greater than 100 percent (115 percent at average ambient to 163 percent at 3-meter windspeed), but all $Q_A/Q_S$ estimates are less than 0.8.

The plume is lofted; concentrations are less than 5 and 2 percent at 400 and 800 meter, respectively, and are not analyzed except for peak concentration values.

Irregular contours were smoothed to be more Gaussian in shape where necessary.

d. Burro 9

The plume at the 57-meter row was bifurcated from 30 to 40 seconds. Nonbifurcated contour heights for 5, 3, 2, and 1-percent contours from 50 to 80 seconds were averaged and input to the curve-fitting program. The fitting

failed, so average heights for 3, 2, and 1-percent contours were used. Contour heights were averaged from 30 to 40 seconds for each lobe. Lobe A is on the left looking back toward the source; Lobe B is on the right. Average heights for the 3, 2, and 1-percent contours were input to the curve-fitting program for Lobe A; 5, 2, and 1 percent for Lobe B. $Q_A$ was calculated for each set of output. Average values of $Q_A/Q_S$, $C_g$, H, and W were found as follows:

$$\frac{\overline{Q_A}}{Q_S} = \frac{Q_A(A) + Q_A(B) + Q_A(\text{single})}{2Q_S} \tag{A-9}$$

$$\overline{C_g} = \frac{C_g(A) + C_g(B) + C_g(\text{single})}{3} \tag{A-10}$$

$$\overline{H} = 2.3^{1/n} \frac{z_e(A) + z_e(\text{single})}{2} \tag{A-11}$$

$$\overline{W} = \frac{\Sigma W}{N} \qquad (N = 6) \tag{A-12}$$

The effective cloud height, $z_e$, of the bifurcated stage was taken to be $z_e(A)$ since it was the maximum between the two lobes. Widths for 30 and 40 seconds were measured as if the cloud were a single plume.

Contour heights and widths from 30 to 110 seconds were averaged at the 140-meter row. Contours chosen were 5, 2, and 1 percent. A weighted least squares Gaussian fit was chosen.

Contour heights and widths from 110 to 150 seconds were averaged at the 400-meter row. Contours chosen were 3, 2, and 1 percent. A weighted least squares Gaussian fit was chosen. The large $Q_A/Q_S$ may result from inaccuracies in measuring low concentrations and the overestimation by the Gaussian model of a lofted plume.

e. Coyote 3.

Contour heights and widths from 50 to 100 seconds were averaged at the 140-meter row. Contours chosen were 5, 2, and 1 percent. A generalized exponential fit with n = 1.419 was chosen because all residuals were 0.

Concentrations at the 400-meter row were not analyzed because concentrations were low (<2 percent).

f. Coyote 5

Contour heights and widths from 100 to 130 seconds were averaged at the 140-meter row. Contours chosen were 5, 2, and 1 percent. The weighted least squares Gaussian fit was then chosen for more reasonable values of the centerline concentration and effective cloud height. $Q_A/Q_S$ was 1.23.

Contour heights and widths from 110 to 140 seconds were averaged at 200 meters. Contours chosen were 5, 2, and 1 percent. A weighted least squares Gaussian fit was chosen, and $Q_A/Q_S$ was 1.881.

Concentrations at the 400-meter row were not analyzed because concentrations were low.

g. Coyote 6

Irregular contours at the 140- and 200-meter rows were smoothed to be more Gaussian in shape.

## REFERENCES


A-1. Rodean, H.C., et al., Vapor Burn Analysis for the Coyote Series LNG Spill Experiments, UCRL-53530, Lawrence Livermore National Laboratory, Livermore, California, April 1984.

A-2. Koopman, R.P., et al., Burro Series Data Report, LLNL/NWC 1980 LNG Spill Tests, UCID-19075, Lawrence Livermore National Laboratory, Livermore, California, December 1982.

A-3. Goldwire, H.C., et al, Burro Series Data Report, LLNL/NWC LNG Spill Tests, Dispersion, Vapor Burn, and Rapid Phase Transition, UCID-19953, Lawrence Livermore National Laboratory, Livermore, California, October 1983.

A-4. Morgan, D.L., et al., Phenomenology and Modeling of Liquefied Natural Gas Vapor Dispersion, UCRL-53581, Lawrence Livermore National Laboratory, Livermore, California, April 1984.

# APPENDIX B

## LLNL DESERT TORTOISE TESTS ($NH_3$)

## A. DESCRIPTION OF TEST SERIES

Four large-scale (15-60 $m^3$) pressurized $NH_3$ spill tests were conducted by Lawrence Livermore National Laboratory (LLNL) for the U.S. Coast Guard, The Fertilizer Institute (TFI), and Environment Canada as part of a joint government-industry study (Reference B-1). Domestic and international ammonia producers participated in the TFI consortium. The $NH_3$ tests, called the Desert Tortoise series, were performed during August and September 1983 on the Frenchman Flat area of the Department of Energy's (DOE) Nevada Test Site (NTS) under the jurisdiction of the DOE Nevada Operations Office (NVO). This test series was designed to measure the atmospheric dispersion of the spilled material under various meteorological conditions. The size, shape, and temperature of the ammonia clouds as well as the extent of hazardous concentrations downwind were determined. To simulate simple cases that could be easily modeled, we performed the tests at constant pressure and over flat terrain under both stable and neutral wind conditions.

Extensive environmental data at Frenchman Flat had been collected for three years. The area is ideal for conducting dispersion tests because the terrain is flat and the wind patterns are regular. Both of these conditions are important for successful modeling and for safety considerations (Reference B-2).

Frenchman Flat is an extremely flat (normally) dry lake bed approximately 4-6 km long and 3 km wide. The average surface layer at the center is less than 0.3 meters below that at the edges. Although normally a dry desert, unusually heavy rain in early and mid August associated with El Nino weather patterns formed a lake at the site. During the calm of the nights before the first and second tests, several inches of water covered the region of the spill point and the array row at 100 meters downwind, with 15-20 cm of water at the 800-meter row. In the mornings, the wind started up. By late in the day, most water in the lake had been blown downwind, leaving the regions nearby relatively free of surface water out to perhaps 400 meters. The second

test, however, was conducted shortly before noon and the region from the spill point to the central part of the 100-meter row of towers was covered by about 0.5 cm of water.

The claylike surface of the playa was saturated with water and numerous small pools of water were present on the first two tests. The lake bed was nearly dry by the third test and was completely dry by the last test. Thus, the atmospheric boundary layer differed considerably from the usual dry desert circumstances, and the tests were conducted under a greater range of humidities and surface conditions than anticipated.

The atmospheric boundary layer, wind field, and turbulence were measured using the meteorological array of stations. Vapor cloud temperature and concentration, surface heat flux, and aerosol property were measured using the mass flux and dispersion arrays. Locations of the various stations and the positions of the camera stations are shown in Figure B-1.

The meteorological array consisted of eleven stations with Met-One two-axis, cup-and-vane anemometers (all at a height of 2 meters), plus a 20-meter tall meteorological tower and station located 50 meters upwind of the spill area.

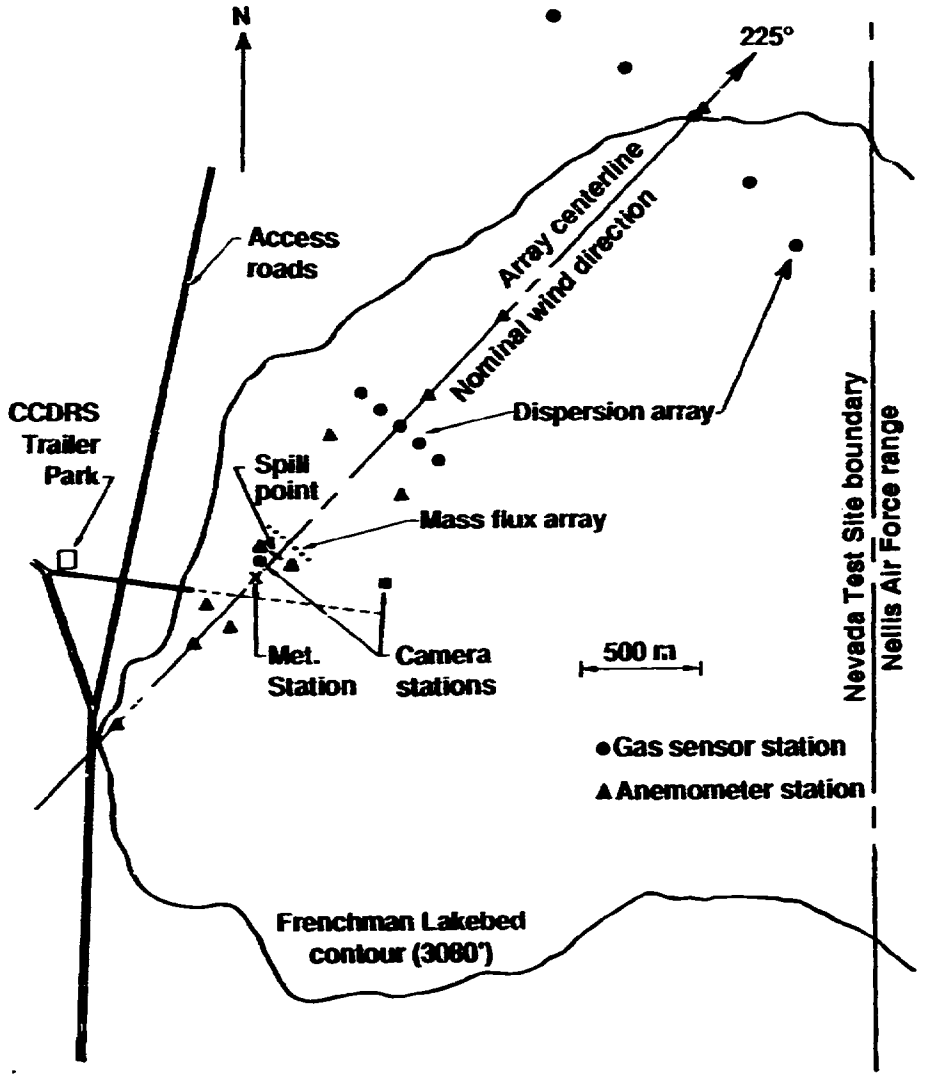


Figure B-1. Sensor Array for the Desert Tortoise Series Experiments.

## B. TEST SUMMARIES

### 1. LLNL Desert Tortoise 2

#### a. Test

| | |
|---|---|
| Name: | Desert Tortoise 2 |
| Date: | August 29, 1983 |
| Material: | Anhydrous liquid ammonia ($NH_3$) |
| Molecular Weight: | 0.017031 kg/mol |
| Liquid Density: | 682.8 kg/m³ at 033.4°C |
| Boiling Temperature: | 239.7 K (-33.4°C) |
| Heat of Vaporization: | 23.3 KJ/mol at -33.4°C |
| Heat Capacity (vapor): | 37.3 J/mol K at 15°C |
| Release Mode: | Steady-state, finite duration, pressurized jet release. Liquid ammonia was released at a constant pressure of 204 psia to the atmosphere via a 0.094-m-diameter orifice and formed a horizontal jet 0.79 m above the ground. The two tanker trailer was pressurized externally using $N_2$ drive gas. |

#### b. Source Data

| | |
|---|---|
| Spill Rate: | 117 kg/s (10.3 m³/min liquid) |
| Spill Duration: | 255 s |
| Spill Mass: | 29900 kg |
| Spill Temperature | 293.3 K (20.1°C) |
| Source Description: | The released ammonia flashed and formed a two-phase (liquid droplet + vapor) jet that expanded radially to about 2 m in diameter within a few meters of the release. The effective liquid velocity at the release point was 23.5 m/s, and an elevated velocity persisted for several hundred meters downwind before slowing to the ambient windspeed. About 0.5 cm of water covered the desert surface in the release area. Elevated temperatures in the area of maximum ammonia pooling at the end of the test indicate exothermic reaction of ammonia with water and definite cloud heating, which was confirmed by heat flux measurements. Wind-blown mist formed above the cold pool in the release area and persisted at least 1000 s after the spill ended. |

#### c. Atmospheric Conditions

| | | | |
|---|---|---|---|
| Avg. Windspeed: | 5.76 m/s at 2 m | $z_o$: | 0.003 m |
| Sigma Windspeed: | 0.68 m/s | $U_*$: | 0.312 m/s |
| Sigma Wind Direction: | 7.54° | $\Theta_*$: | 0.091 K |
| Avg. Temperature: | 303.80 K at 2.46 m | $\Theta_o$: | 310.58 K |
| Barometric Pressure: | 910.3 mb | L: | 83.2 m |
| Relative Humidity: | 17.5% | Stability: | D |
| Cloud Cover: | 4% | | |

d. Vapor Cloud Characteristics (Desert Tortoise 2)

(1) Peak Concentration, $C_p$

| Downwind distance, x (m) | Peak concentration, $C_p$ (vol%) |
|---|---|
| 100 | 11.0 |
| 800 | 1.8 |
| 1400 | >0.5 |

(2) Average Cloud Characteristics

| Downwind distance, x (m) | Average centerline concentration, C(x,0,0) (vol%) | Half-width, W (m) | Height, H (m) | Downwind flux ratio $Q_A/Q_s$ |
|---|---|---|---|---|
| 100 | 8.11 | 32.3 | 5.83 | 0.67 |
| 800 | 1.37 | 172.5 | 8.35 | 0.47 |
| 1400 | >0.5 | >400. | (<10.) | (0.47) |

e. Comments

(1) Peak concentrations at 100 and 800 m downwind were measured at a height of 1 m.

(2) Widths at 100- and 800-m are time-averaged contour widths.

(3) Heights at 100 m are 170-s averaged (from 50 to 210 s) heights for 8.0, 6.0, 4.0, 2.0, 1.0, and 0.5% contours. A 6-point weighted Gaussian fit of averaged centerline vertical values was used to get height parameters, C(x,0,0) and H.

(4) At 100 m, the generalized 3exponential fit turned out slightly better than the Gaussian fits with n = 1.467, but weighted Gaussian was chosen because it provided a better fit to the top of the cloud.

(5) Heights at 800 m were derived from eight 10-s averages (170 s, 230-300 s) for 1.2, 0.8, 0.4, and 0.2% contours. A 4-point weighted least squares Gaussian fit of averaged centerline vertical values was used to get height parameters, C(x,0,0) and H.

(6) At 800 m, the 4-point weighted least squares Gaussian fit errors were less than the 5-point weighted fit, which included 1.6% height values.

(7) Cloud speed at 100 m was assumed to be 10 m/s. The cloud speed decreased to ambient (5.76 m/s) before reaching 800 m.

(8) Calculated height at 1400 m assumes $Q_a/Q_s$ value the same as at 800 m.

## 2. LLNL Desert Tortoise 4

### a. Test

| | |
|---|---|
| Name: | Desert Tortoise 4 |
| Date: | September 6, 1983 |
| Material: | Anhydrous liquid ammonia ($NH_3$) |
| Molecular Weight: | 0.017031 kg/mol |
| Liquid Density: | 682.8 kg/m³ at 033.4°C |
| Boiling Temperature: | 239.7 K (-33.4°C) |
| Heat of Vaporization: | 23.3 KJ/mol at -33.4°C |
| Heat Capacity (vapor): | 37.3 J/mol K at 15°C |
| Release Mode: | Steady-state, finite duration, pressurized jet release. Liquid ammonia was released at a constant pressure of 203 psia to the atmosphere via a 0.094-m-diameter orifice and formed a horizontal jet 0.79 m above the ground. The tanker trailer was pressurized externally using $N_2$ drive gas. |

### b. Source Data

| | |
|---|---|
| Spill Rate: | 108 kg/s (9.5 m³/min liquid) |
| Spill Duration: | 381 s |
| Spill Mass: | 41100 kg |
| Spill Temperature: | 297.3 K (24.1°C) |
| Source Description: | The released ammonia flashed and formed a two-phase (liquid droplet + vapor) jet that expanded radially to approximately 2 m in diameter within a few meters of the release. The effective liquid velocity at the release point was 22.8 m/s, and an elevated velocity persisted for several hundred meters downwind before slowing to the ambient windspeed. A small fraction of the release formed a liquid pool on the desert soil more than 2000 m² in extent and out to 90 m downwind. |

### c. Atmospheric Conditions

| | | | |
|---|---|---|---|
| Avg. Windspeed: | 4.51 m/s at 2 m | $z_o$: | 0.003 m |
| Sigma Windspeed: | 0.65 m/s | $U_*$: | 0.250 m/s |
| Sigma Wind Direction: | 5.02° | $\Theta_*$: | 0.124 K |
| Avg. Temperature: | 305.95 K at 2.46 m | $\Theta_o$: | 312.88 K |
| Barometric Pressure: | 903.1 mb | L: | 39.2 m |
| Relative Humidity: | 21.2% | Stability: | D-E |
| Cloud Cover: | 1% | | |

d. Vapor Cloud Characteristics (Desert Tortoise 4)

(1) Peak Concentration, $C_p$

| Downwind distance, x (m) | Peak concentration, $C_p$ (vol%) |
|---|---|
| 100 | 7.6 |
| 800 | 2.1 |
| 2800 | 0.51 |

(2) Average Cloud Characteristics

| Downwind distance, x (m) | Average centerline concentration, C(x,0,0) (vol%) | Half-width, W (m) | Height, H (m) | Downwind flux ratio $Q_A/Q_s$ |
|---|---|---|---|---|
| 100 | 6.07 | 36 | 6.45 | 0.67 |
| 800 | 2.01 | 236 | 6.31 | 0.60 |
| 2800 | 0.486 | 396 | (15.5) | (0.60) |

e. Comments

(1) Peak concentrations at 100, 800, and 2800 m were measured at a height of 1 m.

(2) Widths at 100 and 800 m are time-averaged contour widths.

(3) Heights at 800 m are 200-s averaged heights for 2.0, 1.6, 1.0, and 0.4%. contours. A 4-point weighted Gaussian fit of averaged centerline vertical values was used to get height parameters C(x,0,0) and H. At 100 m, 250-s averages for heights of 6.0, 4.0, 2.0, 1.0, and 0.5% contours were used in a 5-point weighted Gaussian fit.

(4) Gaussian fits to vertical profile turned out better than the generalized exponential fit.

(5) A 3-point Gaussian fit was used to obtain widths at 2800 m.

(6) At 100 m, we used an observed jet speed of 10 m/s for cloud velocity.

(7) Calculated height at 2800 m assumes $Q_a/Q_s$ value same as at 800 m.

C. TEST SUMMARY NOTES--Desert Tortoise Series

1. General

The general notes given in Appendix A, Section C.1. are also applicable to the calculations for the Desert Tortoise Series.

2. Specific

Our analysis was completed as previously described. Exceptions and difficulties are discussed in the remainder of this appendix.

a. Desert Tortoise 2

Time-averaged concentration contours from the data report were used to obtain fitted average cloud characteristics. In the 100-meter row, the period from 50 to 210 seconds was used for heights of the 8.0, 6.0, 4.0, 2.0, 1.0, and 0.5 percent contours. The parameters reported were from the 6-point weighted Gaussian fit ($n = 2$). Although a generalized exponential fit to the three lowest points (with $n = 1.47$) gave a slightly better fit, it was rejected because it did not fit the top of the cloud well. Cloud speed was taken to be the observed jetting speed, which is larger than the ambient windspeed.

For the 800-meter row, the average heights of the 1.2, 0.8, 0.4, and 0.2 percent contour were determined for 170 to 300 seconds. A 4-point weighted Gaussian fit was used to determine the cloud parameters. Including a 1.6 percent contour in the fits gave poor results.

For the 1400-meter row, only lower limits to the actual gas concentration and cloud width were available experimentally. Assuming that $Q_A/Q_S$ at 1400 meters is the same as at 800 meters, an upper limit to the cloud height can be determined.

b. Desert Tortoise 4

At the 100-meter row, the heights of the 6, 4, 2, 1, and 0.5 percent contours at the cloud center for 50 to 290 seconds were averaged and fit by weighted best squares to a Gaussian height profile. The weighted least squares technique corrects the straightforward least squares Gaussian fit to give equal weighting to all points in concentration space (as opposed to the log of concentration). If these errors are equally distributed, the fit is not forced to pay undue attention to the low concentration values at the higher extremes of the cloud. The exact generalized exponential fit to the 3 lowest heights gave n = 2.07, which is essentially 2. Hence, the Gaussian fit was used. No smoothing of the contour data sets was required. The cloud speed at 100 meters was equal to the observed jetting speed at 100 meters, which was greater than the ambient windspeed.

The 800-m analysis averaged contour data for 300 to 480 seconds. Heights of the 2, 1.6, 1, and 0.4 percent contours were fit, again using a weighted Gaussian fit. The generalized exponential fit to the three lowest contours gave n = 1.85, again essentially 2. The cloud width was the average width.

## REFERENCES


B-1. Goldwire, H.C., et al., Desert Tortoise Series Data Report 1983 Pressurized Ammonia Spills, UCID-20562, Lawrence Livermore National Laboratory, California, October 1985.

B-2. Leitner, P., Miller, G., and Shinn, J.H., Environmental Assessment for Spill Test of $NH_3$ and $N_2O_4$ at Frenchman Flat, Nevada Test Site, UCID-19822, Lawrence Livermore National Laboratory, Livermore, California, June 1983.

# APPENDIX C

# LLNL EAGLE TESTS

## A. DESCRIPTION OF TEST SERIES

### 1. Introduction

During the fall of 1983, the Lawrence Livermore National Laboratory (LLNL) conducted a series of large-scale (3-5 $m^3$) nitrogen tetroxide ($N_2O_4$) spill tests for the USAF Engineering and Services Laboratory, Tyndall AFB (References C-1,C-2). The spill material was nitrogen tetroxide ($N_2O_4$), a rocket fuel oxidizer used in the Titan II missile system. The test series was designed to determine the source strength characteristics and heavy-gas dispersion aspects of large $N_2O_4$ spills. In addition, two spills were performed to evaluate a Portable Foam Vapor Suppression System (PFVSS). The PFVSS tests were directed by the Ogden Air Logistics Center, Hill AFB, with support from USAF Space Division and the Strategic Air Command. The tests were performed at the U.S. Department of Energy (DOE) Nevada Test Site (NTS) under the jurisdiction of the DOE Nevada Operations Office (NVO).

The $N_2O_4$ tests were the fifth in a continuing program of hazardous material spill tests conducted by LLNL and were code-named the Eagle series. Six $N_2O_4$ spill tests were accomplished. Four tests were for the purpose of dispersion and source strength studies (Eagle 1, 2, 3, and 6) and two tests for evaluation of the PFVSS (Eagle 4 and 5). The Eagle series tests were performed between September 17 and October 30, 1983.

### 2. Experiment Description

The $N_2O_4$ was spilled directly onto the surface of the dry lakebed at Frenchman Flat, NTS. The $N_2O_4$ was delivered to the spill area by a 30-meter-long, 7.62-cm-diameter (3-inch) PVC pipe where it was distributed by two different methods. The single-exit, confined spill configuration was used to study evaporation rates as a function of liquid pool depth and windspeed. The multiexit, unconfined spill configuration was designed to distribute the $N_2O_4$ over a large area so that it would evaporate as quickly as it was spilled and

thus produce a large, well-defined source of $N_2O_4$ vapor for the dispersion studies.

Numerous measurements were made in the area of the spill. These included temperature of the $N_2O_4$ at the spill pipe exit, heat flow from the soil, and soil, liquid, and vapor temperatures.

In addition, atmospheric boundary layer, wind field, vapor cloud temperature and concentration, and surface heat flux were measured using an extensive diagnostic system developed by LLNL. The three main array systems were the meteorological array, the mass flux array, and the dispersion array. The locations of these various arrays, along with the positions of the camera stations, are shown in Figure C-1.

The meteorological array consisted of nine two-axis, cup-and-vane anemometers (all at a height of 2 m), plus a 20-m-tall tower located directly upwind of the spill area. The locations of these stations are shown in Figure C-1. Windspeed and direction at each station were averaged for 10 s, and the results, plus the standard deviation of direction for the same 10-sec period, were transmitted to the Command Control and Data Recording System (CCDRS) trailer. The wind-field data were displayed in real time and were the primary information used to determine the optimum time for the spill.

The meteorological boundary layer data were obtained from measurements mounted on a 20-m tower located 50 m directly upwind of the spill point (Figure C-1). This tower had four temperature gauges and three Gill bivane anemometers. The station also measured ground heat flux. Humidity data and local barometric pressure were obtained from the NTS Weather Support Group.

A mass flux array was used to determine the evaporation rate, or source strength, of the $N_2O_4$ by measuring the $N_2O_4$ concentration, vapor cloud temperature, and velocity as the spill passed through the array. Since $N_2O_4$ dissociates rapidly to nitrogen dioxide ($NO_2$), both species must be involved

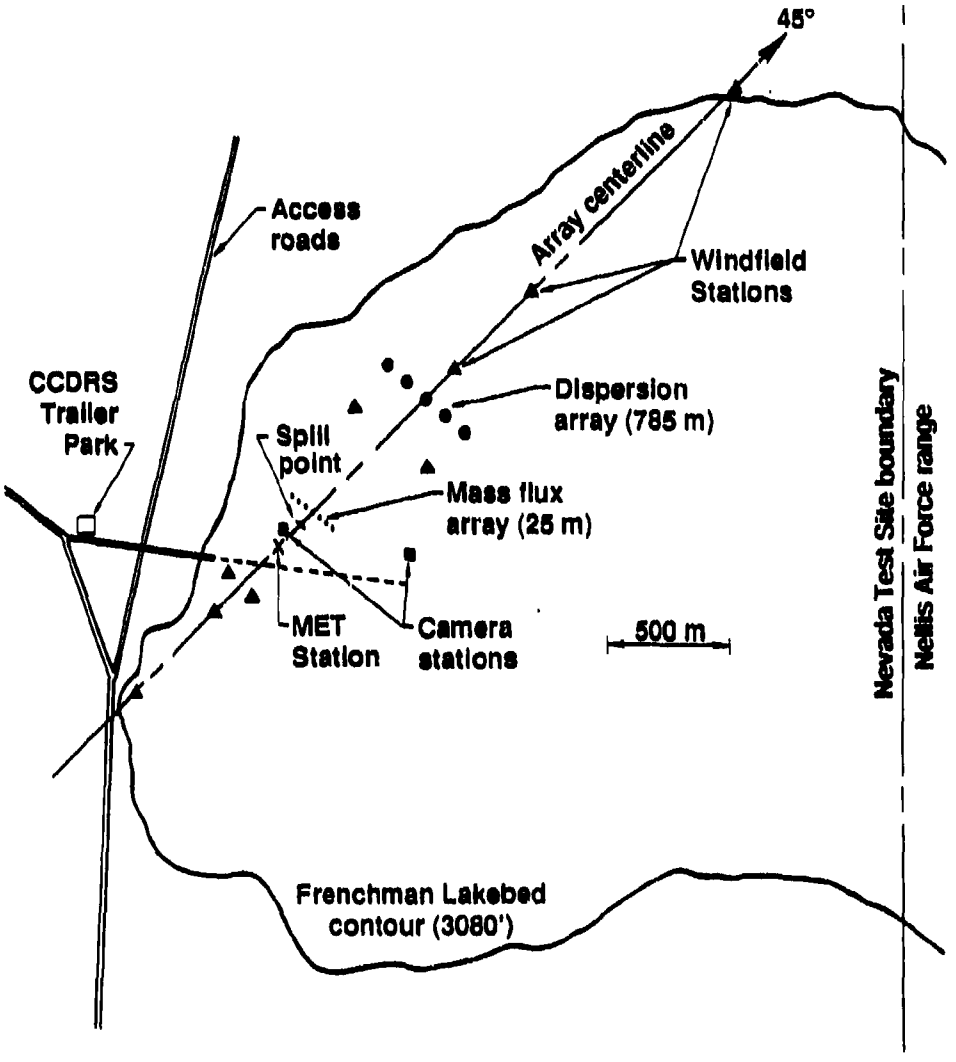


Figure C-1. Sensor Array for the Eagle Series Experiments.

temperature, and velocity as the spill passed through the array. Since $N_2O_4$ dissociates rapidly to nitrogen dioxide ($NO_2$), both species must be involved in the vapor flux calculation. The $N_2O_4/NO_2$ ratio was determined using a well-documented equilibrium reaction rate constant (References C-1, C-2). The cloud temperature data were required for calculations of the rate constant and for conversion from concentration to mass density. The product of the mass density and velocity integrated over the vapor cloud cross section yields the total mass flux passing through the array at any instant. If the entire cloud is "captured" by the array, this mass flux will be equivalent to the vapor source strength of the spilled $N_2O_4$.

The mass flux array was located 25 meters downwind of the spill area and consisted of seven gas stations and two windspeed stations. The centerline station was a 10-meter-tall tower with three bivane anemometers, three LLNL infrared (IR) gas sensors, and three thermocouples. The three anemometers were located at heights of 1.3, 3, and 6 meters for the entire Eagle series. The IR gas sensors and thermocouples were located at different heights for each test. Six additional stations were located at 5-meter intervals on either side of the centerline station (three to each side). Each station had a 6-meter-tall mast, three LLNL IR gas sensors, and three thermocouples.

The dispersion array consisted of five 10-meter towers located 785 meters downwind of the spill area (Figure C-1). This array was used to record the $NO_2$ concentration and the extent of the vertical cross section of the $N_2O_4$ vapors during each spill. Each tower had three $NO_2$ gas sensors and three thermocouples located 1, 3.5, and 8.5 meters above ground. The towers were separated in the crosswind direction by a distance of 100 meters.

B. TEST SUMMARIES

1. LLNL Eagle 3

a. Test

| | |
|---|---|
| Name: | LLNL Eagle 3 |
| Date: | October 7, 1983 |
| Material: | Nitrogen tetroxide $N_2O_4$ |
| Molecular Weight: | 0.0460055 kg/mol ($NO_2$); 0.092011 kg/mol ($N_2O_4$) |
| Liquid Density: | 1446.9 kg/m³ at 20.0°C |
| Boiling Temperature: | 294.30 K (21.15°C) |
| Heat of Vaporization: | 38.116 kJ/mol (Equilibrium mixture at 21.2°C) |
| Heat Capacity (vapor): | 37.0 J/mol K ($NO_2$); 77.3 J/mol K ($N_2O_4$) |
| Release Mode: | Finite duration, steady-state dispersion test. $N_2O_4$ was spilled in a multiexit, unconfined configuration designed to distribute $N_2O_4$ uniformly over a large area and thus evaporate it as quickly as it was spilled. The spill configuration consisted of six 7-m-long spill pipes emanating radially from a center exit point (7 points of release). Below the end of each spill pipe was a splash plate and deflection cone to limit the amount of penetration into the surrounding soil. The $N_2O_4$ tanker was pressurized with gaseous $N_2$. |

b. Source Data

| | |
|---|---|
| Spill Rate: | 33.7 kg/s (4.2 m³ liquid) |
| Spill Duration: | 188 s |
| Spill Mass: | 6350 kg |
| Spill Temperature: | 292. K (19°C) |
| Source Description: | Spill used liquid $N_2O_4$ remaining in tank from previous two tests. Therefore the spill was not terminated by shutting off valve. To ensure the tank was empty, the $N_2$ drive gas was allowed to blow through the system for several minutes after most of the liquid $N_2O_4$ was exhausted, which enhanced the vaporization of the remaining liquid. The lakebed playa surface was claylike and impermeable to water. However, $N_2O_4$ soaked in readily and outgassing from the surface occurred for several hours after the spill terminated. The surface vapor temperature indicates that the liquid $N_2O_4$ froze. Reaction with ambient water vapor produced $HNO_3$ mist near the source, producing uncertainties in source strength. The vapor cloud was totally confined to the 785-m array. |

c. Atmospheric Conditions

| | | | |
|---|---|---|---|
| Avg. Windspeed: | 3.13 m/s at 2 m | $z_o$: | 0.0003 m |
| Sigma Windspeed: | 0.48 m/s | $U_*$: | 0.129 m/s |
| Sigma Wind Direction: | 13.2° | $\theta_*$: | 0.075 K |
| Avg. Temperature: | 295.46 K at 2.46 m | $\theta_o$: | 301.93 K |
| Barometric Pressure: | 901.9 mb | L: | 16.8 |
| Relative Humidity: | 45% | Stability: | E |
| Cloud Cover: | 95% | | |

d. Vapor Cloud Characteristics (Eagle 3)

(1) Peak Concentration, $C_p$

| | Downwind distance, x (m) | Peak concentration, $C_p$ (vol%) |
|---|---|---|
| $N_2O_4$ | 25 | 1.7 |
| $NO_2$ | 25 | 3.7 |
| | 785 | 0.05 |

(2) Average Cloud Characteristics

| | Downwind distance, x (m) | Average centerline concentration, C(x,0,0) (vol%) | Half-width, W (m) | Height, H (m) | Downwind flux ratio $Q_A/Q_s$ |
|---|---|---|---|---|---|
| $N_2O_4$ | 25 | 1.55 | 25 | 0.93 | 0.0864 |
| $NO_2$ | 25 | 4.05 | 25 | 1.02 | 0.1234 |
| | 785 | 0.052 | 125 | 8.32 | 0.0649 |

e. Comments

1. Peak concentrations were measured at a height of 0.3 m, 25 m downwind, and 1.0 m, 785 m downwind.

2. At 25 m, the time-averaged concentration contours at 40- and 90-s were used to determine cloud width and height parameters. Averaged vertical $N_2O_4$ concentration contour heights for 0.1, 0.2, 0.4, 0.6, and 1.0% were fit by a 5-point weighted Gaussian fit to get cloud parameters, C(x,0,0) and H.

3. Generalized exponential fit was poorer than the weighted Gaussian fits.

4. For the 25-m, the gas equilibrium relationship and cloud temperature vs. height were used to calculate corresponding $NO_2$ concentrations. A 5-point weighted Gaussian fit was used to get cloud parameters for $NO_2$.

5. For the 785-m, we used heights for concentration contours at 100, 200, 300, 400, and 500 ppm from 500 to 600 s in 5-point weighted Gaussian fit. Cloud width was determined for the same fit on the contour.

2. LLNL Eagle 6

a. Test

| | |
|---|---|
| Name: | LLNL Eagle 6 |
| Date: | October 30, 1986 |
| Material: | Nitrogen tetroxide |
| Molecular Weight: | 0.0460055 kg/mol ($NO_2$); 0.092011 kg/mol ($N_2O_4$) |
| Liquid Density: | 1446.9 kg/m³ at 20.0°C |
| Boiling Temperature: | 294.30 K (21.2°C) |
| Heat of Vaporization: | 38.116 kJ/mol (equilibrium mixture at 21.2°C) |
| Heat Capacity (vapor): | 37.0 J/mol K ($NO_2$); 77.3 J/mol K ($N_2O_4$) |
| Release Mode: | Finite duration, steady-state dispersion test. $N_2O_4$ was spilled in a multiexit, unconfined configuration designed to distribute $N_2O_4$ uniformly over a larger area and thus evaporate it as quickly as it was spilled. The spill configuration consisted of six 7-m-long spill pipes emanating radially from a center exit point (7 points of release). Below the end of each spill pipe was a splash plate and deflection cone to limit the amount of penetration into the surrounding soil. The $N_2O_4$ tanker was pressurized with gaseous $N_2$. |

b. Source Data

| | |
|---|---|
| Spill Rate: | 16.9 kg/s (0.7 m³/min) |
| Spill Duration: | 296 s |
| Spill Mass: | 5000 kg |
| Spill Temperature: | 290.7 K (17.5°C) |
| Source Description: | The spill used liquid $N_2O_4$ remaining in the tank from previous two tests and therefore was not terminated by shutting off valve. To ensure the tank was empty, the $N_2$ drive gas was allowed to blow through the system for several minutes after most of the liquid $N_2O_4$ was exhausted, which enhanced vaporization of the remaining liquid. The lakebed playa surface was claylike and impermeable to water. However, $N_2O_4$ soaked in readily and outgassing from the surface occurred for several hours after the spill terminated. Reaction with ambient water vapor produced $HNO_3$ mist near the source, producing uncertainties in source strength. The vapor cloud was confined to the 785-m array. |

c. Atmospheric Conditions

| | | | |
|---|---|---|---|
| Avg. Windspeed: | 4.96 m/s at 2 m | $z_o$: | 0.0003 m |
| Sigma Windspeed: | 0.68 m/s | $U_*$: | 0.233 m/s |
| Sigma Wind Direction: | 7.5° | $\theta_*$: | 0.014 K |
| Avg. Temperature: | 295.80 K at 2.46 m | $\theta_o$: | 303.44 K |
| Barometric Pressure: | 909.3 mb | L: | 293.3 m |
| Relative Humidity: | 35% | Stability: | D |
| Cloud Cover: | 85% | | |

d. Vapor Cloud Characteristics (Eagle 6)

(1) Peak Concentration, $C_p$

| | Downwind distance, x (m) | Peak concentration, $C_p$ (vol%) |
|---|---|---|
| $N_2O_4$ | 251.58 | |
| $NO_2$ | 25 | 3.55 |
| $NO_2$ | 785 | >0.05 |

(2) Average Cloud Characteristics

| | Downwind distance, x (m) | Average Centerline concentration, C(x,0,0) (vol%) | Half-width, W (m) | Height, H (m) | Downwind flux ratio $Q_A/Q_s$ |
|---|---|---|---|---|---|
| $N_2O_4$ | 25 | 1.388 | 9.2 | 0.84 | 0.0814 |
| $NO_2$ | 25 | 3.347 | 9.2 | 1.2 | 0.1410 |
| $NO_2$ | 785 | 0.064 | 89.5 | 10.0 | 0.2189 |

e. Comments

(1) Peak concentrations were measured at a height of 0.3 m, 25 m downwind, and 1.0 m, 785 m downwind.

(2) For 25-m, averaged concentration contours at 160, 250, 300, and 360 s were used to determine cloud height and width parameters.

(3) Averaged vertical $N_2O_4$ concentration contour heights for 0.25, 0.5, 0.75, and 1.0% were fit by a 5-point weighted Gaussian fit to get cloud parameters, C(x,0,0) and H.

(4) Generalized exponential fits were poorer than the weighted Gaussian fit.

(5) For the 25-m, the gas equilibrium relationship and cloud temperature vs. height were used to calculate corresponding $NO_2$ concentrations. A 5-point weighted Gaussian fit was used to get cloud parameters for $NO_2$.

(6) At the 785-m, the $NO_2$ cloud had lifted off the ground for most of the spill duration. Cloud heights were computed using the contour at 460 s with a 4-point weighted Gaussian fit.

C. TEST SUMMARY NOTES - Eagle Series

1. General

a. Given the $N_2O_4$ concentration at 25 meters, we found the $NO_2$ concentration by:

$$C_{NO_2} = \sqrt{K_e C_{N_2O_4}} \qquad \text{(C-1)}$$

where C is in volume fraction (0.0 to 1.0) and

$$K_e = \exp \frac{33.815769 + 0.0270486\ T - 2.9114\times10^{-5}T^2 - 12875/T}{1.9871} \qquad \text{(C-2)}$$

where T is in K. From the temperature time series, an average temperature was found at each height during steady-state peak concentration. From these averages, an equation for temperature as a function of height was found. $N_2O_4$ concentration contour heights were measured, and corresponding temperatures were calculated. This temperature was used to find $K_e$ and $C_{NO_2}$ for each concentration of $C_{N_2O_4}$.

b. $NO_2$ concentrations at 785 meters were measured in parts per million (ppm). Concentrations in volume percent were found by multiplying ppm values by $10^{-4}$.

c. Centerline contour heights for the steady-state peak periods at each downwind array were averaged and input into a FORTRAN program that fit the vertical data to four different curves: a generalized exponential fit to the three lowest points, a Gaussian fit to the two lowest points, a least squares Gaussian fit to all points, and a weighted least squares Gaussian fit to all points.

Output consisted of predicted concentration at each given height using each fit. Predicted surface centerline concentration, effective cloud height, and the value of n in the exponential fit were also given.

The fits chosen were those with the smallest residuals overall. When n is close to 2.0, the data nearly have a Gaussian distribution so Gaussian fits were considered.

Although the exponential fit often returned small residuals (always 0 for the lowest three points), it does not estimate cloud parameters as accurately as the Gaussian fits. Exponential fits return larger values for centerline concentration and smaller values for effective cloud height than the Gaussian fits. Among the Gaussian fits, the weighted least squares fit usually returned the smallest residuals, therefore, it was chosen in each instance.

d. Additional information regarding the calculations for the Eagle Series can be found in Appendix A, Section C.1.

2. Specific

Our analysis was completed as previously described. Exceptions and difficulties are discussed in the remainder of this appendix.

a. Eagle 3

At 25 meters, several averages were examined. An average using contour heights from 40, 90, 130, and 180 seconds yielded a questionable surface centerline concentration. We also examined a set of fits for averages from 40 and 90 seconds. Finally, the contours were smoothed to be more Gaussian in shape, averages were taken, and curves fitted. A 5-point weighted least squares Gaussian fit was chosen for the smoothed 40- and 90-second $N_2O_4$ and $NO_2$ data because it was smoother than the previous fits.

b. Eagle 6

At the 785-meter row, the $NO_2$ cloud was lofted for much of the spill. Average contour heights for 430, 460, and 510 seconds were fit. The exponential fit gave n = 0.011. Since this was not close to 2.0, only contour heights from 460 seconds were used because that time looked most Gaussian and nonlofted. Fits were much better and a 4-point weighted least squares Gaussian fit was chosen.

## REFERENCES


C-1. McRae, T.G., et al., Eagle Series Data Report: 1983 Nitrogen Tetroxide Spills, UCID-20063, Rev. 1, Lawrence Livermore National Laboratory, Livermore, California, March 1987.

C-2. McRae, T.G., Analysis and Model/Data Comparisons of Large-Scale Releases of Nitrogen Tetroxide, UCID-20388, Lawrence Livermore National Laboratory, Livermore, California, March 1985.

# APPENDIX D

# SHELL CONTINUOUS RELEASE TESTS (LNG AND LPG)

## A. DESCRIPTION OF TEST SERIES

The Maplin Sands experiments were performed by Shell Research Ltd. in the summer of 1980, to study the dispersion and combustion of releases of dense flammable gases. This study used 34 spills of liquefied gases onto the sea. The materials were refrigerated liquid propane and liquefied natural gas in quantities up to 20 $m^3$. The test series is described in Reference D-1, and additional information is available in References D-2 - D-4.

The site chosen for the releases was on an area of tidal sands with a typical slope of 1/1000 on the north side of the Thames estuary in England. Experiments were conducted during offshore winds for reasons of safety. The point of release was 350 meters offshore, and when possible, spills were performed at high tide. A 300-meter-diameter dike was constructed to retain the seawater around the spill point so that spills also could be performed at low tide. The maximum change in level at the offshore edge of the dike was 0.75 meters. Behind the 5-meter-high seawall was flat farmland.

In the early experiments, liquid was released from the open end of a vertical pipe 0.15 meters in diameter. In four tests the pipe was 2 to 3 meters above the water surface; in subsequent tests it was lower, and in three the pipe end was below the surface. Later, the end of the spill pipe was flared in a vertical-axis cone with a horizontal plate below it at the water surface. The liquid emerged from the slot between the cone and the plate with negligible vertical momentum.

Instruments were deployed on 71 floating pontoons initially in the layout shown in Figure D-1. However, the pattern was changed for the propane spills; more pontoons were concentrated in the nearfield, particularly in the direction covered by the prevailing westerly wind.

About 360 instruments were used in the array. In addition to combustion instruments, three gas sensors were mounted on a standard pontoon, (usually at

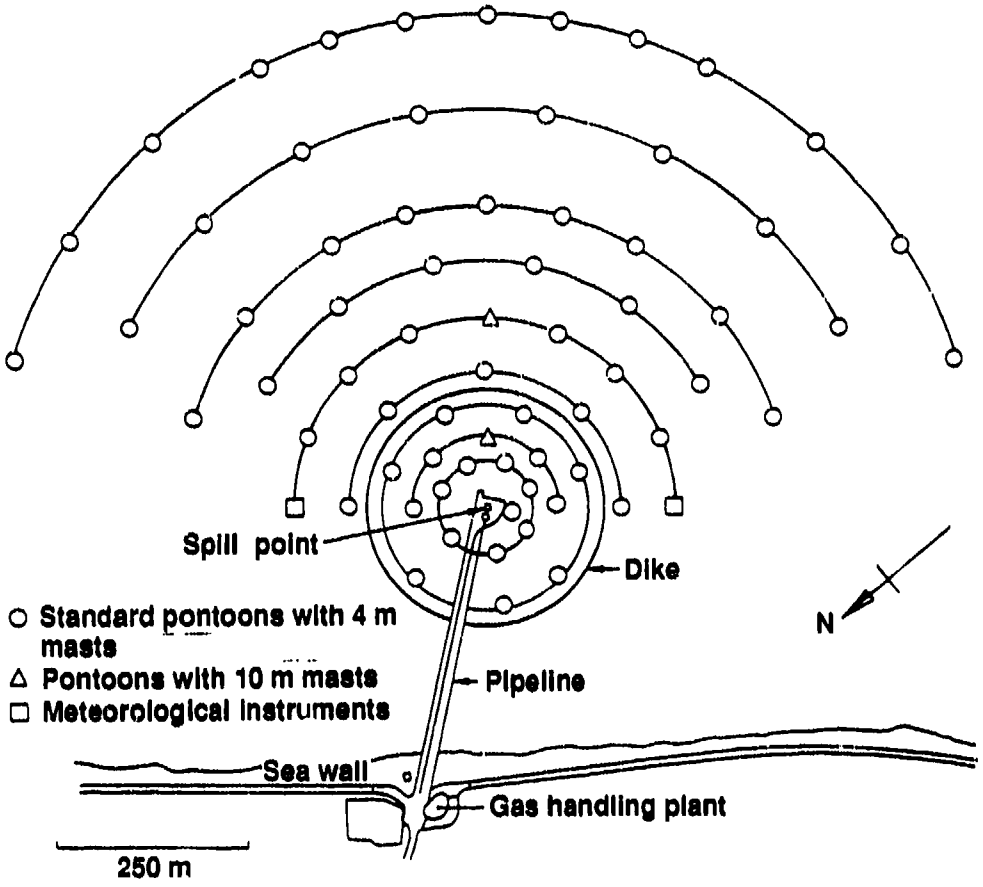


Figure D-1. Sensor Array for the Shell Tests at Maplin Sands.

0.5 to 0.9 meters, 1.4 meters, and 2.4 meters above the sea surface), and one thermocouple, was located close to the lowest gas sensor. The gas sensor is a device based on measurement of the heat loss from a filament under free convection. Two pontoons each had 10-meter masts, six gas sensors, one thermocouple, and two three-axis sonic anemometers. Two sonic anemometers were deployed elsewhere.

Two other pontoons were devoted to meteorological measurements. These provided vertical profiles of temperature and windspeed up to 10 meters, together with measurements of wind direction, relative humidity, insolation, water temperature, and wave height.

Signals from the instruments were sampled 10 times/seconds, digitized on the pontoons, and relayed by cable via multiplexers to the computers onshore.

The spills were photographed from three locations, two land-based towers providing orthogonal views and a helicopter overhead. At each location, still photographs and video recordings were taken.

## B. TEST SUMMARIES

### 1. Shell 15

#### a. Test

| | |
|---|---|
| Name: | Shell 15 |
| Date: | August 18, 1980 |
| Material: | LNG (84.9% methane, 9.7% ethane, 3.2% propane--mol%) |
| Molecular Weight: | 0.016043 kg/mol |
| Liquid Density: | 424.1 kg/m$^3$ at -161.5°C |
| Boiling Temperature: | 111.7 K (-161.5°C) |
| Heat of Vaporization: | 8.18 kJ/mol at -161.5°C |
| Heat Capacity (vapor): | 35.9 J/mol K at 26.8°C |
| Release Mode: | Pressure-driven flow through a precooled 335-m pipe with a volume of about 5 m$^3$ downstream of the control value. The 6-in-diameter end of the pipe pointed downward and terminated about 2 or 3 m above the surface. Much of the LNG apparently evaporated in the air before hitting the surface of the sea. |

#### b. Source Data

| | |
|---|---|
| Spill Rate: | 20.5 kg/s (2.9 m$^3$/min liquid) |
| Spill Duration: | 285 s of steady flow |
| Spill Mass: | 5800 kg during steady flow; 7600 kg total |
| Spill Temperature: | 111.7 K (-161.5°C) |
| Source Description: | The release mode resulted in an appreciable fraction of the LNG evaporating between the end of the spill pipe and the surface of the sea. The result was a cold visible plume that spread considerably laterally and persisted downwind for several hundred meters. No overhead photography was available for documentation. |

#### c. Atmospheric Conditions

| | | | |
|---|---|---|---|
| Avg. Windspeed: | 3.6 m/s at 10 m | $z_0$: | 0.000058 m |
| Sigma Windspeed: | 0.35 m/s | $U_*$: | 0.128 m/s (0.11 m/s) |
| Wind Direction: | 6° | $\Theta_*$: | -0.099 K |
| Avg. Temperature: | 288.28 K at 10 m | $\Theta_0$: | 292.34 K |
| Barometric Pressure: | -- | L: | -71.4 m |
| Relative Humidity: | 88% | Stability | D |
| Cloud Cover: | 84 W/m$^2$ insolation | | |
| Sea Temperature: | -- | | |

d. Vapor Cloud Characteristics (Shell 15)

(1) Peak Concentration, $C_p$

| Downwind distance (m) | Peak concentration (vol%) |
|---|---|
| 58 | 11. at 1.3 m |
| 89 | 11. at 1.3 m |
| 129 | 7.5 |
| 181 | 3.6 at 1.4 m |
| 248 | 3.0 at 1.4 m |
| 322 | 3.6 |
| 399 | 2.1 |
| 650 | 1.1 |

(2) Average Cloud Characteristics

Insufficient data.

e. Comments

(1) Peak concentrations were at an elevation of 0.9 to 1.0 m unless otherwise stated.

(2) Data were insufficient to determine the average cloud characteristics.

2. Shell 27

a. Test

| | |
|---|---|
| Name: | Shell 27 |
| Date: | September 9, 1980 |
| Material: | LNG (93.2% methane, 5.4% ethane, 1.1% propane--mol%) |
| Molecular Weight: | 0.16043 kg/mol |
| Liquid Density: | 424.1 kg/m$^3$ at -161.5°C |
| Boiling Temperature: | 111.7 K (-161.5°C) |
| Heat of Vaporization: | 8.18 kJ/mol at -161.5°C |
| Heat Capacity (vapor): | 35.9 J/mol K at 26.8 K |
| Release Mode: | Pressure-driven flow through a precooled 335-m pipe with a volume of about 5 m$^3$ downstream of the control valves. The 6-in-diameter end of the pipe pointed downward and terminated about 0.5 m above the surface. |

b. Source Data

| | |
|---|---|
| Spill Rate: | 22.6 kg/s (3.2 m$^3$/min liquid) |
| Spill Duration: | 160 s of steady flow |
| Spill Mass: | 3600 kg during steady flow; 5300 kg total |
| Spill Temperature: | 111.7 K (-161.5°C) |
| Source Description: | The short distance between the end of the spill pipe and the water surface together with the downwind momentum of the LNG probably resulted in subsurface and surface evaporation from the spreading pool of LNG. |

c. Atmospheric Conditions

| | | | |
|---|---|---|---|
| Avg. Windspeed: | 5.5 m/s at 10 m | $z_o$: | 0.000058 m |
| Sigma Windspeed: | 0.7 m/s | $U_*$: | 0.203 m/s (0.22 m/s) |
| Sigma Wind Direction: | 5° | $\Theta_*$: | -.134 K |
| Avg. Temperature: | 287.73 K | $\Theta_o$: | 291.32 K |
| Barometric Pressure: | -- | L: | -22.3 m |
| Relative Humidity: | 53% | Stability: | C-D |
| Cloud Cover: | 493 W/m$^2$ insolation | | |
| Sea Temperature: | 288.75 K | | |

d. Vapor Cloud Characteristics (Shell 27)

(1) Peak Concentration, $C_p$

| Downwind distance (m) | Peak concentration (vol%) |
|---|---|
| 58 | 17.5 |
| 88 | 12.0 |
| 129 | 9.0 |
| 181 | 4.5 at 1.4 m |
| 248 | 3.0 |
| 322 | 3.5 |
| 399 | 3.0 |
| 650 | 0.6 |

(2) Average Cloud Characteristics

Insufficient data.

e. Comments

(1) Peak concentrations were at an elevation of 0.9 to 1.0 m unless otherwise stated.

(2) Data were insufficient data to determine the average cloud characteristics.

3. Shell 29

a. Test

| | |
|---|---|
| Name: | Shell 29 |
| Date: | September 9, 1980 |
| Material: | LNG (98.5% methane, 1.4% ethane, 0.1% propane--mol %) |
| Molecular Weight: | 0.016043 kg/mol |
| Liquid Density: | 424.1 kg/m$^3$ at -161.5°C |
| Boiling Temperature: | 111.7 K (-161.5°C) |
| Heat of Vaporization: | 8.18 kJ/mol at -161.5°C |
| Heat Capacity (vapor): | 35.9 J/mol K at 26.8°C |
| Release Mode: | Pressure-driven flow through a precooled 335-m pipe with a volume of about 5 m$^3$ downward of the control valve. The 6-in-diameter end of the pipe pointed downward and was terminated by a short length of flexible hose of the same diameter that just reached the water surface. |

b. Source Data

| | |
|---|---|
| Spill Rate: | 29.0 kg/s (4.1 m$^3$/min liquid) |
| Spill Duration: | 225 s of steady flow |
| Spill Mass: | 6500 kg during steady flow; 9300 kg total |
| Spill Temperature: | 111.7 K (-161.5°C) |
| Source Description: | The penetration of the jet of LNG into the water was clearly greater than in Test 27. Subsurface vaporization was considerable because gas jetted as high as 10 m in the source area. The resulting plume was strongly bifurcated. |

c. Atmospheric Conditions

| | | | |
|---|---|---|---|
| Avg. Windspeed: | 7.4 m/s at 10 m | $z_o$: | 0.000058 m |
| Sigma Windspeed: | 0.9 m/s | $U_*$: | 0.263 m/s (0.20 m/s) |
| Sigma Wind Direction: | 4° | $\Theta_*$: | 0.007 K |
| Avg. Temperature: | 289.19 K | $\Theta_o$: | 289.08 K |
| Barometric Pressure: | -- | L: | 685 m |
| Relative Humidity: | 52% | Stability: | D |
| Cloud Cover: | 143 W/m$^2$ insolation | | |
| Sea Temperature: | 289.95 K | | |

d. Vapor Cloud Characteristics (Shell 29)

(1) Peak Concentration, $C_p$

| Downwind distance (m) | Peak concentration (vol%) |
|---|---|
| 58 | 14.0 |
| 89 | 12.0 |
| 129 | 6.0 |
| 180 | 5.0 |
| 250 | 2.8 at 1.4 m |
| 322 | 1.7 |
| 400 | 1.5 at 2.3 m |

(2) Average Cloud Characteristics

Insufficient data.

e. Comments

(1) Peak concentrations were at an elevation of 0.9 m unless otherwise stated.

(2) Data were insufficient to determine the average cloud characteristics.

4. Shell 34

a. Test

| | |
|---|---|
| Name: | Shell 34 |
| Date: | 17 September 1980 |
| Material: | LNG (95.9% methane, 2.6% ethane, 0.9% propane--mol%). |
| Molecular Weight: | 0.016043 kg/mol |
| Liquid Density: | 424.1 kg/m$^3$ at -161.5°C |
| Boiling Temperature: | 111.7 K (-161.5°C) |
| Heat of Vaporization: | 8.18 kJ/mol at -161.5°C |
| Heat Capacity (vapor): | 35.9 J/mol K at 26.8°C |
| Release Mode: | Pressure-driven flow through a precooled 335-m pipe with a volume of about 5 m$^3$ downward of the control valve. The 6-in-dia. end of the pipe pointed downward and was terminated by a length of flexible hose of the same diameter that ended about 0.7 m above the water surface. |

b. Source Data

| | |
|---|---|
| Spill Rate: | 21.2 kg/s (3.0 m$^3$/min liquid) |
| Spill Duration: | 95 s of steady flow |
| Spill Mass: | 2000 kg during steady flow; 4300 kg total |
| Spill Temperature: | 111.7 K (-161.5°C) |
| Source Description: | The spill conditions were more like those of Test 27 than Test 34 and the vaporization probably occurred below the surface around the downward LNG jet and from the surface of the surrounding LNG pool. There was little lateral spreading of the visible cloud beyond the apparent pool diameter because of the high wind. |

c. Atmospheric Conditions

| | | | |
|---|---|---|---|
| Avg. Windspeed: | 8.6 m/s at 10 m | $z_o$: | 0.000058 m |
| Sigma Windspeed: | 0.6 m/s | $U_*$: | 0.316 m/s (.28 m/s) |
| Sigma Wind Direction: | 4° | $\Theta_*$: | 0.101 K |
| Avg. Temperature: | 288.01 K | $\Theta_o$: | 290.89 K |
| Barometric Pressure: | -- | L: | -71.5 m |
| Relative Humidity: | 72% | Stability: | D |
| Cloud Cover: | 449. W/m$^2$ insolation | | |
| Sea Temperature: | 288.95 K | | |

d. Vapor Cloud Characteristics (Shell 34)

(1) Peak Concentration, $C_p$

| Downwind distance (m) | Peak concentration (vol%) |
|---|---|
| 89 | 12.0 |
| 180 | 4.6 |

(2) Average Cloud Characteristics

Insufficient data.

e. Comments

(1) Peak concentrations were at an elevation of 0.9 to 1.0 m.

(2) Data were insufficient to determine the average cloud characteristics.

5. Shell 35

a. Test

| | |
|---|---|
| Name: | Shell 35 |
| Date: | September 17, 1980 |
| Material: | LNG (97.8% methane, 1.7% ethane, 0.4% propane--mol%) |
| Molecular Weight: | 0.016043 kg/mol |
| Liquid Density: | 424.1 kg/m$^3$ at -161.5°C |
| Boiling Temperature: | 111.7 K (-161.5°C) |
| Heat of Vaporization: | 8.18 kJ/mol at -161.5°C |
| Heat Capacity (vapor): | 35.9 J/mol K at 26.8°C |
| Release Mode: | Pressure-driven flow through a precooled 335-m pipe with a volume of about 5 m$^3$ downstream of the control valve. The 6-in-diameter end of the pipe pointed downward and was terminated by a length of flexible hose of the same diameter that ended about 0.5 m above the water surface. |

b. Source Data

| | |
|---|---|
| Spill Rate: | 27.6 kg/s (3.9 m$^3$/min liquid) |
| Spill Duration: | 135 s of steady flow |
| Spill Mass: | 3700 kg during steady flow; 7800 kg total |
| Spill Temperature: | 111.7 K (-161.5°C) |
| Source Description: | The spill conditions were similar to those for Test 34, which occurred an hour earlier but with somewhat greater windspeed and spill rate. Again, a mixture of subsurface and surface vaporization probably occurred. Little or no lateral spreading of the cloud occurred beyond the diameter of the pool. |

c. Atmospheric Conditions

| | | | |
|---|---|---|---|
| Avg. Windspeed: | 9.8 m/s at 10 m | $z_o$: | 0.000058 m |
| Sigma Windspeed: | 0.9 m/s | $U_*$: | 0.353 m/s (2.8 m/s) |
| Sigma Wind Direction: | 4° | $\Theta_*$: | -168 K |
| Avg. Temperature | 288.76 K | $\Theta_o$: | 293.45 K |
| Barometric Pressure: | -- | L: | -54.0 m |
| Relative Humidity: | 63% | Stability: | D |
| Cloud Cover: | 561 W/m$^2$ insolation | | |
| Sea Temperature: | 289.75 K | | |

d. Vapor Cloud Characteristics (Shell 35)

(1) Peak Concentration, $C_p$

| Downwind distance (m) | Peak concentration (vol%) |
|---|---|
| 129 | 8.0 |
| 250 | 3.5 at 1.6 m |
| 400 | 2.2 |

(2) Average Cloud Characteristics

Insufficient data.

e. Comments

(1) Peak concentrations were at an elevation of 0.9 to 1.0 m unless otherwise stated.

(2) Data were insufficient data to determine the average cloud characteristics.

6. Shell 39

a. Test

| | |
|---|---|
| Name: | Shell 39 |
| Date: | September 24, 1980 |
| Material: | LNG (95.2% methane, 1.7% ethane, 0.6% propane--mol%) |
| Molecular Weight: | 0.016043 kg/mol |
| Liquid Density: | 424.1 kg/m$^3$ at -161.5°C |
| Boiling Temperature: | 111.7 K (-161.5°C) |
| Heat of Vaporization: | 8.18 kJ/mol at -161.5°C |
| Heat Capacity (vapor): | 35.9 J/mol K at 26.8°C |
| Release Mode: | Pressure-driven flow through a precooled 335-m pipe with a volume of about 5 m$^3$ downstream of the control valve. The 6-in diameter end of the pipe pointed downward and was terminated by a length of flexible hose of the same diameter that ended about 0.5 m above the water surface. |

b. Source Data

| | |
|---|---|
| Spill Rate: | 33.2 kg/s (4.7 m$^3$/min liquid) |
| Spill Duration: | 60 s of steady flow |
| Spill Mass: | 2000 kg during steady flow; 4600 kg total |
| Spill Temperature: | 111.7 K (-161.5°C) |
| Source Description: | The greater liquid flow rate probably resulted in increased subsurface vaporization than the earlier spills; photographs show jets of vapor reading considerably higher near the spill pipe. The overhead photography shows a larger diameter pool, and the lower windspeed permitted some lateral spreading of the cloud. |

c. Atmospheric Conditions

| | | | |
|---|---|---|---|
| Avg. Windspeed: | 4.1 m/s at 10 m | $z_o$: | 0.000058 m |
| Sigma Windspeed: | 0.4 m/s | $U_*$: | 0.126 m/s (0.15 m/s) |
| Sigma Wind Direction: | 6° | $\Theta_*$: | 0.036 K |
| Avg. Temperature: | 290.01 K | $\Theta_o$: | 288.92 K |
| Barometric Pressure: | -- | L: | 31.5 m |
| Relative Humidity: | 63% | Stability: | D |
| Cloud Cover: | 39 W/m$^2$ insolation | | |
| Sea Temperature: | -- | | |

d. Vapor Cloud Characteristics (Shell 39)

(1) Peak Concentration, $C_p$

| Downwind distance (m) | Peak concentration (vol%) | |
|---|---|---|
| 36 | 19.0 | |
| 58 | 11.5 | |
| 92 | 9.0 | |
| 128 | 2.5 | at 1.4 m |
| 176 | 2.8 | |
| 248 | 0.8 | at 1.4 m |
| 323 | 2.2 | |
| 399 | 1.6 | |
| 649 | 0.6 | |

(2) Average Cloud Characteristics

Insufficient data.

e. Comments

(1) Peak concentrations were at an elevation of 0.9 to 1.0 m unless otherwise stated.

(2) Data were insufficient to define the average cloud characteristics.

7. Shell 56

a. Test

| | |
|---|---|
| Name: | Shell 56 |
| Date: | October 17, 1980 |
| Material: | LNG (93.3% methane, 4.3% ethane, 1.5% propane--mol%) |
| Molecular Weight: | 0.016043 kg/mol |
| Liquid Density: | 424.1 kg/m$^3$ at -161.5°C |
| Boiling Temperature: | 111.7 K (-161.5°C) |
| Heat of Vaporization: | 8.18 kJ/mol at -161.5°C |
| Heat Capacity (vapor): | 35.9 J/mol K at 26.8°C |
| Release Mode: | Pressure-driven flow through a precooled 335-m pipe with a volume of about 5 m$^3$ downstream of the control valve. The 6-in-diameter end of the pipe was connected by a flexible hose section to an inverted funnel that floated on the water. This device delivered the liquid to the water surface with negligible vertical momentum. |

b. Source Data

| | |
|---|---|
| Spill Rate: | 17.7 kg/s (2.5 m$^3$/min liquid) |
| Spill Duration: | 80 s of steady flow |
| Spill Mass: | 1400 kg during steady flow; no record of total mass |
| Spill Temperature: | 111.7 K (-161.5°C) |
| Source Description: | This LNG spill was the only one to use the above device which delivered the liquid to the water surface with little or no subsurface penetration. Photographs show a low, flat cloud without any vertical jets surrounding the spill pipe. Downwind lateral spreading of the cloud was significant. |

c. Atmospheric Conditions

| | | | |
|---|---|---|---|
| Avg. Windspeed: | 5.1 m/s | $z_o$: | 0.000058 m |
| Sigma Windspeed: | 0.5 m/s | $U_*$: | 0.172 m/s (--) |
| Sigma Wind Direction: | -- | $\Theta_*$: | -0.001 K |
| Avg. Temperature: | 283.66 K | $\Theta_o$: | 283.80 K |
| Barometric Pressure: | -- | L: | -1770 m |
| Relative Humidity: | 83% | Stability: | D |
| Cloud Cover: | -- | | |
| Sea Temperature: | 284.75 K | | |

d. Vapor Cloud Characteristics (Shell 56)

(1) Peak Concentration, $C_p$

| Downwind distance (m) | Peak Concentration (vol%) |
|---|---|
| 58 | 16.0 (22) |
| 92 | 5.5 ( 8) |
| 176 | 4.0 ( 6) |

(2) Average Cloud Characteristics

Insufficient data.

e. Comments

(1) Peak concentrations were at an elevation of 0.6 to 0.7 m unless otherwise stated.

(2) Higher peak concentrations occurred later in the spill after the flow rate suddenly increased to an unknown level. These are given in parentheses.

(3) Data were insufficient to define the average cloud characteristics.

8. Shell 43

a. Test

| | |
|---|---|
| Name: | Shell 43 |
| Date: | September 28, 1980 |
| Material: | LPG (1.22% ethane, 96.98% propane--mol%) |
| Molecular Weight: | 0.044097 kg/mol |
| Liquid Density: | 500 kg/m³ at 20°C |
| Boiling Temperature: | 231.09 K -42.1°C |
| Heat of Vaporization: | 18.774 kJ/mol at 231.0 K |
| Heat Capacity (vapor): | 74.01 J/mol K at 26.8°C |
| Release Mode: | Pressure-driven flow through a precooled 335-m pipe with a volume of about 5 m³ downstream of the control valve. The 6-in-diameter end of the pipe pointed downward and was terminated by flexible pipe that ended about 0.2 m above the water surface. |

b. Source Data

| | |
|---|---|
| Spill Rate: | 19.2 kg/s (2.3 m³/min liquid) |
| Spill Duration: | 330 s of steady flow |
| Spill Mass: | 6300 kg during steady flow; 8600 kg total |
| Spill Temperature: | 231.1 K (-42.1°C) |
| Source Description: | In contrast to the subsequent LPG spills, photographs indicated a smaller opaque cloud center around the spill point surrounded by a thinner cloud through which the surface of the sea was visible. This difference may have been a consequence of the spill pipe configuration from which the liquid propane imported the water. There was considerable lateral spreading of the cloud. |

c. Atmospheric Conditions

| | | | |
|---|---|---|---|
| Avg. Windspeed: | 5.5 m/s at 10 m | $z_o$: | 0.000058 m |
| Sigma Windspeed: | 0.6 m/s | $U_*$: | 0.181 m/s 0.21 m/s |
| Sigma Wind Direction: | 6° | $\Theta_*$: | 0.0001 K |
| Avg. Temperature: | 290.07 K | $\Theta_o$: | 290.17 K |
| Barometric Pressure: | -- | L: | 17,900 m |
| Relative Humidity: | -- | Stability: | D |
| Cloud Cover: | 29 W/m² insolation | | |
| Sea Temperature: | 292.05 K | | |

d. Vapor Cloud Characteristics (Shell 43)

(1) Peak Concentration, $C_p$

| Downwind distance (m) | Peak concentration (vol%) |
|---|---|
| 36 | 3.8 at 1.3 m |
| 58 | 4.8 |
| 88 | 6.0 |
| 128 | 3.5 |
| 179 | 0.9 |
| 248 | 2.0 |
| 400 | 0.7 |

(2) Average Cloud Characteristics

Insufficient data.

e. Comments

(1) Peak concentrations were at an elevation of 0.9 m unless otherwise stated.

(2) Data were insufficient to define the average cloud characteristics.

9. Shell 46

a. Test

| | |
|---|---|
| Name: | Shell 46 |
| Date: | October 1, 1980 |
| Material: | LPG (0.01% methane, 1.05% ethane, 97.32% propane--mol%) |
| Molecular Weight: | 0.044097 kg/mol |
| Liquid Density: | 500 kg/m³ at 20°C |
| Boiling Temperature: | 231.09 K (-42.1°C) |
| Heat of Vaporization: | 18.774 kJ/mol at -231.05 K |
| Heat Capacity (vapor): | 74.01 J/mol K at 26.8°C |
| Release Mode: | Pressure-driven flow through a precooled 335-m pipe with a volume of about 5 m³ downstream of the control valve. For the first time the 6-in-diameter end of the pipe was connected by a flexible hose to an inverted funnel that floated on the water. This device delivered the liquid to the water surface with negligible vertical momentum. |

b. Source Data

| | |
|---|---|
| Spill Rate: | 23.3 kg/s (2.8 m³/min liquid) |
| Spill Duration: | 355 s of steady flow |
| Spill Mass: | 8300 kg during steady flow; 11,100 kg total |
| Spill Temperature: | 231.1 K (-42.1°C) |
| Source Description: | In contrast to Spill 43, photographs indicated evaporation from a liquid pool with little additional lateral spreading. The cloud was opaque for a substantial distance downwind. |

c. Atmospheric Conditions

| | | | |
|---|---|---|---|
| Avg. Windspeed: | 8.1 m/s at 10 m | $z_0$: | 0.000058 m |
| Sigma Windspeed: | 1.0 m/s | $U_*$: | 0.284 m/s (0.25 m/s) |
| Sigma Wind Direction: | 7° | $\theta_*$: | 0.009 K |
| Avg. Temperature: | 291.81 K | $\theta_0$: | 291.64 K |
| Barometric Pressure: | -- | L: | 653 m |
| Relative Humidity: | 71% | Stability: | D |
| Cloud Cover: | 284 W/m² insolation | | |
| Sea Temperature: | 290.45 K | | |

d. Vapor Cloud Characteristics (Shell 46)

(1) Peak Concentration, $C_p$

| Downwind distance (m) | Peak concentration (vol%) | |
|---|---|---|
| 34 | 10.0 | |
| 90 | 5.8 | |
| 129 | 3.5 | |
| 181 | 2.5 | |
| 250 | 1.8 | |
| 322 | 1.7 | |
| 400 | 0.9 | at 2.4 m |

(2) Average Cloud Characteristics

Insufficient data.

e. Comments

(1) Peak concentrations were at an elevation of 0.9 to 1.0 m unless otherwise stated.

(2) Data were insufficient to define the average cloud characteristics.

10. Shell 47

a. Test

| | |
|---|---|
| Name: | Shell 47 |
| Date: | October 1, 1980 |
| Material: | LPG (0.01% methane, 1.78% ethane, 96.86% propane--mol%) |
| Molecular Weight: | 0.044097 kg/mol |
| Liquid Density: | 500 kg/m³ at 20°C |
| Boiling Temperature: | 231.09 K (-42.1°C) |
| Heat of Vaporization: | 18.774 kJ/m² at 231.0 K |
| Heat Capacit (vapor): | 74.01 J/mol K at 26.8°C |
| Release Mode: | Pressure-driven flow through a precooled 335-m pipe with a volume of about 5 m³ downstream of the control valve. The 6-in-diameter end of the pipe was connected by a flexible hose section to an inverted funnel that floated on the water. This device delivered the liquid to the water surface with negligible vertical momentum. |

b. Source Data

| | |
|---|---|
| Spill Rate: | 32.5 kg/s (3.9 m³/min liquid) |
| Spill Duration: | 210 s of steady flow |
| Spill Mass: | 6800 kg during steady flow; 8800 kg total |
| Spill Temperature: | 231.1 K (-42.1°C) |
| Source Description: | Photographs indicated evaporation from a liquid pool with some lateral spreading as the vapor was transported downwind. The cloud was opaque for some distance downwind. |

c. Atmospheric Conditions

| | | | |
|---|---|---|---|
| Avg. Windspeed: | 5.6 m/s at 10 m | $z_o$: | 0.000058 m |
| Sigma Windspeed: | 0.6 m/s | $U_*$: | 0.193 m/s (0.18 m/s) |
| Sigma Wind Direction: | 5° | $\Theta_*$: | 0.015 K |
| Avg. Temperature: | 290.52 K at 10 m | $\Theta_o$: | 290.19 K |
| Barometric Pressure: | -- | L: | 180 m |
| Relative Humidity: | 78% | Stability: | D |
| Cloud Cover: | 100 W/m² insolation | | |
| Sea Temperature: | 290.25 K | | |

d. Vapor Cloud Characteristics (Shell 47)

(1) Peak Concentration, $C_p$

| Downwind distance (m) | Peak concentration (vol%) |
|---|---|
| 34 | 6.0 |
| 90 | 8.0 |
| 129 | 4.0 |
| 181 | 3.0 |
| 250 | 2.0 at 1.5 m |
| 322 | 1.5 |
| 400 | 1.0 |

(2) Average Cloud Characteristics

Insufficient data.

e. Comments

(1) Peak concentrations were at an elevation of 0.9 to 1.0 m unless otherwise stated.

(2) Data were insufficient to define the average cloud characteristics.

11. Shell 49

a. Test

| | |
|---|---|
| Name: | Shell 49 |
| Date: | October 6, 1980 |
| Material: | LPG (2.48% ethane, 96.45% propane--mol%) |
| Molecular Weight: | 0.044097 kg/mol |
| Liquid Density: | 500 kg/m$^3$ at 20°C |
| Boiling Temperature: | 231.09 K (-42.1°C) |
| Heat of Vaporization: | 18.774 kJ/mol at 231.05°C |
| Heat Capacity (vapor): | 74.01 J/mol K at 26.8°C |
| Release Mode: | Pressure-driven flow through a precooled 335-m pipe with a volume of about 5 m$^3$ downstream of the control valve. The 6-in-diameter end of the pipe was connected by a flexible hose section to an inverted funnel that floated on the water. This device delivered the liquid to the water surface with negligible vertical momentum. |

b. Source Data

| | |
|---|---|
| Spill Rate: | 16.7 kg/s (2.0 m$^3$/min liquid) |
| Spill Duration: | 90 s of steady flow |
| Spill Mass: | 1500 kg during steady flow; 4200 kg total |
| Spill Temperature: | 231.1 K (-42.1°C) |
| Source Description: | Photographs indicated evaporation from a smaller liquid pool than in Spill 47. There was some lateral spreading of the visible cloud. |

c. Atmospheric Conditions

| | | | |
|---|---|---|---|
| Avg. Windspeed: | 6.2 m/s at 10 m | $z_o$: | 0.000058 m |
| Sigma Windspeed: | 0.5 m/s | $U_*$: | 0.212 m/s (0.21 m/s) |
| Sigma Wind Direction: | 5° | $\Theta_*$: | 0.058 K |
| Avg. Temperature: | 286.6 K | $\Theta_o$: | 284.98 K |
| Barometric Pressure: | -- | L: | 55.1 m |
| Relative Humidity: | 88% | Stability: | D |
| Cloud Cover: | 337 W/m$^2$ insolation | | |
| Sea Temperature: | 286.15° K | | |

d. Vapor Cloud Characteristics (Shell 49)

(1) Peak Concentration, $C_p$

| Downwind distance (m) | Peak concentration (vol%) |
|---|---|
| 58 | 6.5 |
| 90 | 7.0 |
| 129 | 4.5 |
| 181 | 4.2 |
| 250 | 2.5 |
| 322 | 2.4 |
| 400 | 0.7 |

(2) Average Cloud Characteristics

Insufficient data.

e. Comments

(1) Peak concentrations were at an elevation of 0.9 m.

(2) Data were insufficient to define the average cloud characteristics.

12. Shell 50

a. Test

| | |
|---|---|
| Name: | Shell 50 |
| Date: | September 8, 1980 |
| Material: | LPG (1.18% methane, 97.63% propane--mol%) |
| Molecular Weight: | 0.044097 kg/mol |
| Liquid Density: | 500. kg/m³ at 20°C |
| Boiling Temperature: | 231.09 K (-42.1°C) |
| Heat of Vaporization: | 18.774 kJ/mol at 231.0 K |
| Heat Capacity (vapor): | 74.01 J/mol K at 26.8°C |
| Release Mode: | Pressure-driven flow through a precooled 335-m pipe with a volume of about 5 m³ downstream of the control valve. The 6-in-diameter end of the pipe was connected by flexible hose section o an inverted funnel that floated on the water. This device delivered the liquid to the water surface with negligible vertical momentum. |

b. Source Data

| | |
|---|---|
| Spill Rate: | 35.8 kg/s (4.3 m³/min liquid) |
| Spill Dur tion: | 161 s of steady flow |
| Spill Mass: | 5800 kg during steady flow; 8600 kg total |
| Spill Temperature: | 231.1 K (-42.1°C) |
| Source Description: | Photographs indicated evaporation from a liquid pool, some lateral spreading, and considerable transport downwind before the cloud was no longer opaque. |

c. Atmospheric Conditions

| | | | |
|---|---|---|---|
| Avg. Windspeed: | 7.9 m/s at 10 m | $z_o$: | 0.000058 m |
| Sigma Windspeed: | 0.9 m/s | $U_*$: | 0.260 m/s (0.29 m/s) |
| Sigma Wind Direction: | 6° | $\Theta_*$: | 0.035 K |
| Avg. Temperature: | 283.61 K | $\Theta_o$: | 282.68 K |
| Barometric Pressure: | -- | L: | 137 m |
| Relative Humidity: | 79% | Stability: | D |
| Cloud Cover: | 287 W/m² insolation | | |
| Sea Temperature: | 283.05 K | | |

d. Vapor Cloud Characteristics (Shell 50)

(1) Peak Concentration, $C_p$

| Downwind distance (m) | Peak concentration (vol%) |
|---|---|
| 58 | 10.0 |
| 88 | 7.0 |
| 128 | 3.5 at 1.3 m |
| 181 | 3.5 at 1.3 m |
| 248 | 1.7 at 1.3 m |
| 324 | 1.1 |
| 399 | 1.2 |
| 650 | 0.5 at 1.3 m |

(2) Average Cloud Characteristics

Insufficient data.

e. Comments

(1) Peak concentrations were at an elevation of 0.9 m unless otherwise stated.

(2) Data were insufficient to define the average cloud characteristics.

13. Shell 54

a. Test

| | |
|---|---|
| Name: | Shell 54 |
| Date: | October 15, 1980 |
| Material: | LPG (1.1% ethane, 97.4% propane--mol%) |
| Molecular Weight: | 0.044097 kg/mol |
| Liquid Density: | 500 kg/m³ at 20°C |
| Boiling Temperature: | 231.09 K (-42.1°C) |
| Heat of Vaporization: | 18.774 kJ/mol at 231.0 K |
| Heat Capacity (vapor): | 74.01 J/mol K at 26.8°C |
| Release Mode: | Pressure-driven flow through a precooled 335-m pipe with a volume of about 5 m³ downstream of the control valve. The 6-in-diameter end of the pipe was connected by a flexible hose section to an inverted funnel that floated on the water. This device delivered the liquid to the water surface with negligible vertical momentum. |

b. Source Data

| | |
|---|---|
| Spill Rate: | 19.2 kg/s (2.3 m³/min liquid) |
| Spill Duration: | 120 s of steady flow |
| Spill Mass: | 2300 kg during steady flow; 5800 kg total |
| Spill Temperature: | 231.1 K (-42.1°C) |
| Source Description: | Photographs showed evaporation from a large liquid pool and considerable lateral spreading of the opaque cloud as well as considerable downwind transport. The larger pool size is attributed to probable exit blockage by ice prior to the spill and partial exit constriction resulting in the horizontal liquid jets having greater range than in the preceding tests. |

c. Atmospheric Conditions

| | | | |
|---|---|---|---|
| Avg. Windspeed: | 3.8 m/s at 10 m | $z_o$: | 0.000058 m |
| Sigma Windspeed: | 0.35 m/s | $U_*$: | 0.0126 m/s (.16 m/s) |
| Sigma Wind Direction: | 3° | $\Theta_*$: | 0.020 K |
| Avg. Temperature: | 281.58 K | $\Theta_o$: | 281.06 K |
| Barometric Pressure: | -- | L: | 56.9 m |
| Relative Humidity: | 85% | Stability: | D |
| Cloud Cover: | 191 W/m² insolation | | |
| Sea Temperature: | 282.55 K | | |

d. Vapor Cloud Characteristics (Shell 54)

(1) Peak Concentration, $C_p$

| Downwind distance (m) | Peak concentration (vol%) | |
|---|---|---|
| 58 | 23.0 | |
| 88 | 13.0 | |
| 128 | 4.2 | |
| 181 | 5.5 | |
| 249 | 5.0 | |
| 398 | 2.1 | at 1.4 m |
| 522 | 0.8 | at 1 m |

(2) Average Cloud Characteristics

Insufficient data.

e. Comments

(1) Peak concentrations were at an elevation of 0.5 to 0.7 m unless otherwise stated.

(2) Data were insufficient to define the average cloud characteristics.

## C. TEST SUMMARY NOTES

### 1. Average Cloud Properties for the Shell Experiments

The spatial resolution, especially in the lateral direction, of the gas concentration data is insufficient to determine the cloud widths and the average properties corresponding to that width. Cloud widths are available from overhead images of the visible cloud for all tests but Shell 15. However, information is insufficient to determine the average properties within the visible cloud because the relationship among gas concentration, humidity, and temperature is uncertain. Some unknowns concern heat transfer from the sea to the cloud and enhanced humidity near the water surface, especially above the pool of the boiling cryogen liquid. These problems were identified, but not necessarily solved in the Shell papers (References D-1 - D-4).

### 2. Defining Average Cloud Properties for the Shell Experiments

#### a. Gas concentration data

Table D-1 presents the radial locations (distance from the spill point) at which useful gas concentration data were measured. In many experiments, useful data were obtained at only one station in a given row: LNG--29, 34, 35, and 56; LPG--46 and 50. Data were measured at two stations in some rows: LNG--15, 27, and 39; LPG--43 and 54; and at three stations in only two rows: LPG--47 and 49. Data are limited for gas concentration as a function of azimuth at a given radial distance, and the distances between stations in the rows are large. Therefore, average cloud properties could not be defined in the manner used for the experiments conducted by LLNL.

Numbers in parentheses indicate the number of stations that detected gas.

TABLE D-1. RADIAL LOCATIONS OF USEFUL GAS CONCENTRATION DATA.

| Radial location (m) | LNG spills | | | | | | | LPG spills | | | | | |
|---|---|---|---|---|---|---|---|---|---|---|---|---|---|
| | 15 | 27 | 29 | 34 | 35 | 39 | 56 | 43 | 46 | 47 | 49 | 50 | 54 |
| 35 | | | | | (1) | | (1) | (1) | (2) | | | | |
| 60 | (2) | (1) | (1) | | | (1) | (1) | (1) | | | (1) | (1) | (1) |
| 90 | (2) | (1) | (1) | (1) | | (2) | (1) | (2) | (1) | (3) | (1) | (1) | (2) |
| 130 | (1) | (2) | (1) | | (1) | (1) | | (1) | (1) | (1) | (3) | (1) | (1) |
| 180 | (2) | (1) | (1) | (1) | | (1) | (1) | (1) | (1) | (1) | (1) | (1) | (1) |
| 250 | (2) | (2) | (1) | | (1) | (1) | | (2) | (1) | (1) | (1) | (1) | (2) |
| 325 | (2) | (1) | (1) | | | (1) | | | (1) | (1) | (1) | (1) | |
| 400 | (1) | (1) | (1) | | (1) | (1) | | (1) | (1) | (1) | (1) | (1) | (1) |
| 525 | | | | | | | | | | | | | (1) |
| 650 | (1) | (1) | | | | (1) | | | | | | (1) | |

b. Overhead cloud images

Overhead images of the visible cloud were obtained from a helicopter for all of the Shell experiments except Shell 15 (LNG).

The visible cloud occurs because cloud temperatures are below the local dewpoint; The cloud is a mixture of air, material vapor, and water droplets. The cloud temperature is a function of the degree of vaporization of the LNG or LPG, the mixing of the material vapor and air, heat transfer from the sea to the cloud, and the release of latent heat from the condensation of water vapor.

In principle, the visible water droplet cloud defines a material vapor cloud with a given minimum vapor concentration at the cloud boundaries and with greater concentrations in the cloud. Overhead images of the clouds for specific times are presented in all Shell data reports except that for Test 15.

Shell explored this aspect of the cloud properties in References D-2 - D-4.

Puttock et al. (Reference D-2) compared the observed and calculated (by means of HEGADAS) visible clouds for two LPG spills: Shell 46 and 54. The cloud widths matched well, but the calculated clouds extended considerably downwind of the observed ends of the clouds. The HEGADAS calculations assumed only adiabatic mixing of the humid air with the vaporized material and did not account for the heat transfer from the sea to the cloud, which was indicated by temperature measurements. The observed heat transfer was probably responsible for the difference between the observed and calculated downwind extent of the cloud.

Puttock et al. (Reference D-3) also compared the calculated and observed visible clouds for the Shell 29 spill of LNG, which showed good

agreement for cloud length and width. However, they again found evidence of significant heat transfer from the sea to the cloud. In addition, the humidity in the cloud close to the water surface was significantly greater than that measured at an elevation of 10 meters--the value of humidity used in their calculations.

In a later study, Colenbrander and Puttock (Reference D-4) emphasized the heat transfer from the sea and the enhanced humidity near the water surface within the cloud. Heat-transfer relations were added to the HEGADAS model that they used to simulate Spills 29 and 39 for LNG. They also used significantly higher values of humidity than those measured at an elevation of 10 meters because these values gave calculated temperatures and concentrations that were in agreement with the measurements. In addition, results of laboratory experiments with boiling liquid nitrogen on water showed that water as well as nitrogen was added to the mixture with air close to the liquid surface. This phenomena may account for the enhanced humidity in the visible clouds from the Shell experiments.

Details of their analysis procedures, input data, and assumptions are not given in the references.

c. Conclusions

We cannot determine cloud width and other average cross-section measurements because the spacing for several rows of stations is too large in the lateral direction.

The widths and lengths of visible clouds are available from overhead images obtained at different times for all tests but Shell 15. Boundaries of the visible clouds are a function of the local relative humidity and the local temperature. Temperature is not only a function of the mixing of air with the cold material vapor, but also of heat transfer from the surface of the sea and the release of latent heat from the condensation of

water vapor. Evidence from both the field and the laboratory indicates that water as well as material vapor is mixed with the air above a pool of boiling cryogen liquid. Information is insufficient to use the visible cloud measurements to define the average conditions within the cloud.

## REFERENCES


D-1. Puttock, J.S., Colenbrander, G.W., and Blackmore, D.R., "Maplin Sands Experiments 1980: Dispersion Results from Continuous Releases of Refrigerated Liquid Propane and LNG," in Air Pollution Modeling and Its Application III (C. DeWispelaere, Ed.), Plenum Press, New York, 1983.

D-2 Puttock, J.S., Colenbrander, G.W., and Blackmore, D.R., "Maplin Sands Experiments 1980: Dispersion Results from Continuous Releases of Refrigerated Liquid Propane," Proc. Symp. Heavy Gases and Risk Analysis, Frankfurt, May 1982.

D-3 Puttock, J.S., Colenbrander, G.W., and Blackmore, D.R., "Maplin Sands Experiments 1980: Dispersion Results from Continuous Releases of Refrigerated Liquid Propane and LNG," NATO/CCMS 13th Int. Tech. Meeting on Air Pollution Modeling and Its Application, Isle des Embiez, France, September 1982.

D-4 Colenbrander, G.W., and Puttock, J.S., "Maplin Sands Experiments 1980: Interpretation and Modeling of Liquefied Gas Spills onto the Sea," IUTAM Sym. on Atmospheric Dispersion of Heavy Gases and Small Particles, Delft, 29 August - 2 September 1983.




The reverse of this page is blank.

# APPENDIX E

# HSE CONTINUOUS RELEASE TESTS (FREON)

## A. DESCRIPTION OF TEST SERIES

### 1. Introduction

The Health and Safety Executive's (HSE) Heavy Gas Dispersion Trials (HGDT) project at Thorney Island was set up specifically to study the dispersion of fixed-volume releases of heavy gas. The test series was extended to include trials on steady, continuous plumes. The continuous-release trials became possible because the instrumentation was sold to the contractor (the National Maritime Institute) and the gas container was converted to provide a steady flow rate. The separate series of trials was arranged with the U.S. Department of Transportation. Thus, the continuous-release trials were constrained by the existing inventory of instrumentation, the data-handling capacity, and the limitation on gas supply rate. The test series was not intended to be a comprehensive investigation. Nonetheless, the ad hoc arrangements--which should be seen as a bonus on the main program--were successful, and valuable results were obtained.

### 2. Test Objectives

The main objective was to obtain reliable data to validate the physical and mathematical models of heavy gas dispersion. The configuration was designed to provide, as far as possible, a release condition that, with the fixed-volume results, would bracket the transient release condition typical of many accidental release situations (Reference E-1).

### 3. Terrain

The site chosen was a former Royal Air Force station on Thorney Island in Chichester Harbour about 40 km east of Southampton. Although some buildings and trees obstructed the operational area, the test area had a clear corridor 2 km long with a minimum width of 500 meters. The approach to this corridor was over shallow water to the southwest and the exit was to the

northeast. The site was flat to within about 1 in 100. The only permanent obstruction was a small building (approximately 2 $m^3$). So the adjacent fixed mast was displaced slightly from its planned position. The site was criss-crossed by two tar macadam runways approximately 43 meters wide (see Figure E-1), and the intervening areas are rough grassland (Reference E-2).

Three trials were performed from June 9-15, 1984. In one trial, the coverage of the instrument array by the plume was limited because the wind direction deviated from the array axis. The plume in each trial was characteristically shallow and wide. The visible depth was no more than about 2 meters over much of the plume's extent, and the visible width was as much as 300 meters.

In a trial, the gas container was filled with a mixture of refrigerant-12 and nitrogen in the same way as for the fixed-volume trials. The gas was marked by smoke from successively firing smoke grenades in the delivery duct (Reference E-1).

The source was located 50 meters to the right of the gas container so they did not need to excavate the runway (see Figure E-1). The design windspeed was provisionally selected to be about 2 m/s in both trials, to maximize the detectable extent of the plume within the existing instrument array (Reference E-2).

The source was designed to give a ground-level release with zero vertical momentum, and the design was arranged so the freon was released with no excess horizontal momentum. The diameter of the cap and its height above ground level were such that the horizontal outflow velocity fell below the gravity spreading velocity at a radius within the periphery (Reference E-1).

Release rates averaged 4.2 $m^3/s$ for the three trials with durations of about 400 seconds.

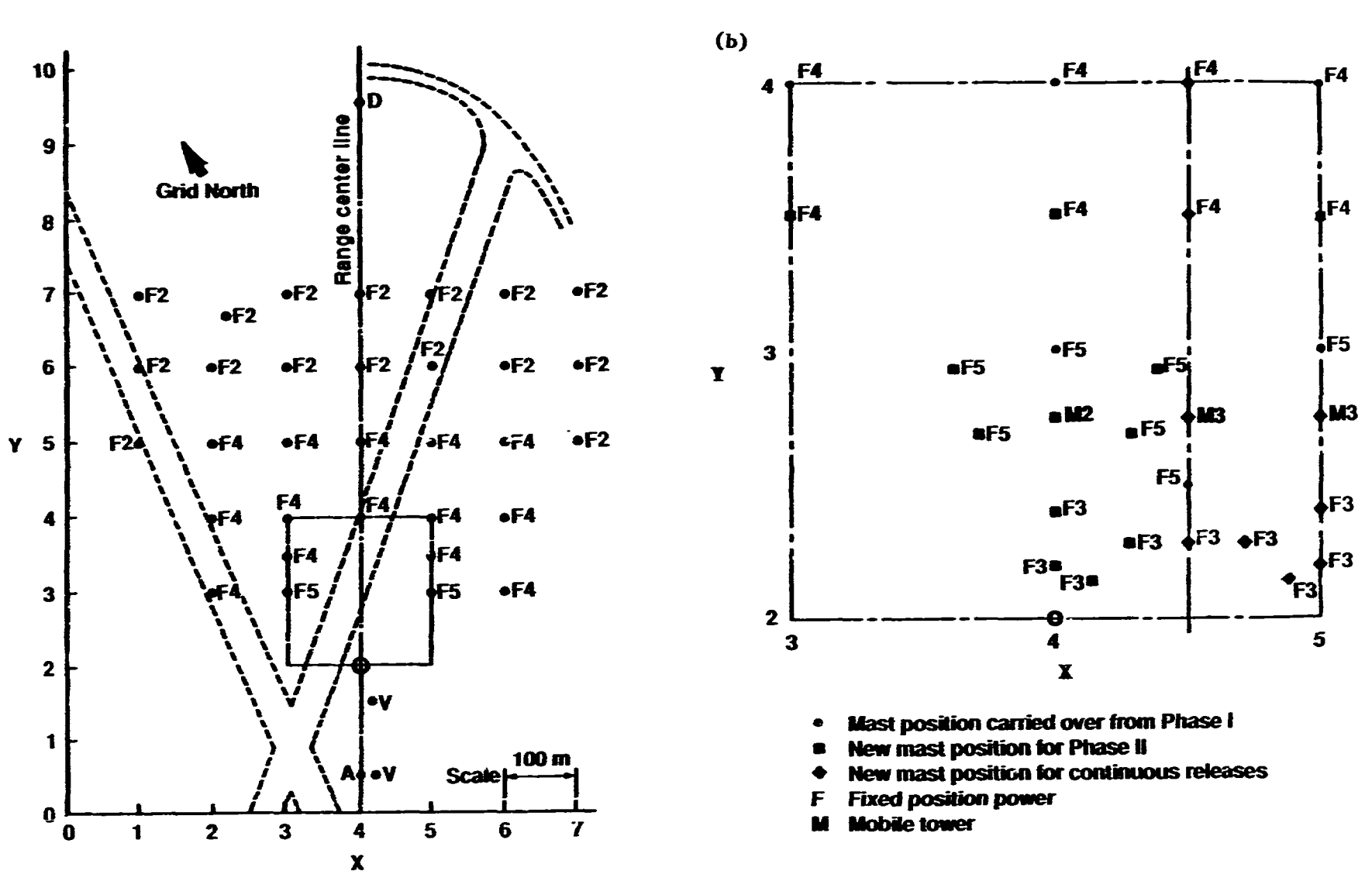


Figure E-1. Sensor Array for the Continuous HSE Tests at Thorney Island: (a) Far-Field Layout; (b) Near-Field Layout.

## 4. Instrumentation

Sensors used during these tests were deployed to maximize the information return, subject to economic constraints (Figure E-1). Thirty-eight type F towers each with five gas sensors comprised the bulk of the instrumentation used during the tests. Four trailer-mounted or mobile masts were deployed, each with four gas sensors mounted at the same height as the type F masts. Eight tri-axiac sonic anemometers were distributed among the four mobile towers. One mobile mast had three sonic anomemeters to provide profile information. One 30-meter-high mast was located 150 meters from the release point. The instrumentation on the mast was designed to provide the data needed to calculate the roughness length ($Z_0$), friction velocity ($U*$), and parameters on which the more common turbulence classification schemes are based.

B. TEST SUMMARIES

1. HSE 45

a. Test

| | |
|---|---|
| Name: | HSE 45 |
| Date: | June 9, 1984 |
| Material: | Freon 12/nitrogen mixture with a relative density of 2 (2.6 kg/m³) |
| Molecular Weight: | 0.058 kg/mol |
| Liquid Density: | -- |
| Boiling Temperature: | -- |
| Heat of Vaporization: | -- |
| Heat Capacity (vapor): | -- |
| Release Mode: | Fan-driven exhaust from a gas bag. |

b. Source Data

| | |
|---|---|
| Spill Rate: | 11.3 kg/s (260 m³/min) |
| Spill Duration: | 455 s |
| Spill Mass: | 5140 kg |
| Spill Temperature: | 289.50 K (16.35°C) |
| Source Description: | The gas was conveyed from the gas bag through an underground duct that terminated in a vertical section. The open end of the duct at ground level was capped by a 2-m-diameter plate that was 0.5 m above the surface. The discharge area was 3.14 m² so the average radial exit velocity was only 1.4 m/s. This velocity is approximately equal to the gravity current velocity for the density ratio of 2. As a result, the material was released with zero vertical momentum and low radial momentum. |

c. Atmospheric Conditions

| | | | |
|---|---|---|---|
| Avg. Windspeed: | 2.3 m/s at 10 m | $z_o$: | 0.005 m |
| Sigma Windspeed: | -- | $U_*$: | 0.083 m/s |
| Sigma Wind Direction: | 7.5°-12.5° | $\theta_*$: | 0.037 K |
| Avg. Temperature: | 286.25 K at 10 m | $\theta_o$: | 285.33 K |
| Barometric Pressure: | -- | L: | 13.3 m |
| Relative Humidity: | 102.4% | Stability: | E/F |
| Cloud Cover: | 13% | | |
| Gross Temperature: | 285.95 K | | |

d. Vapor Cloud Characteristics (HSE 45)

(1) Peak Concentration, $C_p$

| Downwind distance (m) | Peak concentration (vol%) |
|---|---|
| 3.0 | 66.0 |
| 10.0 | 13.0 |
| 20.0 | 17.8 |
| 28.0 | 15.8 |
| 50.0 | 14.5 |
| 52.8 | 13.2 |
| 72.1 | 9.5 |
| 90.1 | 6.4 |
| 111.8 | 4.6 |
| 158.1 | 2.8 |
| 206.2 | 0.9 |
| 250.0 | 0.8 |
| 335.4 | 0.5 |
| 471.6 | 0.4 |
| 522.0 | 0.1 |

(2) Average Cloud Characteristics

The following steady-state concentration values were measured at the locations shown close to the release point.

| Radial distance (m) | Azimuth relative array axis (deg) | Gas concentration (%) z = 0.4 m | z = 1.4 m | z = 2.4 m |
|---|---|---|---|---|
| 38.6 | -68.7 | 11.5 | 0 | 0 |
| 35.6 | -38.2 | 10.5 | 0.2 | 0 |
| 28.0 | 0 | 14.0 | 9.0 | 0 |
| 35.6 | 38.2 | 6.0 | 0.3 | 0 |
| 38.6 | 68.7 | 4.5 | 0.1 | 0 |

e. Comments

(1) Peak concentrations were at a height of 0.4 m.

(2) The pattern of gas concentration data suggests that the cloud moved along the axis of the instrument array (0°) for about 30 to 50 m before it turned to the left and moved along the general direction of the wind vector measured at an elevation of 10 m (-34.5°). This initial movement was slightly uphill; the subsequent cloud track along the wind vector was slightly downhill.

(3) Gas concentration data were available for two or more elevations at nine stations at ranges from 28 to 64 m.

(4) A steady gas concentration greater than a fraction of 1% at elevations greater than 0.4 m was measured at only two stations: 9% at z = 1.4 m at a range of 28 m on the array axis (34.5° to the right of the wind vector), and 1% at z = 1.4 m at a range of 64 m at an azimuth of -51.3° (to the left of the array axis).

2. HSE 47

a. Test

| | |
|---|---|
| Name: | HSE 47 |
| Date: | June 15, 1984 |
| Material: | Freon 12/nitrogen mixture with a relative density of 2 (2.6 kg/m$^3$) |
| Molecular Weight: | 0.058 kg mol |
| Liquid Density: | -- |
| Boiling Temperature: | -- |
| Heat of Vaporization: | -- |
| Heat Capacity (vapor): | -- |
| Release Mode: | Fan-driven exhaust from a gas bag. |

b. Source Data

| | |
|---|---|
| Spill Rate: | 10.8 kg/s (250 m$^3$/min) |
| Spill Duration: | 465 s |
| Spill Mass: | 5020 kg |
| Spill Temperature: | 290.75 K (17.6°C) |
| Source Description: | The gas was conveyed from the gas bag through an underground duct that terminated in a vertical section. The open end of the duct was capped by a 2-m-diameter plate that was 0.5 m above the ground surface. The discharge area was 3.14 m$^2$ so the average radial exit velocity was only 1.3 m/s. This velocity is slightly less than the gravity current velocity of about 1.4 m/s for the density ratio of 2. As a result, the material was released with zero vertical momentum and low radial momentum. |

c. Atmospheric Conditions

| | | | |
|---|---|---|---|
| Avg. Windspeed: | 1.5 m/s at 10 m | $z_o$: | 0.005 m |
| Sigma Windspeed: | -- | $U_*$: | 0.049 m/s |
| Sigma Wind Direction: | 7.5°-12.5° | $\Theta_*$: | 0.017 K |
| Avg. Temperature: | 287.45 K at 10 m | $\Theta_o$: | 287.02 K |
| Barometric Pressure: | -- | L: | 10 m |
| Relative Humidity: | 97.4% | Stability: | F |
| Cloud Cover: | 0% | | |
| Gross Temperature: | 287.65 K | | |

d. Vapor Cloud Characteristics (HSE 47)

(1) Peak Concentration, $C_p$

| Downwind distance (m) | Peak concentration (vol%) |
|---|---|
| 2.0 | 70.0 |
| 10.0 | 17.2 |
| 20.0 | 20.0 |
| 28.0 | 19.0 |
| 40.0 | 16.4 |
| 50.0 | 16.8 |
| 72.1 | 12.0 |
| 90.1 | 8.0 |
| 111.8 | 2.9 |
| 127.3 | 2.5 |
| 212.1 | 1.5 |
| 250.0 | 0.7 |
| 335.4 | 0.5 |
| 471.6 | 0.2 |

(2) Average Cloud Characteristics

The following steady-state concentration values were measured at the locations shown close to the release point.

| Radial distance (m) | Azimuth relative array axis (deg) | Gas concentration (%) z = 0.4 m | z = 1.4 m | z = 2.4 m |
|---|---|---|---|---|
| 38.6 | -68.7 | 14.0 | no data | no data |
| 35.6 | -38.2 | 13.0 | 0.2 | 0 |
| 28.0 | 0 | 17.0 | 12.0 | 0.1 |
| 35.6 | 38.2 | 16.0 | 0.1 | 0 |
| 38.6 | 68.7 | 14.0 | 0 | 0 |

e. Comments

(1) Peak concentrations were at a height of 0.4 m.

(2) The pattern of gas concentration data suggests that the cloud moved along the axis of the instrument array (0°) for about 30 to 50 m before it turned to the left and moved along the general direction of the wind vector (-32.6°). This initial movement was slightly uphill; the subsequent cloud track along the wind vector was slightly downhill.

(3) Gas concentration data were available for two or more elevations at six stations at ranges from 28 to 64 m.

(4) A steady gas concentration greater than a fraction of 1% at elevations greater than 0.4 m was measured at only one station: 12% at z = 1.4 m at a range of 28 m along the array axis (32.6% to the right of the wind vector).

C. TEST SUMMARY NOTES

The pattern of gas concentration data--peak values at 0.4-meter elevation and peak and average values at 1.4-meter elevation--suggest that the cloud first moved along the array axis for 30 to 50 meters before turning left about 30°. Then it followed a track corresponding to the mean wind vector.

Gas concentration data are available at two or more elevations at ranges from 28 to 64 meters. These measurements were made in what appears to be the source or near-source region.

A subset of these measurements was selected in each case to define "average" cloud properties. These stations range in radial distance from 28 to 38.6 meters and azimuths relative to the array axis from -68.7° to + 68.7° (the wind directions were -35.4° for HSE 45 and -32.6° for HSE 47). Measurements are available at elevations of 0.4, 1.4, and 2.4 meters, except for one station where the sensors at 1.4 and 2.4 meters were not operating properly.

REFERENCES

E-1. McQuaid, J., Design of the Thorney Island Continuous Release Trials, Safety Engineering Laboratory, Health and Safety Executive, Sheffield, England, 1985.

E-2. McQuaid, J., and Roebuck, B., Large Scale Field Trials on Dense Vapour Dispersion, Report EUR 10029, Commission of the European Communities, Brussels, 1985.